

# Development of a Computationally Efficient Modelling Framework for Type IV Pressure Vessels

Antonio Johman





# Development of a Computationally Efficient Modelling Framework for Type IV Pressure Vessels

by

Antonio Johman

to obtain the degree of Master of Science  
at the Delft University of Technology,  
to be defended publicly on Thursday January 21, 2021 at 9:30 AM

Student number:	4933664	
Project duration:	April 2020 - January 2021	
Thesis committee:	Prof. Dr. C. Kassapoglou.,	TU Delft, chair
	Dr. Ir. J. M. J. F. van Campen,	TU Delft, supervisor
	Dr. Ir. O. K. Bergsma,	TU Delft
	Dipl. -Ing M. Nebe,	Daimler AG, supervisor

*This thesis is confidential and cannot be made public until January 21, 2023.*

This thesis was sponsored by Daimler AG and Daimler Truck Fuel Cell GmbH  
An electronic version of this thesis is available at <http://repository.tudelft.nl/>.



# Acknowledgments

It seems we have come to the end of another segment of comfortable life - a master's thesis. It is in this section one is asked to be reminded of the fact that, no matter the effort exerted, a difficult task is rarely accomplished by a solitary individual. The thesis that follows is no different. While I was the one that willed it into existence, it is the experience gathered along the way that makes any of the tedious act of "willing" worth it at all. For a considerate individual, writing the acknowledgments is possibly the most difficult sections to write since he is expected to extend gratitude to those that made the process of this thesis memorable. However, as is certainly the case here, some people deserve more than a mention and a simple "thank you". Nevertheless, the thank you's are what this section is for, and so let me name a few that come to mind specifically.

By some cosmic chance, I was paired with mentors whose quality cannot be simply described. Martin Nebe and Julien van Campen are individuals whose standard and demeanor one can only strive towards and their guidance, advice and support in this process cannot be understated. At every step of the way, both Martin and Julien, made sure that I was not straying from this "winding road". To Julien, I am eternally grateful for recommending me for an internship and thesis at Daimler, I still wonder if he was not feeling well the day that came to his mind. And an extra special thank you goes to Martin, his energetic company and genuine spirit were always there to make sure that every student under his wing would not just do well, but would excel at their work - a truly wonderful person and a good friend.

Of all the office mates that have come and gone in the last 12 months, one was irreplaceable - Clemens Braun - an intensely practical person with a profound sense of humor. His help during virtually all manufacturing and testing processes was only matched by the quality of his company and advice. A fantastic person whose perspective made a stronger impact on my own than he may realize.

There were at least 2 other students in the office at any given time during my work at Daimler AG. We shared a common struggle to finish our respective projects to a satisfactory degree and supported each other along the way - making sure that spirits were high and bouncing ideas off each other in order to nudge progress into being. A special thanks goes to Alex, Alejandro, Chiara, Tom and Eleonora for being wonderful peers and for dealing with my periodic existentialism.

Finally, a special thanks must go to the friends I met during my first year at TU Delft, Niz and Sebastian. Together with Alex (the one from above), we formed a close knit group that managed to infuse some life into endless assignments. Thank you for always being willing to share a laugh and spend quality time outside the classroom's tedium.

Contributions to this thesis were not only made through peer support and mentor guidance. Contribution also comes through emotional support, and I was so extremely fortunate to have my parents, Nada and Renato. There is no symbol or action that would sufficiently express how much I've cherished their support. I still do not fully comprehend the sacrifices they've made in order to provide me with the life I've had, and while it is possible that I will never understand the true extent of their sacrifice, I will also never forget it. Hvala mama i tata.

Of course there are many more folks who should be mentioned as having helped me in mentionable ways and if I started listing all of them, the acknowledgments would likely be longer than the thesis itself. To all of those folks, I want to express a heartfelt thank you. You have all helped me to get to this point and your assistance, no matter how big or small, is deeply appreciated.

*Antonio Johman  
Stuttgart, January 2021*



# Nomenclature

## Abbreviations

<b>AE</b>	acoustic emission
<b>BEV</b>	battery electric vehicle
<b>C3D20R</b>	Solid quadratic element type in ABAQUS
<b>C3D8R</b>	Solid element type in ABAQUS
<b>CFRP</b>	carbon fiber-reinforced plastic
<b>CDM</b>	continuum damage mechanics
<b>CLT</b>	classical lamination theory
<b>CNG</b>	compressed natural gas
<b>CPV</b>	composite pressure vessel
<b>CT</b>	computed tomography
<b>DOF</b>	Degree of freedom
<b>DIC</b>	digital image correlation
<b>EoL</b>	end-of-line
<b>ESG</b>	electrical resistance strain gauge
<b>FBG</b>	fiber Bragg grating
<b>FCEV</b>	fuel cell electric vehicle
<b>FC</b>	fuel cell
<b>FEA</b>	finite element analysis
<b>FE</b>	finite element
<b>FPF</b>	first-ply-failure
<b>FVF</b>	fiber volume fraction
<b>ICE</b>	internal combustion engine
<b>ICEV</b>	internal combustion engine vehicle
<b>IFF</b>	interfiber failure
<b>LVDT</b>	linear variable differential transformer
<b>NWP</b>	nominal working pressure
<b>PA6</b>	polyamide 6
<b>S4</b>	Shell element type in ABAQUS

## Symbols

$\alpha$	filament path angle
$\lambda$	slippage coefficient
$t$	layer thickness
$r$	radial coordinate
$N$	in-plane loads
$M$	bending loads
$A$	extensional stiffness matrix
$B$	coupling stiffness matrix
$D$	bending stiffness matrix
$P$	pressure
$V$	volume
$W$	weight
$\sigma$	planar stress
$\gamma$	shear stress
$C_{hoop}$	hoop layer context
$C_{hg}$	hoop group context
$N_h$	number of hoop layers
$i_h$	index of inspected hoop layer
$N_g$	number of hoop groups
$i_g$	index of inspected hoop group
$L_{taper}$	raw tapering length
$C_{helical}$	helical context
$t_{max}$	corrected maximum thickness
$t_{nom}$	raw nominal thickness
$t_{maxCAD}$	raw maximum thickness
$c_{correction}$	thickness correction factor
$x_{maxCAD}$	axial location of raw maximum thickness
$x_{minPO}$	minimum mandrel polar opening
$u_{Mr}$	mandrel displacement vector
$\sigma_{Mr}$	mandrel stresses
$E_M$	Mandrel material Young's modulus
$\nu_M$	Poisson ratio of mandrel material
$a$	internal mandrel radius
$b$	outer mandrel radius

---

$K$	generalized mandrel stiffness
$E_r$	radial Young's modulus
$E_\theta$	hoop elastic modulus
$\nu_r$	radial Poisson's ratio
$\nu_\theta$	hoop Poisson's ratio
$c_i$	boundary condition constants
$S_i$	derived stiffness constants
$\beta$	non-dimensionalized stiffness factor
$h$	layer thickness
$H_i$	substitution variables
$\sigma_\theta^{wt}$	hoop stress due to winding tension
$\sigma_r^{wt}$	radial stress due to winding tension
$\sigma_{11}$	longitudinal/fiber stress
$\sigma_{22}$	transverse stress
$\sigma_{33}$	normal stress
$\sigma_{12}$	shear stress
$\sigma_A$	material longitudinal strength
$\sigma_T$	material transverse strength
$\tau_A$	longitudinal shear strength
$X_{T,C}$	longitudinal tensile or compressive strength
$\nu_{12}$	Poisson's ratio - longitudinal
$E_{11,f}$	fiber Young's modulus
$m_{\sigma,f}$	Puck scaling factor
$\tau_{12}$	shear stress
$p_{ij}^c$	Puck constants for matrix failure

## Definitions

<b>Tangential</b>	Tangent to the circumference of a composite pressure vessel
<b>Meridional</b>	Tangent to the length of a composite pressure vessel
<b>Radial</b>	Through-thickness of laminate material in a composite pressure vessel



# Abstract

The combination of a relatively recent emissions scandal and the ever growing incentive to provide sustainable transportation solutions, led to the fact that the transition to electrically propelled land-based vehicles is more prominent than ever. All prominent European car-makers announced diverse fully and partially electric product portfolios for 2021 and beyond with strong indication that the era of the Internal Combustion Engine (ICE) is slowly fading into history. While Battery Electric Vehicles (BEVs) are already well on their way in establishing a strong market share in the personal vehicle domain, the field of long haul transport is left to search for solutions elsewhere as battery technology does not present an efficient solution at this time. Fuel-Cell Electric Vehicles (FCEVs) pose a solid performance base to close the gap that batteries cannot and provide sustainable, zero emissions solutions, for all heavy transport sectors - automotive, aviation and maritime.

Within fuel cell systems, a component whose criticality is often overlooked or even understated is the hydrogen storage tank. Current state of the art uses type IV composite pressure vessels (CPVs) with a plastic liner and Carbon Fiber Reinforced Plastics (CFRP) composite overwrap to ensure structural integrity. Recognizing the complexity of a CPV is crucial in order to allow for the development of robust and worthwhile design processes that could yield a significant decrease in material use, making FCEVs more cost effective and an attractive long-term solution. This thesis aims to provide some detail on the behavior of CPVs and their depth through the development of an automated numerical analysis framework and the execution of a focused experimental study that examines the impact of laminate stacking sequence as well as manufacturability factors on overall CPV behavior and, in particular the cylinder-dome transition of the vessels.

The details and experimental correlation of the developed numerical analysis framework are shown and discussed. The framework heavily utilizes the outputs of an industry standard filament winding software, Compositcad, which is used as a basis that is then further refined in order to generate a satisfactory geometric description of the vessel and its laminate composition. Major emphasis is placed on the discussion of processes made for the geometry correction and attention is placed on particular factors that were also tested in the experimental study - hoop ply drop-off and stacking sequence. The framework is correlated to experimental results and laminate configurations from previous and current experimental results to showcase its versatility and potential for future optimization studies given the high level of automation involved. Two Finite Element (FE) models are investigated within the scope of the developed framework - a solid and shell element model. The performance and predictive ability for each are presented and discussed.

The experimental study presents data on the impact of stacking sequence effects and hoop ply drop-off on CPV behavior - in particular, the cylinder-dome transition. The influence of both parameters are discussed and contextualized with previous studies in order to identify relevant trends. Novel results were obtained for the relationship between hoop layer placement and burst performance. The results further indicate a delicate interaction between vessel stacking sequence, burst strength and manufacturing robustness.

The results of this study highlight important factors for future numerical studies of CPVs and showcase the development of an analysis approach with low computational cost while retaining acceptable accuracy. Furthermore, the experimental study helps put focus on future areas in need for further investigations in order to identify design-critical performance trends.



# Contents

<b>Nomenclature</b>	<b>v</b>
<b>Abstract</b>	<b>ix</b>
<b>1 Introduction</b>	<b>1</b>
1.1 Composite Pressure Vessels in the Automotive Industry . . . . .	2
1.2 Manufacturing of CPVs . . . . .	4
1.2.1 State-of-the-art Manufacturing Processes . . . . .	4
1.2.2 Path Definition and Thickness Build-up . . . . .	5
1.3 Analysis Methods for CPVs . . . . .	7
1.3.1 Analytical Models . . . . .	8
1.3.2 Numerical Models . . . . .	10
1.4 Experimental Characterization . . . . .	11
1.5 Research Questions and Objectives . . . . .	14
1.6 Thesis Structure. . . . .	15
<b>2 Modelling Methodology</b>	<b>17</b>
2.1 Geometry Correction . . . . .	17
2.1.1 Composicad Output . . . . .	18
2.1.2 Layer Re-arrangement and Context . . . . .	19
2.1.3 Hoop Layer Re-arrangement. . . . .	19
2.1.4 High-angle helical adjustment . . . . .	22
2.1.5 Low-angle Helical Adjustment . . . . .	24
2.1.6 Thickness Adjustment . . . . .	25
2.2 Correlating Corrected Geometry . . . . .	29
2.3 Layer Re-adjustment Limitations and Implications . . . . .	32
2.4 Numerical Modelling . . . . .	32
2.4.1 Shell Model Implementation Plan . . . . .	32
2.4.2 Solid Model Implementation. . . . .	34
2.5 Toward an Automated CPV Analysis Framework . . . . .	36
<b>3 Experimental Plan &amp; Results</b>	<b>39</b>
3.1 Manufacturing and Testing . . . . .	39
3.2 Experimental Plan . . . . .	41
3.3 Overview of Result Consistency . . . . .	43
3.4 Effect of Stacking Sequence Variation . . . . .	44
3.5 Effect of Tangential Stiffness Variation . . . . .	46
3.6 Burst Performance Analysis. . . . .	48
<b>4 Evaluation of Numerical Modelling Methods</b>	<b>53</b>
4.1 Shell Model Performance . . . . .	53
4.2 Solid Model Performance . . . . .	55
4.3 Burst Prediction Overview . . . . .	56
4.3.1 Hashin Failure Criterion . . . . .	57
4.3.2 Puck failure criterion. . . . .	58
4.3.3 Failure Predictions in Solid Model . . . . .	59
4.4 Impact of Inner Contour Variation on Prediction . . . . .	63
4.4.1 Contour Extraction. . . . .	64
4.4.2 Inner Contour Results . . . . .	65
4.5 Summary and Outlook of Modelling Techniques for Fast Behavior Prediction . . . . .	67

---

<b>5 Design Insights</b>	<b>69</b>
5.1 Design Practices and Implications . . . . .	69
5.2 An Improved Stacking Sequence . . . . .	71
<b>6 Conclusions and Outlook</b>	<b>75</b>
6.1 Summary . . . . .	75
6.1.1 Numerical Analysis Framework . . . . .	75
6.1.2 Experimental Plan . . . . .	76
6.2 Conclusions. . . . .	76
6.3 Future Work. . . . .	78
<b>A Mesh Study</b>	<b>81</b>
<b>B Layup Configurations Overview</b>	<b>83</b>
<b>Bibliography</b>	<b>85</b>

# 1

## Introduction

With the ever-growing tendency for governments to recognize the likely negative outcomes of climate change and its apparent connection to human industrial activity, a transition to sustainable alternatives is becoming a highly incentivized activity that has finally been recognized in the automotive industry at large. This was most obviously manifested in an increasing number of battery electric vehicles, BEVs, on the market. The transition to an electric drive train offers some performance improvements expressed as high torque and power conversion efficiency capable of rivaling even high-performance internal combustion engines ICE. However, the necessity to use batteries as a power source comes with major restrictions given how stored power translates to range and battery weight. For example, the average energy density of commercially available battery packs is 0.15 kWh/kg - which translates into 650 kg for a desired range of a 500 km with a conservative 180 Wh/km power consumption. Additionally, one is beset with inconvenience when the question of recharging is set since most vehicles in circulation today do not have fast-charging functionality and require a substantial amount of time to charge fully. To give a more specific example, using a conventional 3.7 kW plug, a 2019, 75kWh Tesla Model S would require 20 hours to charge from completely empty to full capacity. Granted, that time is reduced to a mere hour if a Tesla fast-charging socket is used which operates at 150 kW. While the inconvenience of maintaining full charge in a BEV is a factor to consider, the market has shown trends of centering personal transportation on BEVs since the average person generally has the ability to charge the car during a significant portion of the day. Where this inconvenience become a critical issue is freight transport and industry-relevant logistics. If long-haul trucks are to become sustainably powered, the prospect of a battery-electric propulsion system quickly dwindles - hence an alternative solution is necessary.

Alongside the growth of BEVs, hybrid applications combining both battery and ICE systems have been growing in popularity. The selective use of a battery powered drive and a relatively small ICE allows for significant reduction in emissions compared to vehicles relying solely on an ICE for propulsion. However, the goal of the automotive industry is ICE elimination which implies that hybrid drives are effectively a transitory phase until fully sustainable solutions reach performance requirements that can match performance of current ICE vehicles.

Fuel-Cell Electric Vehicles, FCEVs, represent an 'in-development' product that has relatively recently started appearing in the personal vehicle market and more recently has been announced as the major direction for the development of long-range land freight transport. A FCEV, as described by Eshanie et al. [1], is a electrically driven vehicle fueled by electrical energy produced as a result of stripping hydrogen gas of its electrons through a galvanic cell. Hydrogen fuel is constantly fed through the galvanic cell, ensuring a steady potential difference which allows for power output similar to that of a Li-ion battery. Recent FCEVs that can be found on the market are Toyota Mirai, Honda Clarity and the Mercedes-Benz GLC F-Cell. Other than fuel-cell drivetrain principle that all of these vehicles share, they also share an additionally similarity - high pressure hydrogen storage. More specifically, high pressure hydrogen storage. The need to pressurize hydrogen gas stems from its low density in gaseous form of just 0.09 g/L. For personal transport applications, fuel cell systems are capable of providing 100km of range per 1kg of hydrogen. This results in a need of about 5kg of Hydrogen to achieve a range that is competitive to current BEVs - 500km. According to EU regulation No 134, the standard operating pressure for gaseous hydrogen storage is 700 bar [2] at a safety factor of 2.5. To satisfy safety regulations and operating pressure conditions using metallic storage would result in unacceptably heavy solutions which would greatly affect vehicle performance. Therefore, the use of

lightweight materials is necessary and has been the industry standard approach through the use of Carbon Fiber Reinforced Polymers CFRP. An exemplary pressure vessel can be seen in Figure 1.1. In this chapter, relevant background information on Composite Pressure Vessels, CPVs, will be provided. The chapter will cover common manufacturing methods, numerical and analytical analysis described in literature as well as experimental methods used in this study and previous studies describing CPV behavior. Additionally, the chapter will serve to identify knowledge gaps and establish a set of research questions for the main body of work presented in this report.

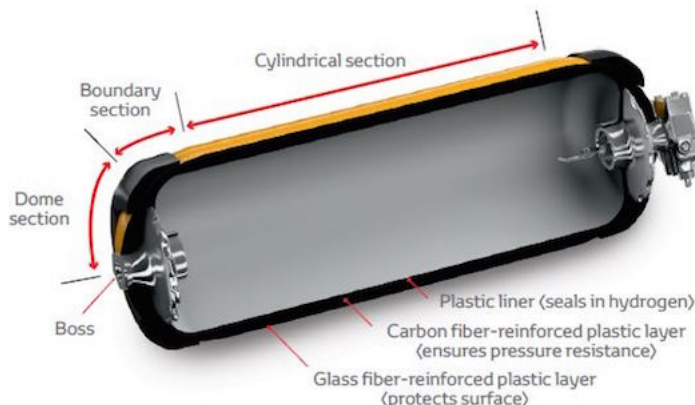


Figure 1.1: Schematic depiction of a type IV vessel used in Toyota Mirai - taken from [3]

## 1.1. Composite Pressure Vessels in the Automotive Industry

Storing a fuel in a highly pressurized storage system is not novel technology as it was the main method of storing compressed natural gas CNG for decades. However, the benefit of this effective 'experience' is the presence of already established regulations and frameworks that detail the requirements of such storage solutions for the automotive industry - as a result, the set of regulations developed to specifically target the certification processes of pressurized hydrogen storage (ISO 19881 [4]) shares many similarities for regulations created for CNG storage (ISO 11439 [5]). Other than the required operation pressure of 700 bar [2], the regulations referred to here [2, 4, 5] also outline the requirements for certifying safety and operational stability for CPVs by defining a set of tests required prior to production. These tests include static and cyclic loading tests to gauge the overall strength and performance during tests that simulate use during a predicted product life-cycle.

Schematics describing the durability and static loading tests as well as the on-road performance test can be seen in Figures 1.2 and 1.3. While these tests are somewhat complex and consisted of multiple various stages and conditions to which a certifiable CPV needs to be exposed to, their relevance to this study lies in the fact that all of them require pressurization to much higher than nominal working pressure, NWP.

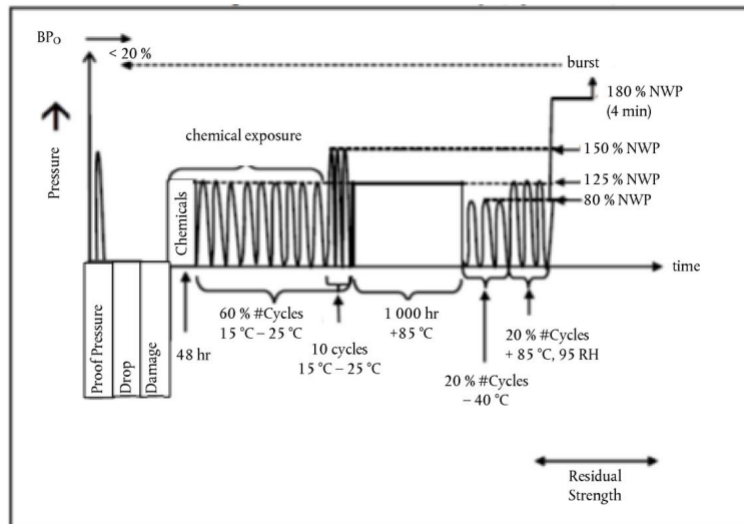


Figure 1.2: Verification of vessel durability graphical description of cyclic testing, taken from [2]

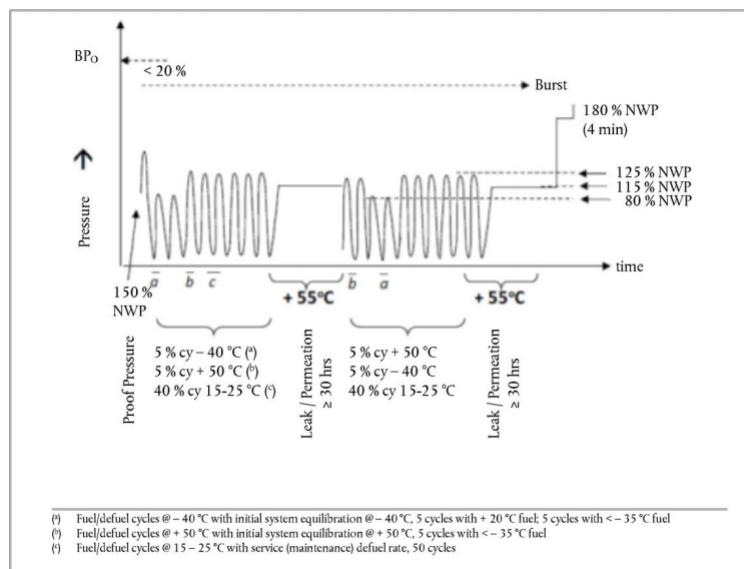


Figure 1.3: Verification of on-road performance graphical description of cyclic testing - taken from [2]

The repercussions of catastrophic failure in CPVs in real-life use are substantial as they pose a major threat both to the integrity of the vehicle the vessel is in, and the vehicles in close proximity to it. Therefore it is necessary to ensure a high level of certainty that burst failure will be avoided.

The design of a CPV in relation to the tests described above will depend on the material used for vessel manufacturing. For this purpose, CPVs have been characterized into 5 types graphically depicted in Figure 1.4. Currently popular CPV configurations can be described in terms of the material composition of their two main constituents - mandrel(liner) and reinforcement material:

- Type I: Metal mandrel without additional reinforcement
- Type II: Metal mandrel with composite overwrap in the cylinder region
- Type III: Metal mandrel with composite overwrap of the entire vessel
- Type IV: Plastic mandrel with composite overwrap of the entire vessel and metal boss-ends

- Type V: Absent mandrel and full composite overwrap with metal boss-ends

Type IV CPVs are state-of-the-art in automotive uses with aspirations to progress towards Type V configurations in the future. Current materials make it impossible to develop a Type V configuration that will effectively contain hydrogen gas without leaking. While Type I to Type V effectively increases the amount of composite materials used, it also increases cost of manufacturing as less standardized processes are necessary and more expensive materials need to be used.

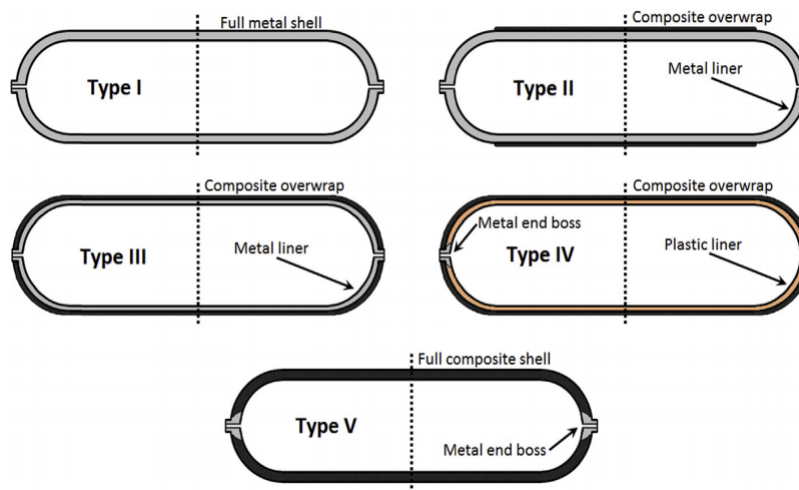


Figure 1.4: Different CPV configurations - taken from [5]

All current commercially available FCEVs use Type IV CPVs. The manufacturing processes for this configuration have already been certified and shown to be a viable solution for application within the automotive industry.

## 1.2. Manufacturing of CPVs

The serialization of CPVs is highly dependent on their composition and currently available manufacturing processes. The choice of currently available manufacturing processes is heavily based on previously available knowledge and process certification. Current state-of-the-art for CPV manufacturing is filament winding where dry fibers are impregnated with resin in-line (also called wet winding). Because CNG solutions also used wet wound CPV solutions, the adoption of the manufacturing process for the development of CPVs was a natural first step.

The manufacturing process of CPVs is also the source of significant design problems. This is mainly exhibited in the material thickness build-up resulting from overlapping fiber paths during winding. The prediction of thickness build-up around the polar openings of CPV domes is a topic of extensive study and has also been shown as a design-critical area of the vessel [6–8].

The following section briefly describes current manufacturing processes, their benefits and drawbacks. Additionally, the topic of thickness build-up is discussed with reference to previous studies in order to touch upon some relevant nomenclature as well as provide further context for the manufacturing processes of CPVs.

### 1.2.1. State-of-the-art Manufacturing Processes

CPVs are manufactured through filament winding, a process in which a mandrel is moved and rotated in front of a fiber deposition apparatus in a particular pattern that allows the fibers to be wrapped around the mandrel to provide reinforcement to the vessel structure. The filament winding process can be divided into two main categories, wet-winding and pre-preg winding. Wet winding is industry standard according to current regulation and all currently available FCEVs contain wet-wound CPVs. Wet winding differs from pre-preg winding in the state of the material upon deposition/winding. In wet-winding, dry fibers are impregnated with resin prior to being applied to the vessel while in pre-preg winding, a pre-impregnated resin-fiber material is wound onto the vessel [9]. The basic principle is the same between both approaches but each has some benefits and drawbacks. [10]

Wet winding, as depicted schematically in Figure 1.5, requires a relatively complex configuration to allow for the manufacturing process since the dry fibers need to be wetted in-situ prior to winding. This means that control systems for resin viscosity, resin flow, fiber deposition need to be in place in order to ensure a consistent properties of the material deposited on the vessel. This separation of the composite material into dry fibers and resin comes with a benefit of effectively infinite shelf-life as dry fibers effectively don't deteriorate with age and most resins can be split into their non-reactive components which can be stored for long periods of time.

Pre-preg winding comes with the benefit of a relatively simple configuration as the fibers are already impregnated with resin, meaning that effectively all fiber processing parts shown in Figure 1.5 can be eliminated. The fiber and resin components are replaced with a set of rollers compatible with industry standard pre-preg fiber scales that guide the impregnated fiber onto the rotating vessel during winding. However, impregnated fibers introduce cost-raising effects in their effective shelf-life. The resin that covers the fibers is technically in a constant state of reacting, the rate of which is dependent solely on environment temperature.

Upon the completion of vessel winding, the vessel is placed into an oven and the composite material cured via a heating cycle appropriate for the resin used. It should be said that the wet winding and pre-preg winding each have a profound impact on the resulting composite laminate quality as a result of the materials used during winding. The interaction of the material with the physics of the winding process has a direct impact on the final laminate quality in terms of porosity and layer orientations [11]. Wet winding implies a low resin viscosity during winding which implies that fiber tension during winding can cause resin flows during manufacturing - possibly causing resin-dry areas in the laminate. In pre-preg winding, the resin is highly viscous during winding which implies that high tension during winding can be caused to directly affect layer compaction without the risk of adverse resin flow during winding. In both processes, the resin goes through a low-viscosity state during curing where resin will inevitably flow and layers will reorganize [? ]. Resin flow during manufacturing causes a variation in material porosity through thickness which was also confirmed by Nebe et al [12].

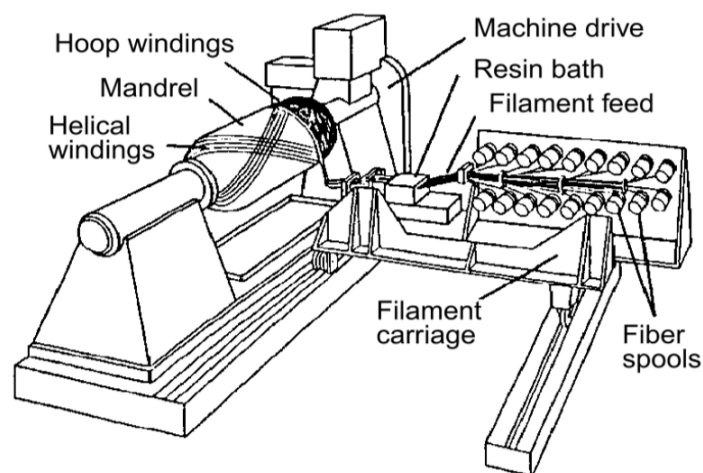


Figure 1.5: Wet winding schematic - taken from [9]

### 1.2.2. Path Definition and Thickness Build-up

The proper definition of filament paths during winding is perhaps the most important aspect of CPV manufacturability. The complexity in CPV filament winding is introduced by the dome end-caps of the vessel which necessitate the deviation from nominal fiber angle in the cylinder in order to achieve full coverage. The deviation from cylinder nominal fiber orientation also results in each wound layer having a turn around region or *polar opening* where thickness build-up increases substantially as a result of multiple fiber passes over that region to achieve full coverage [6]. Fiber orientation variation has a direct impact on the stiffness and load distribution of the CPV [7]. The combination of thickness build-up and stiffness variation poses a major design challenge as different stacking sequence variations will have a direct impact both on the manufacturing process and the resulting stiffness distribution of material in the dome.

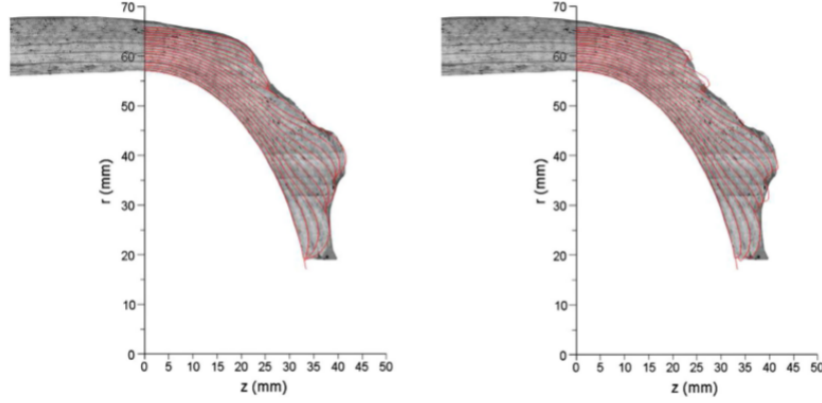


Figure 1.6: Thickness buildup in dome region - taken from [6]

The layer definition of CPVs stacking sequences can be divided into two main branches, geodesic and non-geodesic. The difference between the two being present in the variation of angles in the helical layers wound around the vessel. To solely use geodesic angles is to severely narrow the available design space of a CPV and, as shown by Zu et al. [7], geodesic solutions are more usually not optimal to achieve desired vessel performance. Non-geodesic fiber paths open the design space of a CPV significantly, but introduce a variety of effects that have implications on the load distribution and pressure vessel performance [6, 8]. In either case, the correct depiction of vessel geometry was shown to be crucial in the reproducing those effects in the context of numerical modelling in multiple papers [6, 12]. Analytical tools for the prediction of thickness build-up have been developed by Leh et al. [6] to account for thickness build-up of helical layers with a focus on the thickness behavior around the polar opening of successive layers. Figure 1.6

The complex geometry around layer polar openings developing as a result of layer deposition is a difficult problem to solve. The importance of solving this problem is further emphasized by the possible impact seemingly small variations in material build-up around polar openings can have on vessel performance and burst pressure [7]. Leh et al. [6] presents a variation of the thickness predictions methods developed by Zu et al. [7] who based their method on CLT. Equation 1.1 shows the definition of a fiber path between two points on a curved surface [6].

$$\frac{d\alpha}{dz} = \lambda \left[ \frac{\sin(\alpha)\tan(\alpha)}{r} - \frac{f''}{1+r'^2} \cos(\alpha) \right] - \frac{f' \tan(\alpha)}{r} \quad (1.1)$$

where  $\alpha$  denotes the angle between fiber path and axial direction,  $\lambda$  defines the slip potential between the surface and fiber, while  $r$  represents the radial coordinate. A schematic view of these parameters is shown in Figure 1.7. Slip potential was mathematically described by De Carvalho et al. [13] as the ratio of transverse and normal forces acting on a fiber or rowing applied on a surface (Equation 1.2)

$$\lambda = \frac{f_b}{f_n} \quad (1.2)$$

Where  $f_b$  and  $f_n$  are body and normal forces acting on a fiber respectively. Normal forces represent force applied by the surface onto the rowing/fiber and the transverse force is caused by the angle of application of the fiber onto the surface and is countered by surface friction that keeps the fiber in place after application. Logically, as long as friction between the surface and the fiber is larger than the tangential force, the fiber will not slip. The normal force additionally reduces the fiber from slipping by adding component-wise to the friction force.

Practically, the slip potential is never exactly zero for a fiber on a double-curved surface. To obtain a solution to the differential equation 1.1, standard solving methods, such as the Runge-Kutta algorithm [14]. To ensure the manufacturability of non-geodesic filament paths within the context of this definition, a continuity condition is enforced as follows [6]:

$$\lambda = \lambda_{max} \cos\left(\frac{\pi * (r - r_{turn})}{R - r_{turn}}\right) \quad (1.3)$$

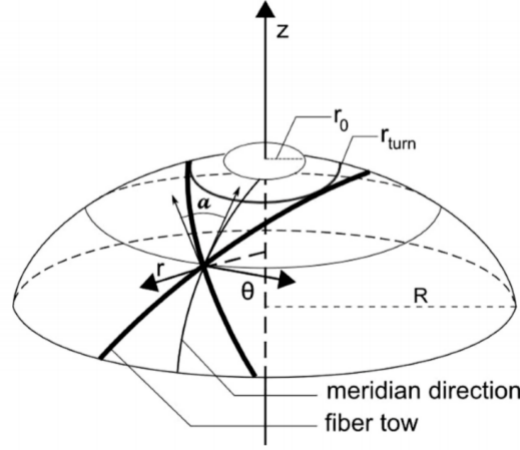


Figure 1.7: Schematic of path definition on a double curved surface - taken from [6]

In Equation 1.3  $R$  denotes cylinder radius,  $r_{turn}$  is the smallest radial distance from the polar opening,  $\lambda_{max}$  is an arbitrary maximum value of slip potential that would allow for the combination of friction and normal forces to be greater than tangential forces. The problem gets more complicated when multiple stacked layers are considered since each layer changes the geometry upon which the succeeding layer is applied. Wang et al. [15] show that major differences in performance can be pinpointed to material used for winding, surface roughness and winding tension and goes to conclude that slip potentials lower than 0.1 and 0.5 are viable for wet winding and pre-preg winding respectively.

The thickness build-up of a layer is defined by Leh et al. [6] in the Equations 1.4:

$$t(r) = \frac{n_R m_R t_p}{\pi} [\arccos(\frac{r_{turn}}{r}) - \arccos(\frac{r_b}{r})] \quad \text{for } r_{2b} \leq r \leq R$$

$$t(r) = A + Br + Cr^2 + Dr^3 \quad \text{for } r_{turn} \leq r \leq r_{2b}$$
(1.4)

These equations are originally presented by Wang et al [16]. In the equations  $r_b$  is pole opening radius,  $r_{2b}$  is the distance of 2 tow-width radii from the two turn-radius,  $r_{turn}$ . The turn-around point is defined as the polar opening of each individual layer.  $n_r$  and  $m_r$  represent the number of pseudo-ply confined to the cylinder section of the CPV. A pseudo-ply being defined as the set of interwoven fibers in the cylinder section oriented at  $\pm\alpha$  degrees. A group of pseudo-ply of the same winding angle  $\alpha$  in the cylinder are defined as a layer.  $t_p$ ,  $b$ ,  $t_R$  and  $\alpha_R$  are thickness, tow width, layer thickness and layer angle in the cylinder respectively.

The determination of thickness build as described by Leh et al. [6] requires an iterative process that shows promising results and good match with manufactured vessels. The impact of thickness description on numerical model accuracy was outlined in [6] and then further corroborated by [12] where a manual thickness correction was applied in order to achieve a good numerical correlation to experimental results. A major limitation of current works on geometry description of CPVs is the focus on helical angles. The unique loading case of CPVs more often than not requires a high amount of hoop layers confined to the cylinder to tackle the high tangential stresses in the region. This results in asymmetric stacking sequences and significant thickness build-up of hoop layers which are subject to movement during the manufacturing (winding and curing). To describe these phenomena mathematically or physically should be a major focus for future studies.

### 1.3. Analysis Methods for CPVs

The modelling of CPVs is not a new endeavor and has been hypothesised since as early as 1973 [17]. Meanwhile, a variety of methods have been developed that represent a chronological increase in modelling complexity as the body of knowledge pertaining to CPVs increased. This is most aptly visible through the variety of optimization studies that came about as a result of new analysis methods being developed. Perhaps the essence of our understanding of CPVs lies in the accurate identification of design-critical areas. Hence, a relatively large body of academic work was identified that focuses on the design of CPV domes, the reinforcement placement on dome regions and their optimization [18–23]. From relatively simple netting analysis which only considers geodesic paths and assumes all loads are carried exclusively by fibers [19, 24], toward

analysis including material via Classical Lamination Theory, CLT, [18, 23, 25], and finally with emerging analyses that also account for through-thickness effects with the use of FE methods and numerical modelling [26–28]. Some of the results of these methods are briefly discussed in the following sections and their limitations/implications for future work highlighted.

### 1.3.1. Analytical Models

#### Analysis of Composite Cylinders

While CPVs are not a new topic at this point, they are far from being entirely understood. Therefore, one will find that a substantial chunk of the available academic work is focused on structures that can, to an extent, be projected to the context of CPVs. This is especially the case for developed analysis methods on cylindrical pipes which are effectively equivalent to the cylinder section of a CPV. When not considering wall thickness, the analysis of composite pipes is equivalent to the conventional analysis - meaning that, when applicable, the thin wall assumption allows for an effective use of netting analysis [29] and CLT analysis [30] to obtain valuable results that can potentially be used to obtain an optimized design. However, the high pressures to which CPVs are exposed often lead to what could be considered thick laminates. In fact, the definition of a thick-walled CPV was formalized by Parnas and Katirci [31] as vessels whose ratio of outer to inner radius is larger than 1.1. In thick laminates, the internal variation of stresses can be significant and, as a result, have a major impact on structural deformation. To account for through thickness effects in composite pipes, a 3D elasticity theory approach was described by Xia et al. [32]. 3D elasticity theory, as presented in [32], allows for the calculation of internal stress and strain variation of a symmetric and balanced stacking sequence around pipes. To limit ones design to symmetric and balanced laminates is a valid assumption when considering the design of composite pipes but is fairly constricting when attempting to apply the same model to the analysis of CPVs since those laminates are more often than not asymmetric. Withal, the model presented by Xia et al. [32] was successfully applied to various CPV stacking sequences by Asijee [33] with the yield of fairly good strain accordance. In more recent work, Ramos et al. [34], have shown an application of 3D elasticity theory for thick composite pipes under various loading cases. Additionally, [34] also show the comparison of their analytical approach to FE analysis and demonstrate good accordance with some relevant conclusions about the sources of failure in composite pipes. Additional work presented by Mertiny et al. [35] introduces the apparent impact of the relative placement of tangential reinforcement plies on composite pipe performance and highlight the apparent improvement in results by placing hoop layers towards the outside of the laminate. However, Mertiny et al. [35] do not describe the possible impact of the real boundary conditions used in the test-bench on the impact of the results and do not refer to the differences in the laminate's interaction with said boundary conditions as a result of stacking sequence changes.

Overall, there are multiple tools at one's disposal for the analysis of cylinder related behavior in CPVs. From netting theory to 3D elasticity theory, one can seemingly accurately describe the internal development of stresses and strains under multiple loading cases depending on the requirements of the problem at hand. Regardless, to claim the cylinder behavior is the sole determinant of vessel burst performance would be to comically simplify CPVs as a family of composite structures.

#### CPV Analysis

A general understanding of pressurized structures is required prior to building understanding of CPVs since the two share a similar load case. The fundamental analysis of isotropic pressure vessels is based on classical works by the likes of Love, Reissner, Timoshenko etc - an overview of which can be found in a book by Vinson [36]. A description of the loading case of isotropic pressure vessels with ellipsoidal domes was presented by Baličević et al. [37]. In [37], the cylinder-dome transition is identified as a highly critical area due to the manifestation point of the bending moments caused by geometric non-linearities in the pressure vessel structure. A schematic of the bending moment variation in the cylinder-dome transition can be seen in Figure 1.8. It should be noted that this analysis makes use of the thin wall assumption and constant wall thickness in the whole vessel.

An additional study regarding isotropic pressure vessels accounts for varying thickness between cylinder and dome regions of a pressure vessel was shown by Magnucki et al. [38]. The major conclusion of this study is that a change in the wall thickness between cylinder and dome does not change the general behavioral trend in the cylinder-dome transition, but it can have a major effect on the stresses induced in the region as a result of stress concentration at the cylinder-dome joint. Additionally, a variation in the thickness between

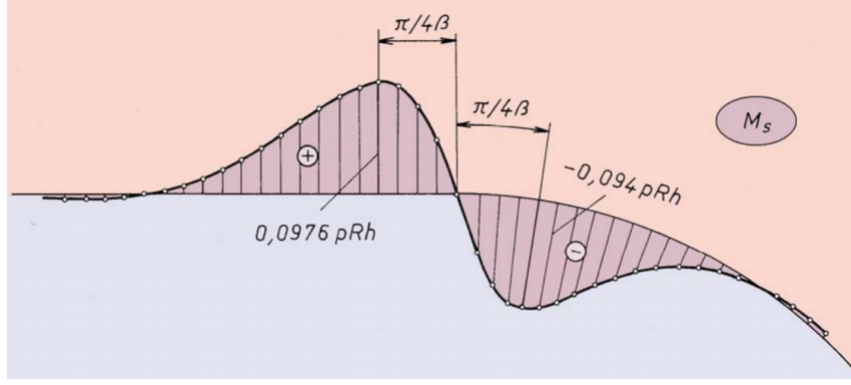


Figure 1.8: Variation of meridional moments in an isotropic pressure vessel - taken from [37]

the two regions causes a shift in the bending moment curves as seen in Figure 1.8.

To account for material orthotropy, multiple approaches can be applied. The principles mentioned earlier in the discussion on composite pipe analysis can also be extended to the context of the entire CPV. For example, netting theory - which assumes that all loads are exclusively carried by fibers - can be used as a rudimentary design tools [24]. The implicit result of using netting theory to design a CPV is that the obtained optimal result will by definition be an isotensoid solution [39]. The extension of netting theory to account for non-geodesic filament paths was described by Zu et al. [40]. The extension of netting theory to non-geodesic filament path descriptions within a CPV makes for netting theory to be a reasonable and fast starting point for CPV analysis despite the limitations imposed by thin wall and unidirectional reinforcement assumptions inherent to it.

Unlike netting theory, CLT allows for a more robust accounting of material orthotropy of a structure. The basis equation relating strains to loads is expressed as follows:

$$\begin{bmatrix} N \\ M \end{bmatrix} = \begin{bmatrix} A & B \\ B & D \end{bmatrix} \cdot \begin{bmatrix} \epsilon \\ \kappa \end{bmatrix} \quad (1.5)$$

where  $N$  and  $M$  represent the in-plane and bending loads applied;  $A$ ,  $B$  and  $D$  represent the extensional, bending-extensional and bending stiffness matrices respectively; while  $\epsilon$  and  $\kappa$  are strains and curvatures. The application of CLT to CPV analysis was readily found in the field of vessel optimization where the improvement relative to netting theory was found in CLT accounting for transverse strength which has a major effect on the load distribution within the CPV - hence, a variety of studies were found detailing the process to determine optimal dome shapes based on CLT analysis [20–22]. Hojjati et al [20] the influence of matrix strength is shown to have a demonstrable influence on the optimal dome shape solution compared to netting theory solutions. Liang et al. [21] shows a comparison of optimal dome shapes when using CLT and results demonstrated by Fukunaga [19]. Their work concludes the optimum dome shape for a CPV to be an ellipsoid whose shape can be determined by a shape factor definition shown in Equation 1.6

$$\bar{K} = \frac{PV}{W(\sigma/\gamma)} \quad (1.6)$$

Where  $P$ ,  $V$  and  $W$  are internal pressure, volume and dome weight respectively. Another major conclusion from [19] is the finding that failure in the dome stems from a lack of transverse strength around the polar opening and cylinder-dome transition. Granted, the limitations of this work need to be recognized since thin wall assumptions were made in this study.

Much like netting theory, the benefit of CLT is its low computational cost. With comparable complexity to netting theory, a significant improvement in results and number of effects captured is present in the analysis of CPVs through CLT. Alcantar et al. [41] showed a method to optimize stacking sequence and layer thicknesses in CPVs using a CLT based approach. However, this study also utilizes some FE methods and genetic algorithms in tandem in order achieve an optimal solution. Overall, while CLT is confidently shown to be a strong tool for the analysis of CPVs that can capture some of the effects induced by material orthotropy. However, its reliance on the thin wall assumption implies the need for more in-depth analysis that can account for through thickness effects better.

At this time, a comprehensive analytical framework that can describe the stress state of a CPV does not exist. Because of this, current FE methods can be utilized to describe the impact of the through thickness effects that are not entirely understood.

### 1.3.2. Numerical Models

The development of FE models in the past has been strongly biased towards enabling the prediction of CPV failure. For this purpose, a set of works presented by Leh et al. [6, 42, 43] show a methodology for the geometric description of CPVs with arbitrarily defined stacking sequence layer (geodesic and non-geodesic), a FE modelling approach based on modelling an axi-symmetric slit of the vessel, and subsequent optimization procedure. An example of the FE model developed in [42, 43] is shown in Figure 1.9. The figure depicts the result thickness build-up computations (described in Section 1.2.2) applied into an FE environment.

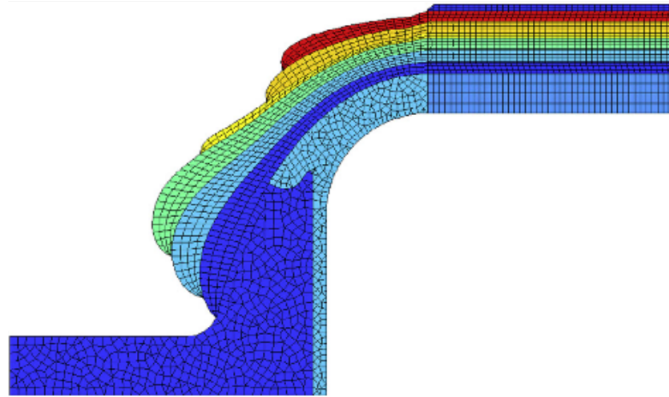


Figure 1.9: axisymmetric FE model as developed by Leh et al. - taken from [42]

A major aspect of this modelling approach was to capture damage progression trends and pressure at structural failure. To account for damage progression, a Hashin-Rottem criterion was used [44]. The burst pressure prediction from the models were generally underestimated compared to experimental results - this was likely linked to the fact that axial stiffness was found to be underestimated during experimental correlation. A variety of effects were suggested to have caused inaccuracies, but focus was pointed towards possibly inadequate depiction of material properties as a result of layer compaction, not accounting for material porosity variation in the dome region where layer relaxation often occurs during manufacturing, and likely inaccuracies in the damage progression models [43].

Ramirez et al. [45] also developed a model that captures damage progression with intent to accurately predict CPV failure. The model suffered similar problems as the models presented by Leh [43] where errors axial stiffness prediction was identified as the source of the error in the burst pressure prediction. The source of the axial stiffness error was eventually narrowed down to processes involving mandrel deformation during manufacturing which, once accounted for, improve the axial stiffness prediction of the vessel significantly.

A more recent work by Nebe et al. [12] tackles the modelling of CPVs by attempting to develop a highly detailed depiction of a select few configurations for which an extensive data-set existed. The modelling approach was based on defining every layer as an individual entity within a FE environment and connecting them through a tie connection. Within the model, a manual correction for the vessel geometry and the mandrel deformation was made in order to depict the overall vessel geometry and the internal distribution of layers as closely as possible via user input. An example of one such model is seen in Figure 1.10.

This model was correlated to full-field DIC measurements and was shown to provide highly accurate predictions of deformational behavior. Furthermore, the model was made to capture damage progression trends by the application of a damage model developed by Leone [46] which allowed it to predict the burst pressure to a relatively high degree of accuracy with some variation in results depending on the vessel configuration being modeled. The development of this model could be seen as a wrapper of previously accumulated knowledge that aimed to describe CPVs in a high detailed FE environment in order to capture as many details of CPV behavior as possible.

The benefit of these *high fidelity* solutions is unambiguous as they pose the possibility to provide answers where understanding is lacking. However, the execution of these models comes at a great computational cost which is not compatible with design procedures within an industrial context. There is a need to focus

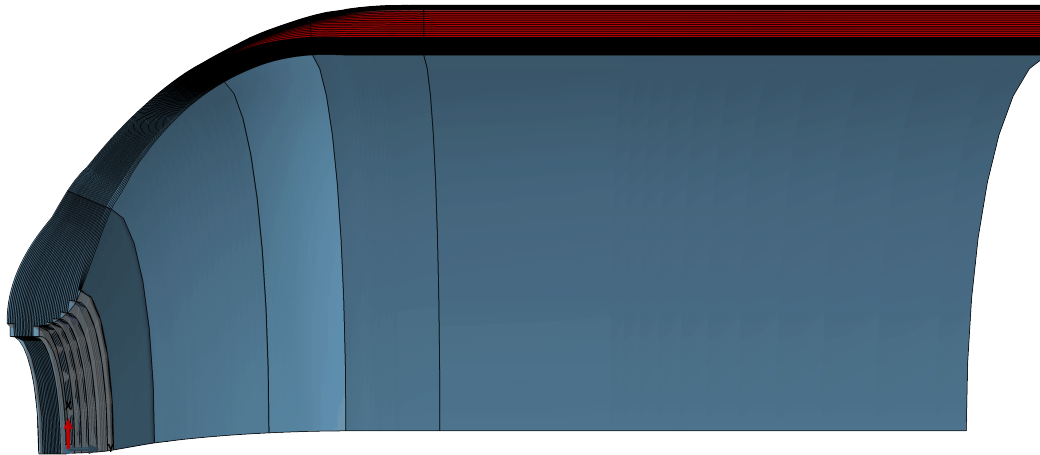


Figure 1.10: FE model as depicted by Nebe et al. - taken from [12]

on building computationally inexpensive models capable of capturing critical features in CPV behavior that allow the engineer or an optimization procedure to integrate seamlessly within an industrial context while providing relevant information to the engineer user. These models would, in principle, put less focus on being able to capture *all* damage mechanisms that may be occurring within a CPV and instead focus more on the accurate depiction of deformational trends and design critical damage mechanisms that have a major impact on burst pressure. The need for this modelling approach becomes even more apparent when emerging trends in the automotive sector are considered - where deadlines for emission goals are approaching rapidly and viable solutions will require the utilization of FCEVs with safe and efficient solutions for hydrogen storage.

## 1.4. Experimental Characterization

The experimental study of CPVs is made complicated by the multiple sources of non-linearities that make both analysis and experimental measurement complicated. Regardless, progress is a necessity mandated by both market and industry forces as well as human curiosity. A significant amount of work was done in order to make valuable measurements in composite pipes, which are somewhat representative of a cylindrical section in a CPV [35] as well as complete CPV structures [33, 47–51]. The following section outlines currently available measurement techniques in the experimental sphere of CPV development as well as provides an overview of previous studies relevant to the work in this project.

A CPV presents unique challenges in the extraction of information that allows for in depth interpretation. The models currently in circulation, be they analytical or numerical in essence, often attempt to describe the vessel as a whole. However, their validation is limited when the experimental methods for the extraction of continuous data are limited to a few select methods which can provide a narrow view of the system's behavior. Perhaps the most rudimentary measurement one can make about a CPV pressurization test is its burst pressure. This parameter is useful for a number of reasons as it is an absolute measure of the vessel's performance and is the straightforward parameter by which to gauge a vessel's safety. However, noting the burst pressure of a CPV alone says close to nothing of the way in which the vessel failed, or what exactly caused its failure. And while there is a significant effort to predict the burst pressure of pressure vessels in various models, there seemed to have been a distinct lack of focus on first trying to accurately depict vessel behavior in said models. To do this, it is necessary to capture this behavior quantitatively within an experiment as only then can we comfortably make claims about validity of a developed model. To get a more complete picture of CPV behavior, the measurements of strains and displacements are crucial.

During pressurization, the measurement of axial displacement can be made using Linear Variable Differential transducers LVDT which are elements by which a rule between voltage output and geometric extension can be established. An LVDT is essentially a metal core inside an electromagnetic coil - upon relative movement of the core and coil, a current is produced and a voltage can be measured which can then be converted into relative extension. The measurement of the axial extension of a CPV is a good first step, however still leaves much to be desired in terms of depicting vessel behavior since it does not allow the identification of

local behaviors on the vessel. However, it can serve as an indicator of non-linear behavior during the axial expansion of the vessel. This was shown by Ramirez et al. [45] where a discrepancy between measured and model strains was identified as a result of onset non-linearities during vessel pressurization.

Strain measurements on a surface is traditionally done using strain gauges. A relatively simple contraption where a small metallic foil is laminated in a particular pattern inside a polymer. The metallic foil is first adhesively applied to a surface and connected to a circuit. As the surface the gauge is attached to is deforming, the shape of the foil changes which effectively changes the resistance of the strain gauge element. The relative change in resistance can be correlated to a change in length which can then be converted into strain in the lengthwise direction of the strain gauge. Figure 1.11 shows a generic strain gauge after being applied to a surface and appropriately connected to a measuring circuit.

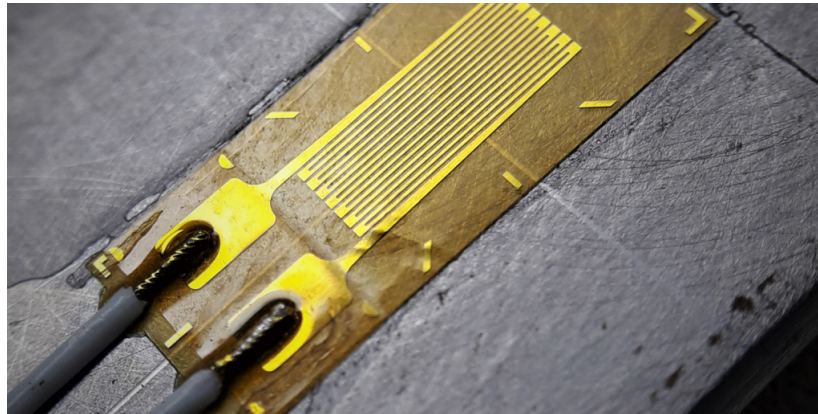


Figure 1.11: A strain gauge after application to a surface and connected to a circuit - taken from [52]

The main limitation of strain gauges within the context of CPVs is the nature of their measurement. Namely, the strain gauge only provides an average strain measurement over the length of the foil within it (usually 0.5cm). This would imply that, to obtain a full-field strain measurement along the surface of a vessel, one would have to implement an unreasonable amount of strain gauges. Additionally, strain gauges are highly susceptible to measurement error as a result of improper orientation [53]. So to expect that the use of a large number of strain gauges on a single surface would result in highly accurate results is not realistic. However, strain gauges are, at this point, a traditional method of measuring surface strains and can be used for validation purposes of other measurement systems.

To obtain measurements through thickness, Fiber Bragg Gratings (FBG) could be used within the context of CPVs. By embedding an optical fiber with a known refractive index into a structure, the through thickness strains can be measured by measuring the changes in the measured refractive index of the fiber [54]. FBGs and strain gauges share the same limitation in as much they are both effectively discrete sensors. In other words, they can only provide local data and provide information limited to the area of their application. And while, FBGs could provide highly important information of the through-thickness strain distribution, the application of FBG sensors within a CPV is not straight-forward given the winding manufacturing procedure. A successful implementation of these sensors was made by Kang et al. [55] who aimed to show the possibility of embedding FBG sensors into CPVs for structural health monitoring. The study was successful but the methodology used was rather difficult to rationalize within an industrial context due to the level of monitoring required during manufacturing and sensor embedment.

An alternative to the measurement methods described above, and one that bypasses the discrete measurements provided by them, is Digital Image Correlation (DIC). DIC uses an array of cameras recording a surface with a high contrasting pattern to measure the relative changes in the surface's pattern and determine surface strain continuously along the entire surface. DIC was shown to be effectively used in the testing of CPVs by Gasio et al. [49]. This principle was further corroborated on by Nebe et al. [47] where DIC was used to identify a rather substantial amount of trends of CPV behavior among a variety of test configurations. The main drawback of DIC is that it can only provide surface strains. However, this measurement can be made continuously along the entire surface of a CPV [47] which makes it significantly more valuable for the purpose of correlation with numerical or analytical models.

The testing of CPVs for the automotive industry is made complicated mainly by the high pressures the structures are supposed to endure in order to present a viable direction for development. This perhaps comes

at the expense of understanding since, within an industrial context, it is often seen as crucial that the main tested specimens within an experimental set come close to satisfying the pressure conditions of a vessel that could hypothetically be used within a vehicle. This of course comes with the benefit of the configurations tested resembling, in constitution, the configurations that may be used in a commercial application eventually, but comes at the expense of significantly higher material costs and manufacturing times.

In the academic context, experimental studies were often aimed at observing phenomena in composite tubes [35] whose results could to some extent be extended to the study of CPVs. On the other hand, in more recent times, a number of studies tested full CPV structures [33, 47–51].

The work by Mertiny et al [35] describes the result of an investigation of composite pipes where the influence of stacking sequence on the structures performance is measured through burst pressure. An apparatus to fix a composite pipe at both ends was developed (shown in Figure 1.12) to allow for consistent boundary conditions between configurations. A major conclusion of the work is the reported effect of hoop group placement within the laminate. Mertiny reports that placing hoops on the outside of the cylinder has a beneficial effect on the cylinder strength and can be directly related to the loading case of composite tubes. Mainly, by placing the hoop group on the outside of the laminate, the hoops are effectively loaded marginally less at the same pressure - effectively raising burst pressure.

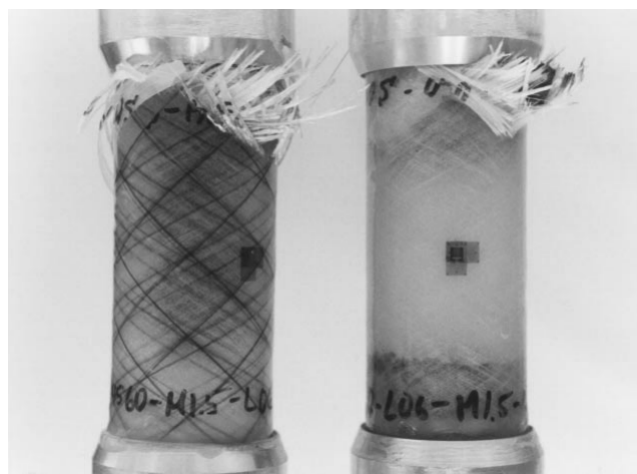


Figure 1.12: Post burst photo taken from Mertiny et. al experiment - taken from [35]

The essential drawback of the work presented in [35] is the fact that it only deals with cylinders and not drawing more focus on the possible effects laminate properties may have on the cylinder's interaction with the fixed boundary condition in the experiment. Even in Figure 1.12 it is visible that at least some of their experiments failed at the boundary condition application while other tests failed in the cylinder proper - implying a fundamentally different response. These effects are likely to also be present in CPVs but more difficult to observe given that it is not trivial to describe the boundary condition between the dome and cylinder as a combination of rudimentary boundary conditions.

A comprehensive study by Nebe et al. [47] shows a full-field DIC system implementation on the measurements of strains of a CPV. The paper shows an overview of strain development in the dome and cylinder regions of the tested vessels with the aim of recognizing effects of stacking sequence on CPV performance. The thesis by Aijee [33] that came out in tandem with the paper by Nebe et al. [47] serves to further corroborate the findings and identifies some major trends that came about as a result of stacking sequence changes. An interesting find aligns with the findings of Mertiny et al. [35] where the placement of hoop groups on the outside of the cylinder laminate in a CPV went to significantly increase the burst pressure reported. This study is heavily inspired by the work presented by [33, 47] and aims to provide further information on the behavior of CPVs based on stacking sequence effects by accounting for the effects changing of changing laminate properties on CPV manufacturing and testing. It should be noted that, while the work presented by Nebe et al. [47] presents a large amount of information, it focuses on presenting average strain trends in the cylinder and dome region. While this decision is valid for the cylinder which is inherently a stable and symmetric construct, it is likely to not yield highly representative results for the dome region where non-linearities from both vessel geometry and laminate properties are likely to manifest in a highly irregular response between configurations.

Additionally, the study of CPVs extends past strain measurements. During first pressurization, a CPV is a highly active structure and emits a substantial amount of Acoustic Emissions (AE). These acoustic emissions can provide insights into damage progression and current status of the vessel. In studies by Nebe et al. [56], Torres [50] and Cesari [51] a system capable of localizing the AE of a CPV in pressurization is described and used to localize, accurately, the sources of emissions on the surface of a CPV. These emissions were related to the progression of inter-fiber damage during first pressurization [51]. Additionally, the effects of stacking sequence on general trends in AEs were described by both Torres and Cesari [50, 51] where a significant variation in both amplitude and number of emissions was recorded between different stacking sequence configurations.

## 1.5. Research Questions and Objectives

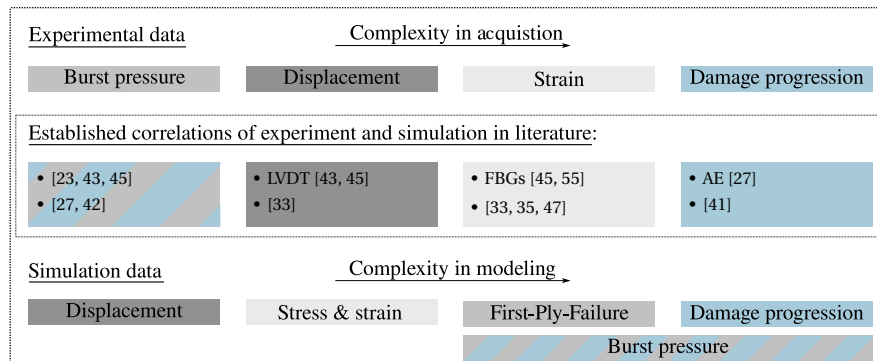


Figure 1.13: Schematic overview of experimental and numerical correlation with indicated literature sources - adapted from Nebe [57]

Figure 1.13 shows an overview of the current state-of-the-art on CPV development where the number of sources on each also serves to highlight the apparent representation of academic/research effort historically applied to certain topics - Of course, it should be stressed that this only serves to visualize the perceived amount of historical effort applied into each area and not to imply that *all* literature on CPVs was reviewed over the course of this study. As was mentioned earlier, a substantial amount of effort was placed on modelling for damage progression and burst pressure estimation. Investigating increasingly complex methods of modelling CPVs in order to potentially depict occurrence of catastrophic failure better is suitable for academic purposes as these models can provide a substantial amount of information and insight into the inner mechanisms of CPV behavior. However, the estimation of burst pressure is perhaps the last validating step in quantifying vessel performance and, more often than not requires a substantial amount of time to be somewhat accurately predicted. There is a distinct gap in the knowledge of viable techniques in the transitory segments shown in Figure 1.13 - mainly the prediction of stress and strain in tandem with first-ply-failure (FPF) calculations. The development of these techniques should in principle allow the evaluation of deformational behavior for a large number of CPV configurations in a short amount of time. The development of highly cost efficient numerical tools capable of providing a reasonably accurate prediction of CPV behavior is also a crucial step for product development processes in an industrial context where long computation times almost directly translate into higher expenditures. Therefore, a major focus of this study is to provide an overview of methods that, while preserving low computation time, provide an accurate depiction of the deformational behavior of CPVs. Furthermore, a a minimum-input CPV analysis framework is developed and described as a foundation for future integration of optimization protocols for CPVs.

This being a study supported by Daimler AG, strong focus was set on the experimental works previously presented and published by groups affiliated with Daimler AG that have worked on the topic of CPV development in the past which clearly identified the cylinder-dome transition of CPVs as a highly critical design region whose response to various stacking sequence configurations is not entirely understood [33, 47, 56] . The work presented here puts strong focus on identifying trends in behavior of the cylinder-dome transition due to changes in stacking sequence configurations and other parameters that were identified and further elaborated in later chapters of this report.

Consequently, a main research question is formulated as part of this study:

*How can computationally efficient predictive numerical models capture phenomena related to the cylinder-dome transition and what design rules can be derived from it?*

This research question was separated into a set of more detailed sub-questions listed below together with the chapters that aim to provide insights and answers:

- How can the influence of manufacturing related phenomena as well as distinct laminate responses be captured by computationally efficient numerical models? - **Chapter 2; 4**
- How does changing laminate properties of the cylinder affect the behavior of the cylinder-dome transition region? - **Chapter 3**
- How sensitive is the cylinder-dome transition to varying tangential stiffness by introduction of hoop layer tapering into the transition region? - **Chapter 3**
- How do laminate properties and changing hoop layer tapering affect burst performance? - **Chapter 3; 4**
- What design rules can be determined from the experimental set provided in this study? - **Chapter 5**

## 1.6. Thesis Structure

The following report is divided into a series of chapters that address the subquestions presented in Section 1.5. In this section, a brief summary of each chapter's contents is presented in order to provide more clarity on the documents structure and flow.

Chapters 2 and 4 present a comprehensive discussion on the development and performance of a modelling framework for CPVs. In Chapter 2, the methodology for vessel geometry correction is described. The geometry correction methodology is used as a significant segment of the automated analysis framework which deals with ensuring a usable geometry of a CPV is generated for use in FE models. Additionally, the chapter briefly discusses the setup of the FE models that were used to analyze a large variety of CPVs configurations as part of this study.

Chapter 4 discusses the performance of the FE models and their correlation to previous and current experimental data. The ability of the models to predict vessel response and its ability to predict burst pressure is evaluated. The model is evaluated critically and a summarized overview of suggested improvements is listed at the end of the chapter.

Chapter 3 goes into depth on the experimental study executed for this thesis. The experimental study tackles the impact of two design-critical variables for CPVs design - stacking sequence and tangential stiffness variation in the cylinder-dome transition. The chapter also provides an overview of nomenclature for vessel configuration description as well as a brief overview of the configurations developed for the experimental plan (Section 3.2). The results of the experimental plan are analyzed and discussed at length with valuable trends in vessel deformation and burst performance being identified.

Chapter 5 shows a potential use case for the analysis framework developed as part of this thesis. The framework is applied to a hypothetical set of CPV configurations in order to gain insight on potential future studies and areas of improvements for the best-performing configuration in the current experimental plan.

Lastly, Chapter 6 provides a brief set of conclusion reviewing the work presented here and adds to the discussion on future work and recommendations. The subquestions are explicitly focused on in order to provide a brief review of the discussion from previous chapters.



# 2

## Modelling Methodology

Industrial development of high-performance products requires an ever increasing concept-to-result rate in order to ensure competitiveness and novelty in the market. CPVs, as components of immense criticality, are one such product that requires development of rapid analysis methods which allow engineers to evaluate design concepts in a way conducive to further mass savings or safety increase. Previous knowledge now allows the exploration of 'middle-ground' models that aim to model the critical aspects of CPV response in order to preserve a quality prediction without sacrificing computational efficiency. Within this study, two modelling approaches were developed in order to examine their viability within a streamlined design framework. The novelty of the models can be found in their integration with a geometry correction procedure.

Nebe et al. [12] demonstrated that the accurate depiction of through-thickness geometry can lead to a high-degree of accuracy in FE modelling of CPVs. The geometry correction protocol presented here depicts an engineering solution aiming to provide a satisfactory description of CPVs and their through-thickness layer distribution. The protocol is based on substantial modification of outputs generated by industry-standard software - Compositcad and tackles the correction of hoop layer drop-off regions, thickness and angle correction.

In this chapter an overview of the methods used within the scope of this study are documented. A major motivator for the work presented here, other than the acquisition of worthwhile results of scientific significance, was the need to demonstrate a potential framework for design and data analysis of CPVs within an industrial context. All of the tools and methods described below are part of a fully automated system that requires minimal input from the user and yields results within a short amount of time.

### 2.1. Geometry Correction

The importance of geometry correction within the context of modelling was discussed to some extent by Soriano [27] where the accurate depiction of through-thickness layer distribution was crucial for the accurate reproduction of deformational behavior of CPVs. The problem of layer distribution in a CPV is fairly complicated as the context of filament winding as a manufacturing process introduces a variety of parameters that affect the behavior of layers between winding and curing. Winding tension, liner rigidity, internal liner pressure, resin properties and even stacking sequence have an effect on how layers will interact with each other and how much they will or can move during the entirety of the manufacturing process. To model the actual process of layer re-arrangement during manufacturing process is a task well outside this thesis' scope and could pose a topic for a future PhD project.

Within this project, an engineering approach was developed that would tackle the problem of layer re-arrangement in a systematic way that results are of sufficient quality for use in numerical models while disregarding the physical intricacies of the problem at hand. This engineering process makes heavy use of industry standard software - Compositcad. Compositcad is software whose main purpose is the definition of winding protocols for a variety of filament winding machines. It allows a user to define a stacking sequence of a CPV with relative ease and, in addition to machine code for the filament winding process, it allows the user to extract some estimative information about the general geometry of the vessel regarding the distribution of layers. To produce satisfactory predictions on the final vessel geometry, the problem of geometry prediction is divided into two separate processes - layer re-arrangement and layer compaction.

Layer re-arrangement is tackled through the development of a representative variable named *context*, which helps to determine the amount any given layer is to be displaced from its intended deposition location. Layer compaction is approached by applying previous academic work on the modeling of compaction in wound CFRP cylinders such as seen in the work presented by Kang et al.[58] with additional assumptions which are later discussed in this chapter.

### 2.1.1. Compositcad Output

While its primary purpose of generating winding and machine motion programs is more often than not satisfied to a high degree of accuracy, Compositcad's secondary functionality leaves much to be desired. This primarily applies to the thickness and angle variation prediction of the software. A graphical representation of layer thickness variation along the vessel length as produced by Compositcad is shown in Figure 2.1. A few key points need to be made about this figure to ensure understanding of the underlying issues which make these results incompatible with well-performing numerical models.

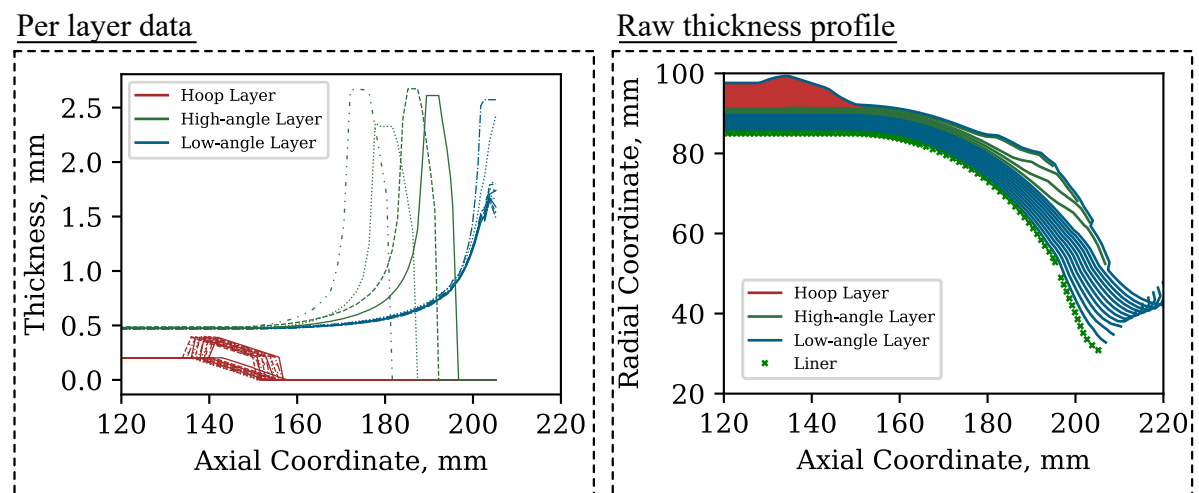


Figure 2.1: Graphical depiction of Compositcad thickness output

In Figure 2.1 a clear distinction can be made between hoop layers and two types of helical layers. This information can be inferred by observing the thickness prediction for the cylinder part of the vessel - where hoop and helical layers are predicted to have exactly nominal and 2x nominal thickness respectively. There is no apparent thickness adjustment per layer as a result of compaction forces developed during winding - this is a result of the lack of any thickness gradient between layers in the cylinder. The distinction between two types of helical layers (high angle and low angle) is visible mainly in the thickness prediction around the polar openings of these layers. As the layer reaches its desired polar opening, its thickness prediction exponentially grows to roughly 5.5x of the layer thickness in the cylinder. This prediction is, to an extent, rooted in reality since a thickness increase around the polar opening of a helical layer is expected. However, it is fundamentally wrong to claim that the thickness increase of a layer around its polar opening is effectively independent of the polar opening diameter. When observing the hoop layer thickness prediction, it is easy to notice unexpected behavior around the layer drop-off points. This is mainly manifested as 2x thickness increase for some layers just prior to layer tapering. This thickness increase is related to the definition of a dwell in the winding protocol that is used to ensure full circumferential coverage. However, including this winding dwell causes issues with Compositcad's thickness prediction as it does not account for any layer interaction which would effectively cause layer re-arrangement in that region and result in a smooth thickness distribution.

The result of these thickness prediction issues is shown in Figure 2.1 which shows a rather unrealistic depiction of a CPV geometry. What follows is a description of the efforts made to account for the issues identified in Compositcad's thickness prediction. The geometry correction algorithm is divided into two main sections - layer re-arrangement and thickness correction. These two are treated as additive components of the geometry prediction problem and as such are solved separately and consequently superimposed.

### 2.1.2. Layer Re-arrangement and Context

The behavior of layers during CPV winding is a complicated topic to tackle due to the variety of factors that influence it and the variability of those factors depending on the configuration being manufactured. Some of the main parameters that have been identified can be grouped as physical and chemical. The physical factors that require accounting for are fiber tension, fiber angle and order of layers being deposited. Additionally, there are chemical factors such as choice of fiber and resin. The chemical factors play a role in determining the friction coefficient of the winding material to some extent but play a far greater role during the curing process of the laminate where the resin has to go through significant viscosity changes - thereby affecting the ability of individual layers to slip and move before curing completely.

The physical factors are rather important since their understanding would allow for a preliminary estimation of the final vessel geometry. The fiber tension play a role in the compaction rate of individual layers. Higher winding tension implies a higher radial pressure being applied to the plies below and can cause the transverse expansion of said layers. The effect the angle of a layer has on the layer distribution below depends on the angle itself. Low-angle helical layers will inevitably apply higher meridional forces on the layers below - causing them to shift. As the angle tends towards a circumferential tangent, these friction forces reduce and more compaction is applied to the layers below. Additionally, low-angle helicals can have an impact on the length of the vessel since the majority of their compaction will be found at their polar openings. The contraction of the vessel depends on liner stiffness.

While a solid foundation of academic work already exists that deals with the prediction of thickness build-up for helical layers [6, 7, 59], no significant research was done to attempt to describe the re-arrangement of hoop layers in CPV winding. This is possibly due to the fact that most research on CPVs in the past is not specifically looking to extend their knowledge to automotive applications where loading conditions are so high they necessitate a large amount of tangential reinforcement. Since the topic of physically describing material re-arrangement in CPVs can easily be the topic of a PhD study, an engineering solution that provides satisfactory results was developed as part of this thesis.

The approach considers the three types of layers mentioned above, and adjusts the initial Compositcad output in order to achieve a geometry that resemble manufactured vessels to a satisfactory degree as well as provides a geometry description of sufficient quality for use in numerical models with substantive predictive ability. The layer re-arrangement procedure described here seeks to separate the problem into individual units that can be tackled independently in order to simplify the problem as much as possible while opening up the opportunity to fine tune the parameters that affect the layer re-arrangement process.

### 2.1.3. Hoop Layer Re-arrangement

Within a CPV, hoop layers play crucial role as they provide the most tangential reinforcement in the vessel. This is especially important for the cylinder where the presence of tangential loads are highest. The distribution of hoops plays a major role in the development of laminate stress states and directly determines the cylinder's bending-extensional response - the effects of which are also a focus of the work presented in this report. However, it is unclear whether the bending-extensional response or the hoop distribution through-thickness is the dominant the parameter in the determination of laminate response in CPVs. The main focus of the hoop layer re-arrangement procedure is the cylinder-dome region of the vessel where the layers taper off. In this region Compositcad inaccurately predicts that some layers experience a factor two thickness increase which manifests itself in a highly local thickness increase which is unrepresentative of reality. This inaccuracy mainly stems from Compositcad's inability to capture individual hoop layers interacting with each other. As previously mentioned, to attempt to predict the extension of the hoop layers, a mathematical solution that applies a few rules that were established as a result of observing the filament winding process at Daimler. Figure 2.2 shows a graphical summary of the adjustments made to the Compositcad output with per-ply thickness plots and layer contour plots.

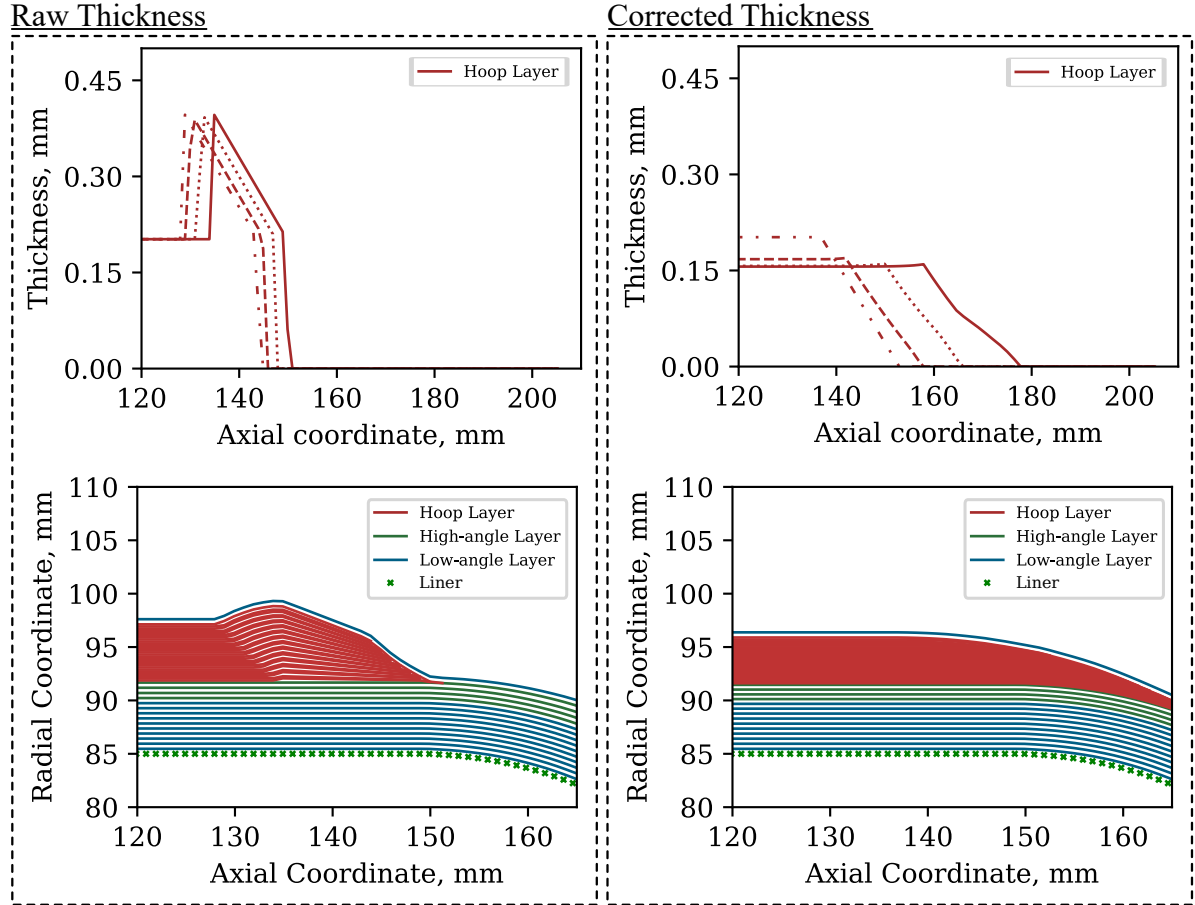


Figure 2.2: Comparison of Composicad and corrected layer thickness profile output

The goal of hoop layer re-arrangement is to determine the amount any given hoop layer extends from its intended placement position. This is achieved by accounting for the position of the layer within the laminate - its *context*. The two effects that *context* attempts to account for are changes in vessel dimensions and the interaction of hoop layers and hoop groups within the vessel laminate. The entire procedure is based of the assumption that the tapering length,  $L_{taper}$ , predicted by Composicad is correct and preserved throughout the manufacturing process. This tapering length is normalized to start at nominal layer thickness and then shifted by the amount determined by *context*. To predict the behavior of a hoop layer within its hoop group, a simple linear relationship is established and described in Equation 2.1.

$$C_{hoop} = \frac{N_h - i_h}{N_h} \quad (2.1)$$

The  $C_{hoop}$  stands for hoop layer context,  $N_h$  is the total number of hoops stacking sequence,  $i_h$  is the cardinal number of the inspected hoop within its hoop group. The desired behavior of the fraction is such that the value varies linearly between 1, starting at the bottom hoop of the inspected hoop group, and 0 at top hoop of the stacking sequence. This behavior ensures that hoops at the bottom of any given hoop group extend by a given maximum amount, and hoops at the top of a hoop group do not extend while intermediate hoops extend following a linear trend between the two extremes. Equation 2.1 is combined with Equation 2.2 in order to finalize this aspect of hoop group context definition.

$$C_{hg} = \frac{N_g - i_g}{N_g} \quad (2.2)$$

In Equation 2.2,  $C_{hg}$  stands for hoop group context - where  $N_g$  is the total number of hoop groups and  $i_g$  is the cardinal number of the hoop group being inspected. The desired behavior achieved by this equation is, similar to Equation 2.1, a linear variation between one, starting at the bottom hoop group, and zero at the

top hoop group. Which, similar to Equation 2.1, implies that a hoop group on the bottom of the laminate can extend the most, while comparatively a hoop group on the top of the laminate cannot extend. Equations 2.2 and 2.1 combined yield the first half of the definition of *context* within the hoop layer re-arrangement procedure. As is visible in Equation 2.3, These two serve as a base by which the initial tapering length, as defined by Compositcad, is scaled in order to determine how far it will be offset.

$$C = L_{taper} C_{hoop} C_{hg} \quad (2.3)$$

During the manufacturing of CPVs the vessel length changes due to forces applied onto the mandrel. Figure 2.3 shows the variation in length of a representative vessel configuration and highlights the potential severity of this effect. As is visible in figure 2.3, the length of a vessel can vary by a few millimeters. While this 3% change in length can seem trivial, the work presented by Nebe et al. [12] and Soriano [27] strongly emphasize the importance of capturing these perceivable minor changes in geometry in order to enable numerical models to capture the vessels' mechanical response well.

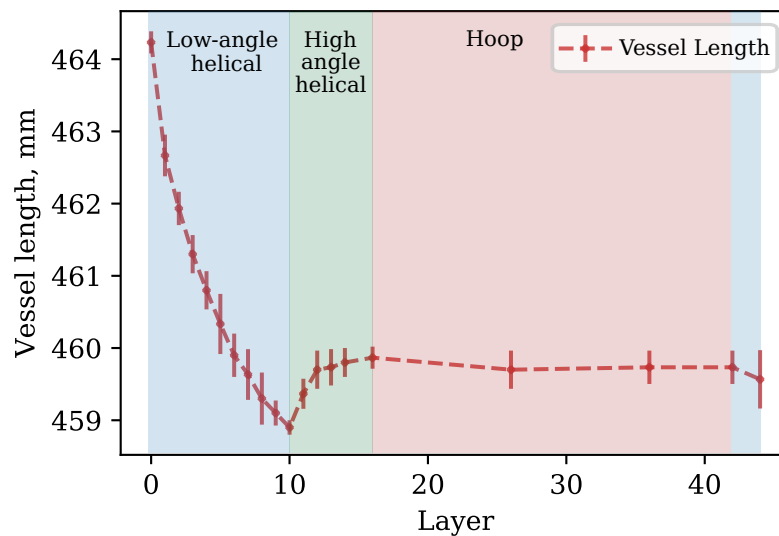


Figure 2.3: Representative vessel length variation as a result of different layer type winding

While it is almost certain that the variation in vessel length during manufacturing is manifested as a modification of the inner vessel contour, the quantification of liner deformation during winding is outside the scope of this study - therefore the following assumption is made: Liner shape does not change during winding. This is a major assumption to make as the shape of the liner can have a profound effect on the internal load distribution of the vessel. Regardless, this allows a simple solution to account for vessel length change within the definition of *context*. During the manufacturing process, the vessel length was measured after the application of every helical layer as these were found to be the most influential on vessel length. It is important to note that every type of layer has either an additive or deductive effect to the overall vessel length. So for example, hoop and high angle helicals tend to increase vessel length, while low angle helicals decrease it. The apparent increase in length is assumed to be confined to the dome and is therefore not accounted for in the layer re-arrangement protocol.

The severity that changes in inner contour can have on mechanical response have not been adequately described in previous studies. In this study, changes in mandrel geometry are not accounted for, but the changes in internal layer distribution as a consequence of mandrel deformation have been taken into account as they have been shown to have a significant effect on the internal distribution of layers within a vessel laminate [27]. The degree to which the layer distribution is affected by changing in vessel length depends on the stacking sequence configuration of the vessel. Consider a stacking sequence where all the helical layers precede all hoop layers within a vessel layup. In this case all of the major changes in vessel length occur *prior* to the winding of hoop layers which inherently changes the location of their application. In contrast, if all the hoop layers of a stacking sequence were applied before any of the helical layers were applied to the mandrel, the hoops would only be affected by their own interaction with themselves. Therefore, it is important to

account for the number of helicals that exist *above* any given hoop group to additionally adjust the amount of extension that any given hoop layer will have to better approximate the internal distribution of layers within a vessel. From Figure 2.3, the average reduction in length as a result of low angle helical application was determined to be 0.58 mm.

To account for the additional extension that any given hoop layer experiences as a result of low-angle helical application, the following expression is added to the definition of context:

$$C_{helical} = 0.58 * N_{lh} \quad (2.4)$$

Equation 2.4 describes the absolute extension (in mm) of hoop layers as a result of the low angle helicals wound prior to the application of the inspected hoop layers. In the equation  $C_{helical}$  stands for *helical context* while 0.58 is a value, in mm, to denote the average axial contraction of a vessel for one helical layer and  $N_{lh}$  denotes the number of low angle helical layer wound before the hoop in question.

Equation 2.4 is then combined with the definition of *context* in shown in Equation 2.3 in order to provide its full definition:

$$C = L_{taper} C_{hoop} C_{hg} + C_{helical} \quad (2.5)$$

With *context* defined fully, it is applied to every hoop layer in a stacking sequence of CPV and used to determine the extension of all the hoops given their relative position within the laminate. The tapering length as defined by Composicad is then shifted by the amount defined by *context* and the tapering slope replicated as it was defined by Composicad. The values preceding the newly defined tapering region are replaced by cylinder nominal thickness values.

#### 2.1.4. High-angle helical adjustment

The adjustment of high-angle helical layers is comparatively less structured than the correction of hoop layers. As noted earlier, the main issues with the high-angle helical thickness profile, as it is defined in Composicad, are the exaggerated thickness prediction around polar opening and the apparently perpendicular layer edge caused by a lack of tapering.

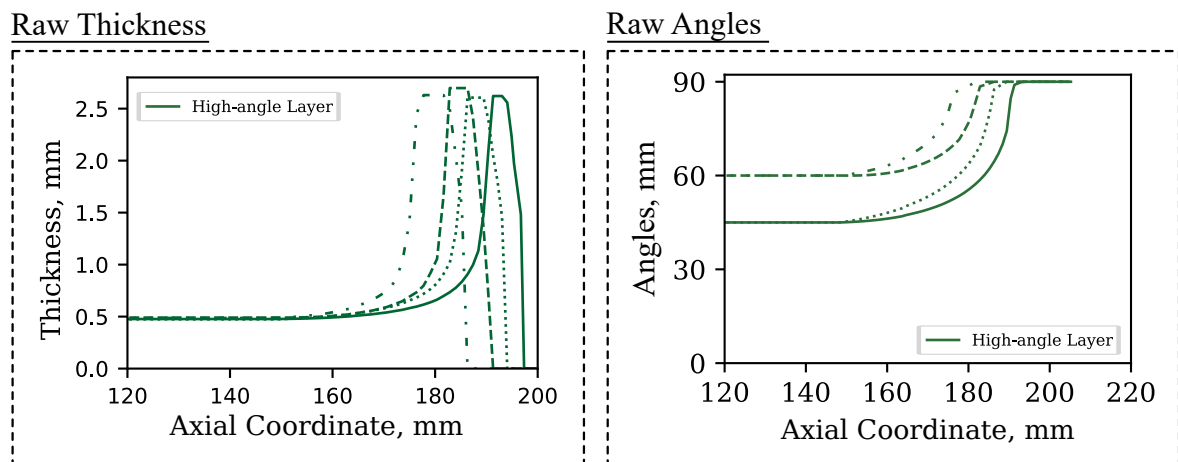


Figure 2.4: Side-by-side comparison of Composicad thickness and angle variation prediction for high-angle helicals

The thickness build-up around the polar opening of a layer is related to the diameter of the polar opening [6] so it is unlikely that the Composicad output for the thickness prediction of high-angle helicals is correct. Due to confidentiality restrictions, it is not possible to know how the thickness build-up prediction at the polar opening of a helical layer is determined within Composicad. However, it is likely that the thickness prediction of the polar opening is strongly linked to the angle prediction of a layer - meaning that regardless of the polar opening diameter, the thickness prediction at the polar opening of a layer will be roughly the

same. This behavior is shown in Figure 2.1 where the thickness prediction of high-angle helical layers is fairly similar to the thickness prediction of low-angle helical layers around their respective polar openings. Figure 2.4 shows a side by side comparison of the thickness and angle variation output for a high-angle helical layer generated by Compositcad. One should notice that the thickness profile of the presented high-angle helical layer is a 1-to-1 scaling of the angle variation profile, though it is unclear how the limit for layer thickness is determined exactly as it currently seems to be set at an arbitrary 5x nominal layer thickness. In reality, the thickness build-up around the polar opening increases with the decrease of the polar opening diameter. This is caused by the necessity of filament continuity during winding. For example, consider a fully closed spherical end-cap on a CPV. If 100% coverage of the vessel is to be achieved with longitudinal layers (polar opening diameter = 0), every layer would have to cross the pole of the spherical end-cap - resulting in substantial thickness build-up. If the polar opening diameter is now increased, the area over which layers need to overlap is now increased - causing a decrease in thickness build-up around the polar opening.

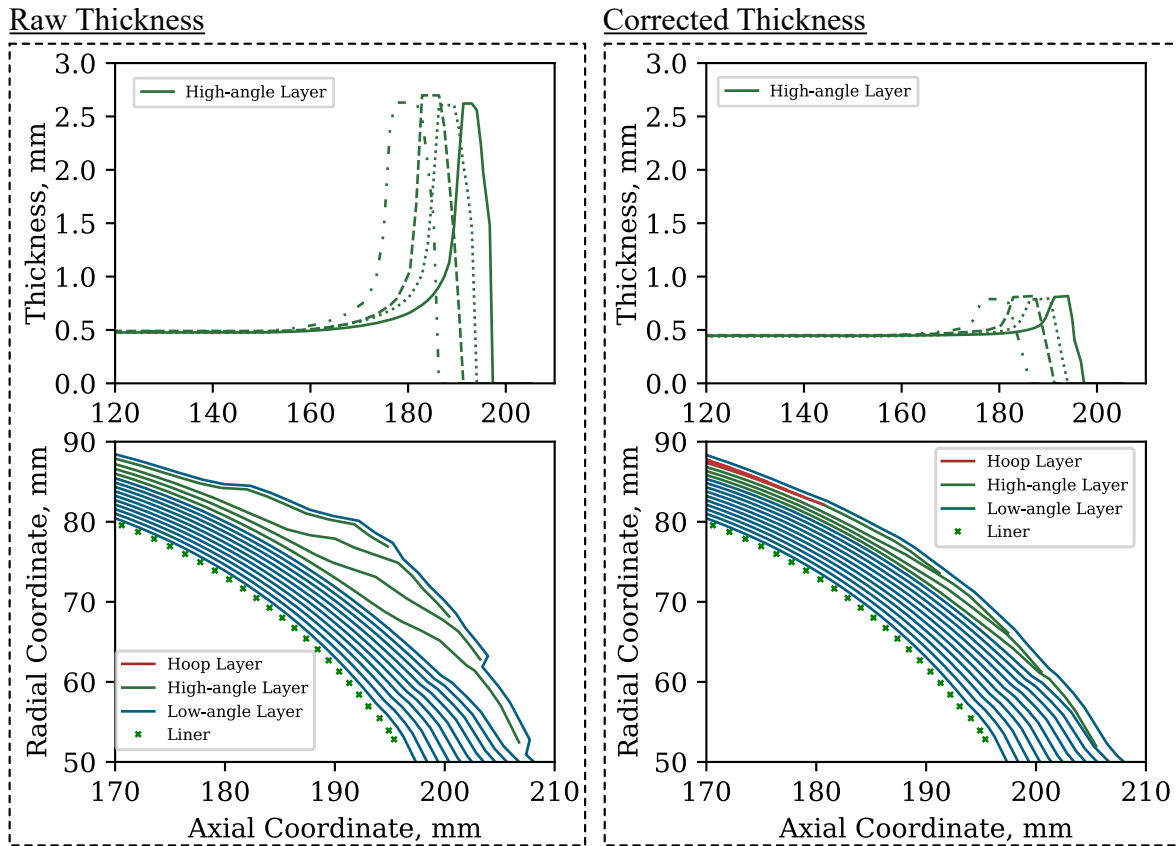


Figure 2.5: Comparison of Compositcad and corrected layer thicknesses profile output - High-angle helical example

To adjust the thickness build-up around the polar opening of the high-angle helicals, the maximum thickness is scaled by a simple linear relationship presented in Equation 2.6 presented below:

$$t_{max} = t_{nom} + (t_{maxCAD} - t_{nom}) * c_{correction} \quad (2.6)$$

Where  $t_{max}$  is the corrected maximum thickness,  $t_{nom}$  is nominal layer thickness,  $t_{maxCAD}$  is maximum layer thickness as defined by Compositcad and  $c_{correction}$  a non-dimensional factor expressed as the ratio of axial locations of the Compositcad maximum thickness and the minimum polar opening on the mandrel  $\frac{x_{maxCAD}}{x_{minPO}} * \frac{1}{3}$ . The definition of the correction factor is rather arbitrary - the main idea behind it was to have the maximum layer thickness increase linearly as the polar opening of the layer decreases. However, during development and testing, it was clear that linearly scaling the Compositcad maximum predicted thickness is insufficient and further scaling is required. Hence, the division by 3 was implemented as a result of fine tuning the thickness prediction protocol through comparison with measured vessel data.

To account for layer tapering, the high-angle helical thickness profile was made to adopt a similar trend to the one found in the description of hoop layers. After the initial thickness correction of high-angle helical

layers, the tapering range was found to be unrepresentative of reality. Hence the region after the perceived plateau of each high-angle helical layer was modified to have a linear tapering trend. The slope of the tapering was fine-tuned until a smooth outer contour could be ensured. Figure 2.5 summarizes the changes made to Compositcad's prediction of thickness build-up in high-angle helical layers.

### 2.1.5. Low-angle Helical Adjustment

Similar to high-angle helicals, low-angle helical layers are plagued by inaccurate predictions within Compositcad's framework. The apparent link between angle and thickness prediction is more apparent in the case of low-angle helical layers. Figure 2.6 highlights this effect well by showing the nearly one-to-one mapping trends of raw thicknesses to raw angles. The result is unphysical and implies that some low-angle helical layers reach their polar opening at an angle other than a  $90^\circ$ . To correct this, the angle prediction was adjusted from the Compositcad prediction by applying a 6th degree polynomial that ensured a smooth increase of angle towards  $90^\circ$  for each low-angle helical layer.

Correcting the thickness prediction was a far less trivial task since Compositcad's prediction predicts thickness build as a function of the normal to the mandrel geometry - resulting in intersecting thickness region around the polar opening (see Figure 2.7). The thickness adjustment approach was based on a significant amount of empirical measurements that served to establish trends in outer contours around the polar opening. It was noticed that good accordance can be made by fitting a parabolic curve to the thickness prediction region around the polar opening. An arbitrary starting point was chosen for each layer and matched with a scaled ending point based on the liner geometry and Compositcad faulty thickness prediction. Knowing the slope conditions at the starting point and the ending point allowed to fit a parabolic curve for each layer and ensure a smooth thickness buildup around the polar opening region of the CPV.

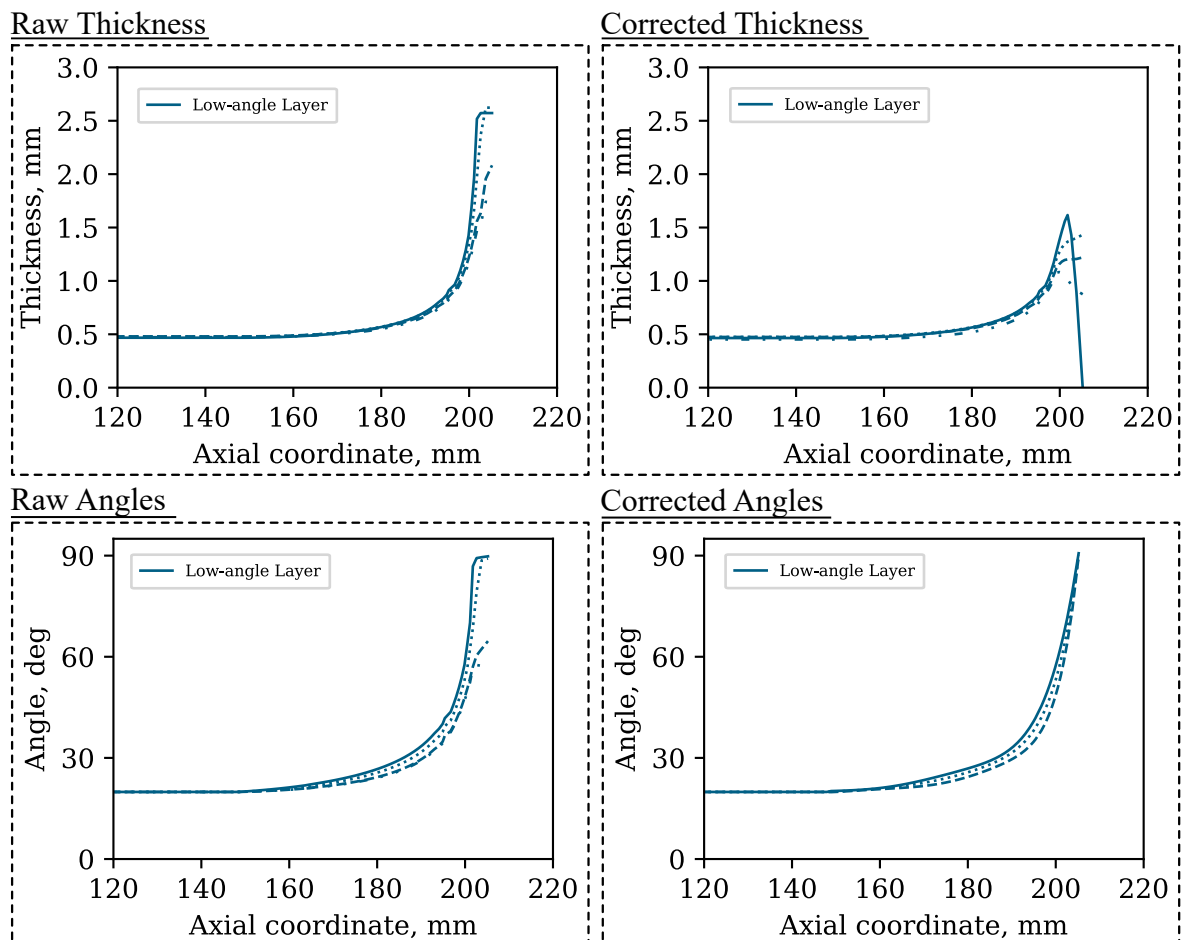


Figure 2.6: Comparison of raw and corrected thickness profiles for low-angle helicals

Finally, 2.7 shows the raw and corrected results of the layer contours for low-angle helical layers around

the polar opening.

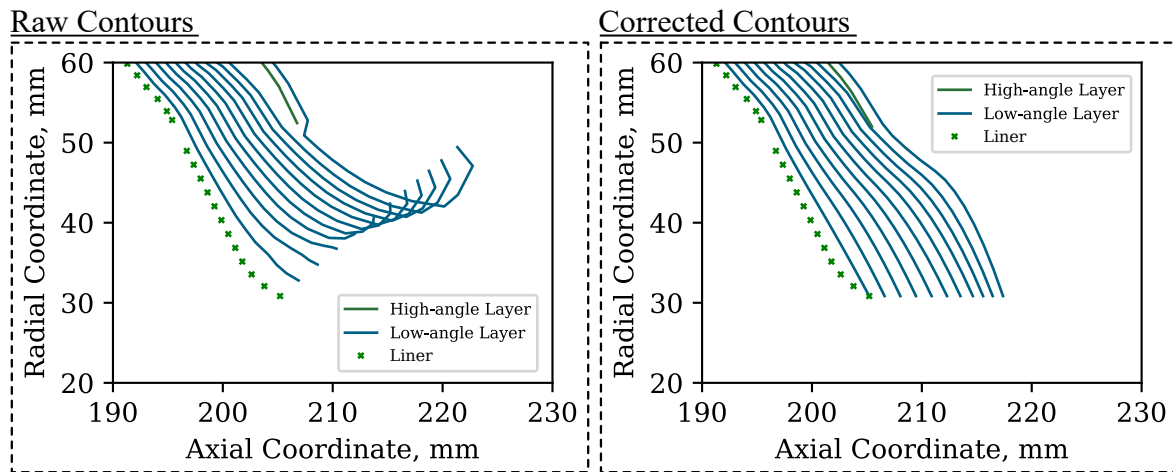


Figure 2.7: Comparison of raw and corrected thickness profiles around polar opening

### 2.1.6. Thickness Adjustment

With the layer re-arrangement algorithm complete, the other half of the process is a thickness correction algorithm that looks account for the compaction of any individual layer as a result of the layers surrounding them, their respective winding tensions and its own winding tension. The thickness correction algorithm is mainly based on the implementation of the work presented by Kang et al. [58].

The model presented by Kang et al. [58] outlines a model to determine the development of stresses in wound cylinders. As shown in Figure 2.8, the model takes into account winding stresses, thermal and chemical shrinkage induced stresses. Because the calculation of stresses due to the curing process of the laminate requires material information that was not available during the development of this tool-set, the curing process stresses are not accounted for in this work.

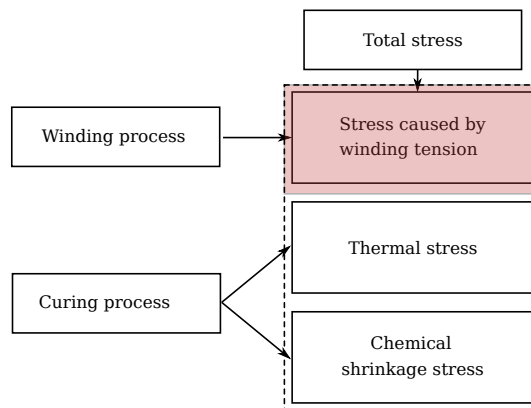


Figure 2.8: Overview of internal stress calculation captured by model presented in Kang et al. [58]

To account for winding stresses, the model presented in [58] makes a series of assumptions:

- plane stress
- layers are discrete and the stress in each individual ring is acquired through superposition
- mixing rule is valid to determine composite modulus
- the mandrel is isotropic and linear-elastic

Geometry parameters and loading case description are shown in Figure 2.9. In accordance with thick cylinder theory, the displacement and radial stress of the mandrel can be represented as follows

$$\begin{bmatrix} u_{Mr} \\ \sigma_{Mr} \end{bmatrix} = \begin{bmatrix} r & \frac{1}{r} \\ \frac{E_M}{1-\nu_M} & \frac{E_M}{1+\nu_M} \frac{1}{r^2} \end{bmatrix} \begin{bmatrix} A \\ B \end{bmatrix} \quad (2.7)$$

where  $u_{Mr}$  and  $\sigma_{Mr}$  are the displacement and mandrel stress in the radial direction.  $\nu_M$  is Poisson's ratio of the mandrel and  $A$  and  $B$  are constants and  $r$  is mandrel radius. The boundary conditions of the cylinder can be defined as shown in Equations 2.8:

$$\sigma_{Mr} = 0, \quad r = a; \quad \sigma_{Mr} = -P_1, \quad r = b, \quad (2.8)$$

where  $a$  and  $b$  are internal and external mandrel radii respectively and  $P_1$  is external pressure. The generalized mandrel stiffness is introduced in the radial direction:

$$K = \frac{\sigma_{Mr}|_{r=b}}{u_{Mr}|_{r=b}} \quad (2.9)$$

By substituting 2.7 into 2.8 and then forwarding the result into 2.9 - the generalized stiffness of the mandrel follows as shown in Equation 2.10

$$K = \frac{(b^2 - a^2)E_M}{b[b^2(1 - \nu_M) + a^2(1 + \nu_M)]} \quad (2.10)$$

To determine the stresses in the cylinder itself, linear constitutive equations are presented below:

$$\begin{bmatrix} \epsilon_r \\ \epsilon_\theta \end{bmatrix} = \begin{bmatrix} \frac{1}{E_r} & \frac{-\nu_\theta}{E_\theta} \\ \frac{\nu_r}{E_r} & \frac{1}{E_\theta} \end{bmatrix} \begin{bmatrix} \sigma_r \\ \sigma_\theta \end{bmatrix} \quad (2.11)$$

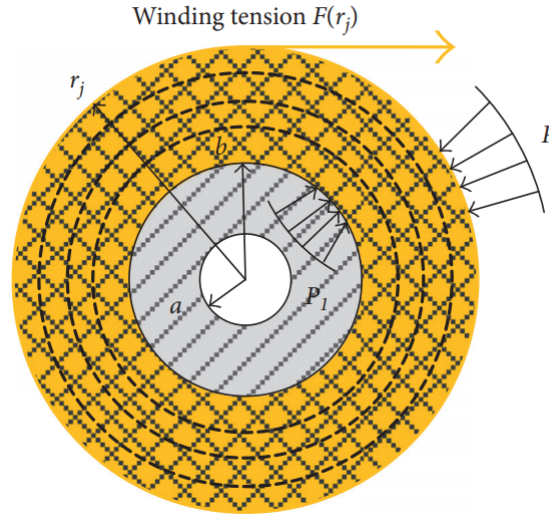


Figure 2.9: Cylinder geometry and load definition - taken from Kang et al. [58]

Where  $E_r$  and  $E_\theta$  are radial and hoop elastic moduli,  $\nu_r$ ,  $\nu_{theta}$  denote Poisson's ratios of radial and tangential directions, while  $\sigma_r$  and  $\sigma_\theta$  are the stresses in radial and tangential directions respectively.

Additionally, mechanical equilibrium is defined as:

$$\frac{d\sigma_r}{dr} + \frac{\sigma_r - \sigma_\theta}{r} = 0 \quad (2.12)$$

Through some simple algebra relating Equations 2.11 and 2.12 the following equation is derived:

$$u_r'' + \frac{1}{r}u_r' - \frac{\beta^2}{r^2}u_r = 0 \quad (2.13)$$

Where  $\beta^2 = \frac{E_\theta}{E_r}$ . The solution for displacement can be given as follows:

$$u_r = c_1 r^\beta + c_2 r^{-\beta} \quad (2.14)$$

where  $c_1$  and  $c_2$  are constants determined by boundary conditions. Through further algebra using equations 2.11, 2.12 and 2.14, the following expressions are derived for stresses in the composite cylinder:

$$\sigma_r = c_1 S_1 r^{\beta-1} - c_2 S_2 r^{-\beta-1} \quad (2.15)$$

$$\sigma_\theta = c_1 S_3 r^{\beta-1} - c_2 S_4 r^{-\beta-1} \quad (2.16)$$

Where the S coefficients are defined as:

$$\begin{aligned} S_1 &= \frac{\beta + \nu_\theta}{1 - \nu_r \nu_\theta} E_r \\ S_2 &= \frac{\beta - \nu_\theta}{1 - \nu_r \nu_\theta} E_r \\ S_3 &= \frac{1 + \beta \nu_r}{1 - \nu_r \nu_\theta} E_r \\ S_4 &= \frac{1 - \beta \nu_r}{1 - \nu_r \nu_\theta} E_r \end{aligned} \quad (2.17)$$

Boundary conditions for the composite cylinder can be given as shown in equations 2.18 through which expressions for  $c_1$  and  $c_2$  can be derived (equation 2.19).

$$\begin{aligned} \sigma_r &= K \cdot u_r, & r &= b \\ \sigma_r &= -P, & r &= r_j \end{aligned} \quad (2.18)$$

$$\begin{aligned} c_1 &= -\frac{H_2 (r_j/b)^{2\beta}}{H_1 S_2 + H_2 S_1 (r_j/b)^{2\beta}} \left( \frac{1}{r_j^{\beta-1}} \right) P, \\ c_2 &= \frac{H_1 r_j^{\beta+1}}{H_1 S_2 + H_2 S_1 (r_j/b)^{2\beta}} P \end{aligned} \quad (2.19)$$

Where  $H_1 = Kb - S_1$  and  $H_2 = Kb + S_2$ . From this, full expressions for the tangential and radial stresses in the composite cylinder are derived. Lastly, following the superposition assumption, it can be concluded that the stress in the  $i$ th layer is determined through the sum of the stresses introduced by all layers  $i$ th to the final layer in the manufacturing process.

$$\sigma_\theta^{wt}(r_i, r_n) = \frac{F(r_i)}{h} + \sigma_\theta(i, i+1) + \dots + \sigma_\theta(i, n) = \frac{F(r_i)}{h} + \sum_{j=i+1}^n \sigma_\theta(i, j) \quad (2.20)$$

Where  $h$  is the layer thickness and  $F(r_i)$  is the tension of at which the  $i$ th layer is wound. This summation can be expressed in the form of a continuous integral since the thickness of any given ply is relatively small.

$$\sigma_\theta^{wt}(x) = \frac{1}{h} [F(x) + (H_1 S_4 - H_2 S_3 (x)^{2\beta}) (x)^{-\beta-1} \int_x^m \frac{\zeta^\beta F(\zeta)}{H_1 S_2 + H_2 S_1 \zeta^{2\beta}} d\zeta] \quad (2.21)$$

Similarly, the expression for radial stresses can be expressed as follows.

$$\sigma_r^{wt}(x) = -\frac{1}{h} [(H_1 S_2 - H_2 S_1 (x)^{2\beta}) (x)^{-\beta-1} \int_x^m \frac{\zeta^\beta F(\zeta)}{H_1 S_2 + H_2 S_1 \zeta^{2\beta}} d\zeta] \quad (2.22)$$

To actually apply this model to the thickness distribution of CPVs, radial stresses are calculated along the length of the CPV. Since this model is only valid for wound cylinders, the vessel is discretized into a series of cylinders of varying radius along its length in order to allow for the application of the model to the entire

vessel. Once the radial stresses along the entire vessel are calculated each cylinder section is investigated individually and its radial stresses are converted to strains and subsequently to a thickness reduction of each layer.

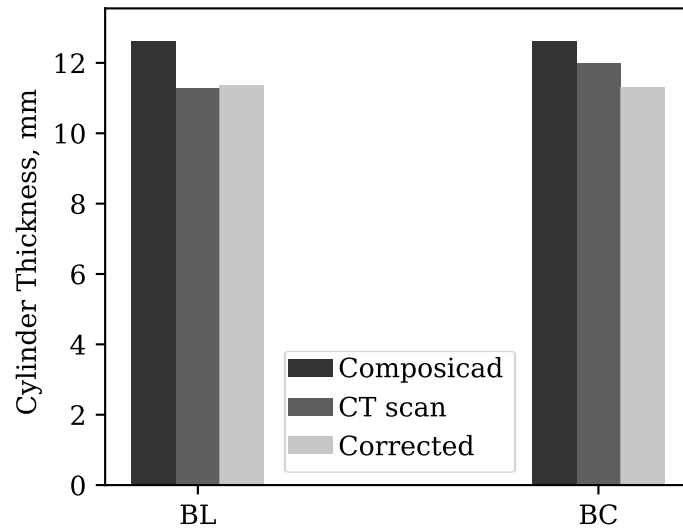


Figure 2.10: Overview of calculated cylinder thickness reduction for representative would cylinder configurations

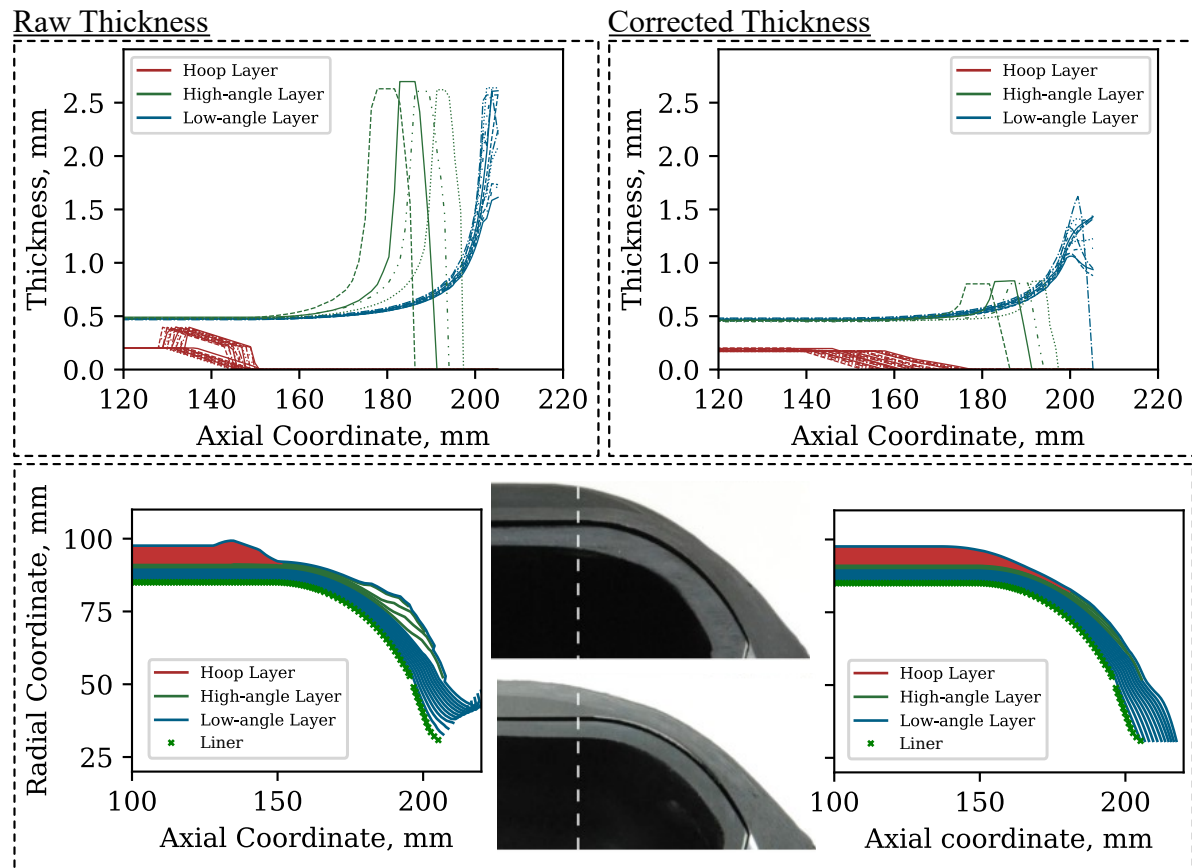


Figure 2.11: Summary of effects of layer re-arrangement and thickness correction on vessel geometry

The results of this procedure applied to a cylindrical section of a CPV can be seen in 2.10. In this particular example, correcting for thickness via the described methods results in a total thickness reduction of 5.4%. Lastly, the thickness correction combined with the layer re-arrangement algorithm produces a reasonable vessel geometry. The complete summary of changes and their effects is depicted in Figure 2.11.

## 2.2. Correlating Corrected Geometry

The development of the the geometry correction algorithm described in Section 2.1 was strongly influenced by trends observed in correlation behavior with old datasets on CPV manufacturing. A substantial amount of outer contour data was preserved from the studies conducted by Asijee [33]. This data was used as a benchmark for performance of the geometry correction protocol. Figure 2.12 shows an overview of the configurations used in [33] experimental study.

As shown in Figure 2.12, all of the configurations associated with [33] study make use of low-angle helical and hoop layers but do not include high-angle helical layers. This was quite useful for the development of the geometry correction tool since it allowed a focus on relatively simple cases prior to introducing configurations including high-angle helical layers. In the following section, an overview of the geometry correction algorithm's performance is described in relation to representative cases from the configurations present in Figure 2.12. Additionally, the performance of the geometry correction algorithm applied to the configurations tested as part of this work's experimental study are shown.

Figures 2.14 and 2.15 show an overview of the geometry correction algorithm performance when compared against configurations shown in Figures 2.12 and 2.13 respectively. The measured outer contour in the figures was captured using stripe light projection. Stripe light projection allowed for the accurate measurement of the outer contour of all tested vessels. With current measurement methods found at Daimler AG, it is only practically possible to make measurements of the outer contour for each vessel tested since the vessel must be CT scanned or cut in order to get an estimate of the inner contour. Additionally, to compare the actual layer thicknesses to reality is nearly impossible to do. Some rough measurements could be made by cutting or grinding the vessel surface however, this was not attempted during this study.

The vessel configurations shown in Figure 2.12 show a good correlation between measured vessel contours and predicted contours using the geometry correction results. For configurations without high-angle helical layers, the overall match is quite good in sections of the vessel with a noticeable decrease in accuracy with a significant increase in the number of hoop groups.

From Figures 2.15 and 2.14 it is apparent that a fairly consistent performance of the geometry correction algorithm can be expected between different configurations. Even with the addition of high-angle helicals, as is the case for the configurations shown in Figure 2.15, the accuracy of the prediction in comparison to the outer contour remains mostly unchanged in comparison to the benchmark configurations. With the introduction of high-angle helical layers to the configurations, a small high-error region was introduced to the area prior to the polar opening of the vessel contour. It is not entirely clear whether that high-error region is caused by the introduction of the high-angle helical layers or by something else. The deposition of high-angle layers should not affect the polar region of the vessel domes and should instead cause a thickness build-up increases around the layers' respective polar opening. A potential source of the high error region is the fact that the robot paths generated by Compositcad do not take into account for the wound surface changes caused by preceding layers. It is possible that the robot paths effectively change substantially enough for the layer correction code pertaining to the low-angle helical layer polar openings loses its representativeness.

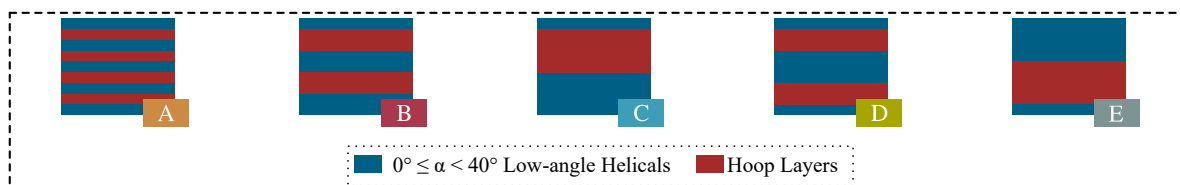


Figure 2.12: Summary of configurations used for geometry correction performance evaluation

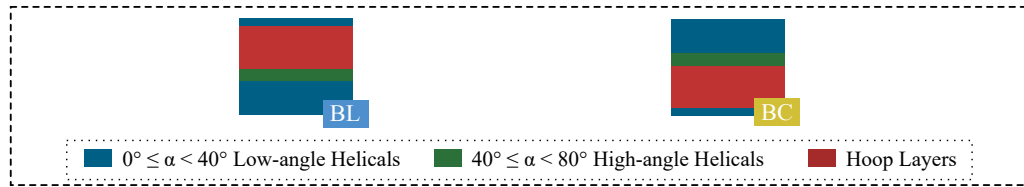


Figure 2.13: Overview of representative configurations within the current study

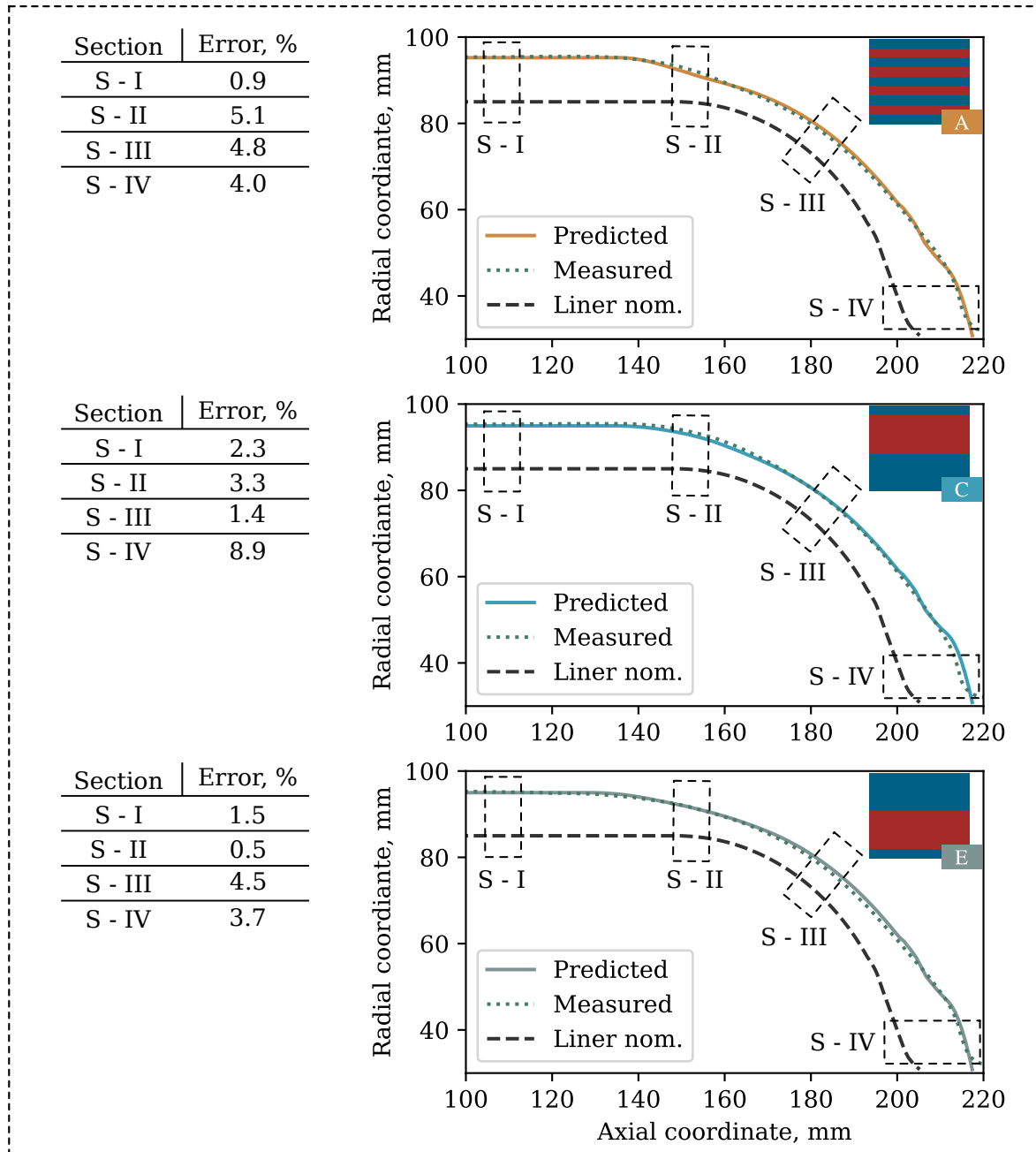


Figure 2.14: Overview of geometry correction algorithm performance on the experimental plan shown in Asijee [33]

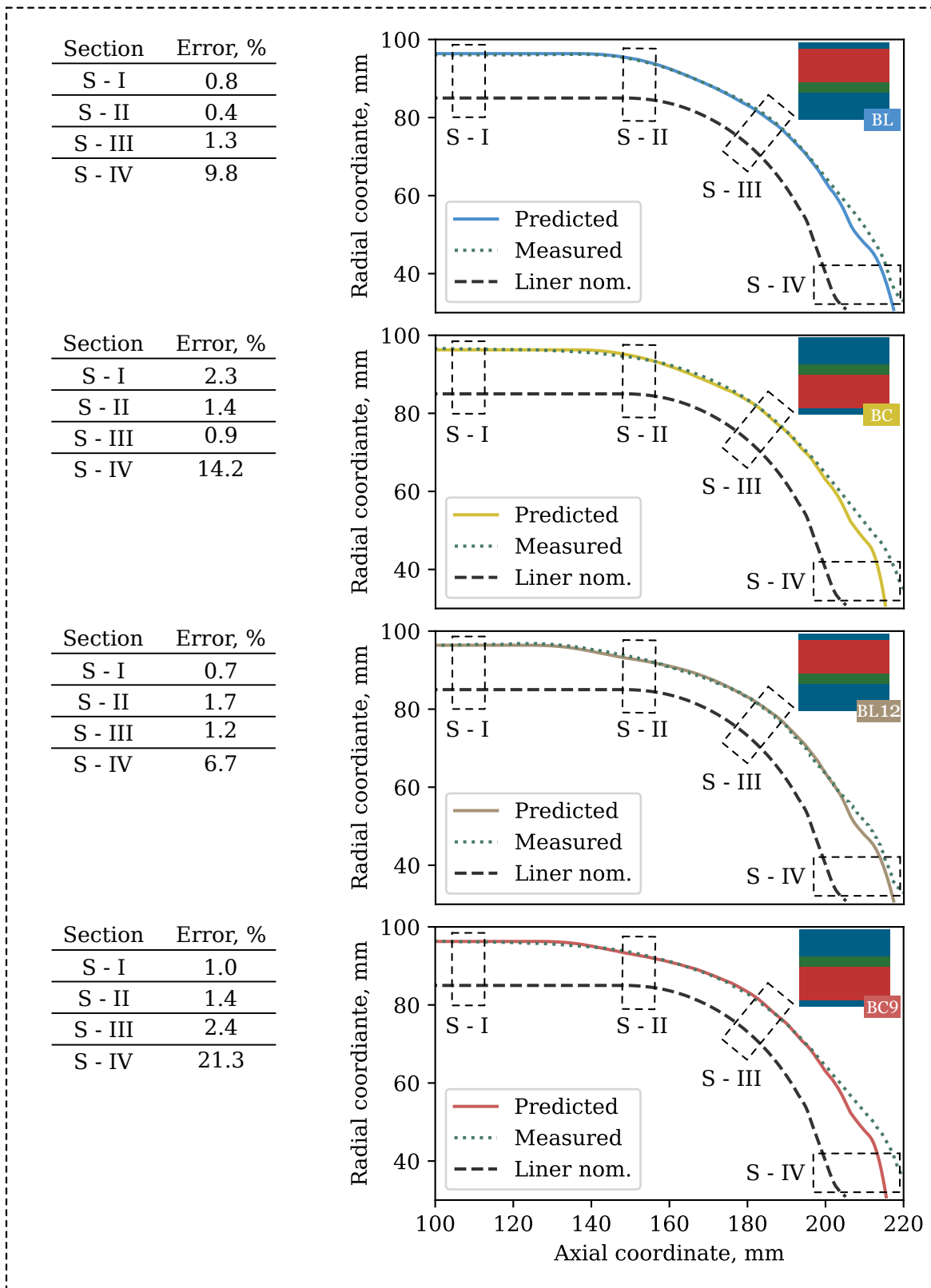


Figure 2.15: Overview of geometry correction algorithm performance on current experimental plan

### 2.3. Layer Re-adjustment Limitations and Implications

The layer re-adjustment procedure described above completed half of a geometry correction algorithm used for the prediction of vessel geometry within the scope of the manufacturing processes and facilities currently used at Daimler AG. This in itself is a major limitation to the universality of this protocol as it would likely require adjustment if either the manufacturing process or the material worked with were to change significantly.

Assuming a rigid mandrel is likely the most critical assumption of the layer re-arrangement process as the inner contour of the vessel is certainly changing with the depicted reduction in vessel length. Currently, the liner contraction is tackled by an average extension of the hoop layers to compensate for contraction due to low-angle helical layer placement. The magnitude of this extension is likely to change with a major overhaul of the angles used in the laminate or a change of the liner material. Additionally, the current method of accounting for vessel liner deformation also implies an addition of non-existent material. The non-physicality of this tool must be emphasized as all the changes to the predicted amount of material deposited essentially reduce the total amount of material predicted to be deposited by Compositcad.

The thickness correction procedure is more robust than the layer re-arrangement procedure since it is based on a physical model. Regardless, it faces limitation due to lack of information on material properties for the material used in the manufacturing of CPVs at Daimler AG. The model implemented requires knowledge of fiber and transverse direction properties of the uncured material. The fiber direction properties can be reasonably assumed to be the same as fiber direction properties as cured material. The transverse direction properties were inferred through benchmark testing and were adapted based on a sensitivity analysis considering all existent configurations. Additionally, the model presented by Kang et al. [58] is also capable of accounting for compaction effects during curing. These effects are not considered in this study and, with adequate approximation of material properties, would likely yield better results for cylinder compaction.

Lastly, the thickness correction protocol is limited in as much as the model applied was not designed to be applied to double-curved geometries such as the dome. The discretization of the dome into discrete cylinder segments yields good results for the cases examined here however it is not clear whether the recorded accordance is circumstantial.

### 2.4. Numerical Modelling

With the geometry correction algorithm described and developed, it is necessary to apply the established tool-set for geometry depiction into a numerical modelling context which would support the effort to validate the performance of geometry validation algorithm as well as provide insights into viable modelling techniques for CPVs. Viable, in this particular case, is interpreted as models that provide quality and meaningful results while being computationally efficient and applicable into future design processes. While previous work focused on highly developing models with a high degree of complexity [12, 42] whose aim is to allow to either capture damage propagation mechanisms or capture previously unknown effects, in this study the aim is to develop fast models that can accurately predict trends in a variety of vessel configurations without manual adjustment.

Within this study, the performance of two modelling strategies are investigated - one based on 2D shell elements, and the other 3D solid elements. All models were developed with ABAQUS, an industry standard FE software. The decision to approach CPV modelling with these strategies was inspired primarily by the work presented by Asijee [33] and Soriano [27] where shell and solid element models have been discussed respectively.

The shell model described in the following subsections aims to further investigate the viability of using shell elements in the numerical description of CPVs by applying the geometry correction algorithm presented earlier and correlating predictions with experimental data. Additionally, the solid element model aims to investigate the level of model simplification that can be made while preserving predictive ability.

#### 2.4.1. Shell Model Implementation Plan

The shell element model discussed by Asijee [33] highlighted the potential plausibility of using shell element based models in the numerical description of CPVs but the work was limited in the lack of geometry correction procedures, instead the models presented in [33] used the raw thickness output of Compositcad which inevitably caused large discrepancies in the predicted response of the vessel. Figure 2.16 shows an overview of results of the model developed in [33] where the geometry and the strain response are shown. The figure highlights the issues when geometry is not described adequately since all three configurations shown are

presented to have the same deformational patterns which is not the case in reality. The development of the geometry correction algorithm allowed for further evaluation of shell element model performance in predicting relevant trends in CPVs.

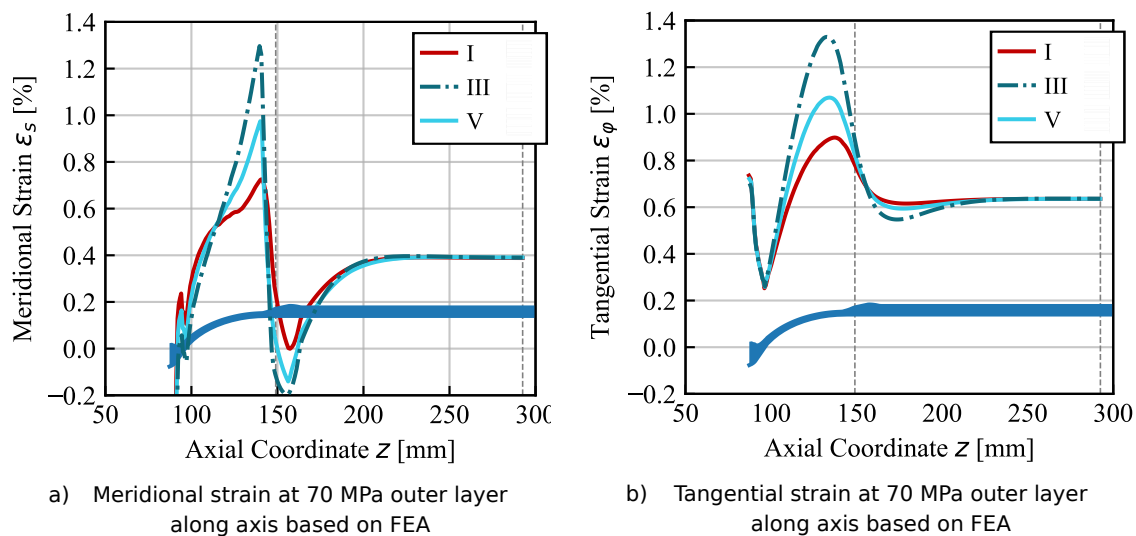


Figure 2.16: FE results of shell model presented by Asijee [33] - Figure acquired from the same study

The shell model developed for this study is based on the S4 shell element which is a fully integrated finite-membrane strain shell element with 6 degrees of freedom (3 translational and 3 rotational). Due to the element being fully integrated, no zero energy bending modes, hourglass stabilization or bending mode stabilization is used. The element assumes that the shear strain is constant over the element - implying that all integration points will have a constant and equal shear strain, transverse shear force and shear stress. Shear locking can occur when using S4 elements but was not observed in the examples tested in this study.

The vessels investigated within this study fall under the definition of thick walled CPVs [31]. This has direct implications on the expected performance of shell element models which cannot account for through-thickness effects due to the plane stress assumption inherent to conventional shell elements in the FE software, ABAQUS. The plane stress assumption in the context of modelling CPVs manifests itself as a lack of stress gradient through-thickness of the laminate structure in the cylinder. This basically means that a variation in stacking sequence will not yield a difference in prediction for the displacement of the cylinder if no change in stacking sequence composition was made.

The model aims to describe an 8th of a sub-scale CPV corresponding to the geometry of the vessels tested in the experimental plan described in Chapter 3. Figure 2.17 shows the shell element model as defined within ABAQUS.

The model is defined by two shell type parts, one to define the inner vessel contour and the other to define the boss end-cap. The vessel part is bounded by symmetry conditions on all free edges and the surface segments in contact with the boss are tied to the boss surface. The vessel part is divided into 121 sections along its meridian. These sections are predefined by Compositcad. The decision to keep a significant part of the model definition tied to Compositcad definitions was intentional as it allowed for better automation and ease of use for by other engineers in the development team at Daimler AG. Each of the sections is assigned a composite layup section with the data for layer thicknesses and distribution being provided by the geometry correction algorithm.

The boss is a simplified version of the actual geometry. The original boss geometry consisted of threaded features and minor features such as a wrench attachments - these were eliminated since they made the meshing process unnecessarily complex while not contributing to the prediction of the vessel behavior. The final mesh of the shell model can be seen in Figure 2.18

The shell model consisted of 6,000 elements which sum to a total of 6,171 nodes with an average solving time of 10 minutes.

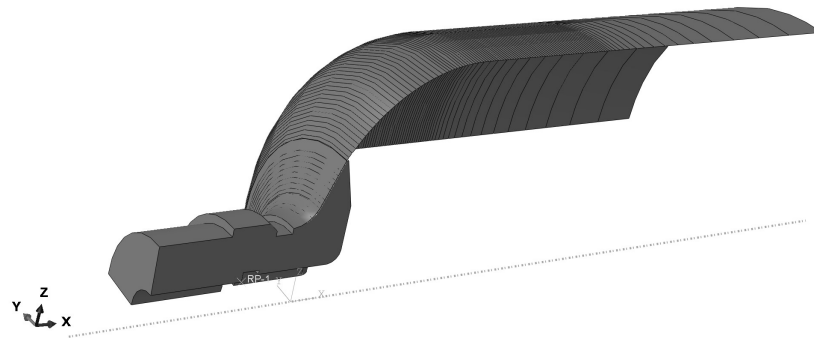


Figure 2.17: Shell element model defined in ABAQUS

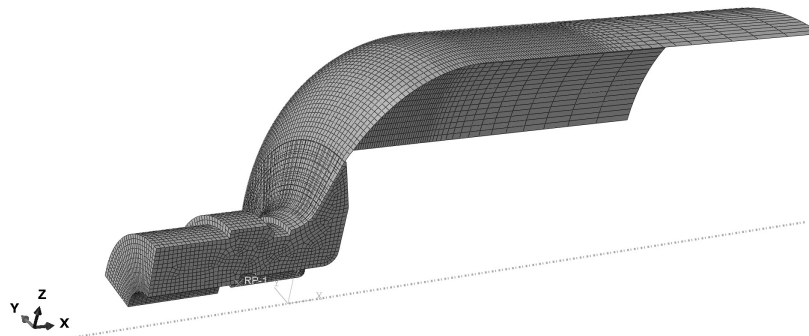


Figure 2.18: Shell element model mesh definition

### 2.4.2. Solid Model Implementation

The application of solid elements to the numerical description of CPVs was initially inspired by the results shown by Soriano and Nebe et al. [12, 27]. The necessity of capturing through thickness effects in, what can be defined as, thick-walled CPVs is even more clear when the context of the most usual stacking sequences is taken into account. As mentioned earlier, the severe loading case CPV structures are exposed to generally lead to highly asymmetric stacking sequences. These, if additional effort is not made to minimize through-thickness stress gradients, amplify through-thickness effects.

The solid elements used in the development of this model are C3D20R which is an the quadratic formulation of the C3D8R element with three translational degrees of freedom. This element brings the benefit of being able to depict through thickness stresses which are manifested as the translations of each individual node during loading. However, the formulation of the element assumes there are not rotational degrees of freedom - implying it overestimates stiffness in bending deformation. The elements used in this simulation use reduced integrations and, as a result can experience issues with hourglassing. However, hourglassing was not encountered to a noticeable degree within this study and the used mesh strategies. The quadratic formulation of solid elements was used in order to allow for better through-thickness mesh density which was difficult to control given the through-thickness geometry partitioning strategy.

The solid model is also strongly founded on Compositcad output. After geometry correction, the inner and the outer contour are exported and used to generate a single solid part. The solid part is then partitioned through-thickness and along the meridian and each section assigned the appropriate stacking sequence - layer orientations and thicknesses. Similar to the shell model described in the previous section, the number

of meridional sections is determined by Compositcad while the number of through thickness sections was determined by the user - at the time of writing, processes were established to partition the vessel through-thickness in the 2 partitioned sections.

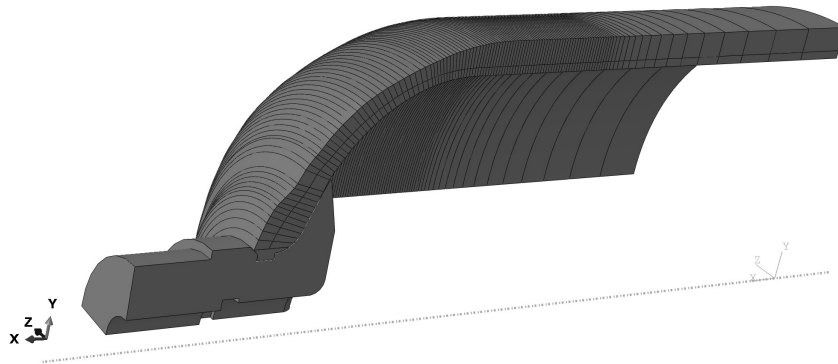


Figure 2.19: Solid element model defined in ABAQUS

Figure 2.19 shows the solid element model as is seen in the ABAQUS interface. The same boss end-cap model was used in the solid model as was used in the shell element model. The tip of the laminate length is not originally depicted by the Compositcad output. The Compositcad output does not fully extend down the length of the vessel inner contour. To eliminate the need for additional boundary condition definitions at the laminate end, the vessel surface was extended to fully adhere to the boss contour. The vessel tip was assigned pure matrix material properties. This was deemed to be a reasonable assumption since the number of layers that are present in that region of the vessel is relatively small and likely do not play a significant role in the vessel's structural integrity. Lastly, a depiction of the vessel mesh can be seen in Figure 2.20

Through a simple mesh refinement study, the decision to use fully integrated quadratic elements with one through-thickness partition was deemed to be suitable for the functioning of the models shown here. The use of quadratic elements, in combination with the partitioning, effectively allows for the evaluation of the vessel at 5 points through-thickness. The model contains 69,660 elements with 383,415 nodes and an average solving time of 30 minutes. More details on performance variation with respect to mesh variation can be seen in Appendix A

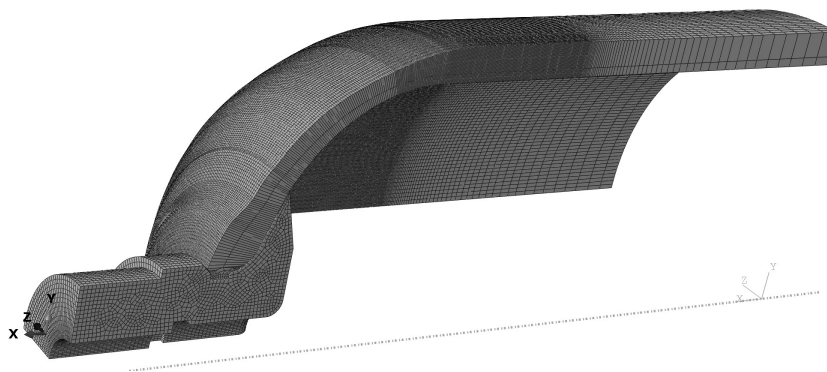


Figure 2.20: Solid element model mesh definition

## 2.5. Toward an Automated CPV Analysis Framework

The meaningful analysis of CPVs is a substantial task which lacks appropriate and structured definition. An additional goal of this study was to outline the potential processes required to establish a streamlined workflow in the numerical analysis of CPVs. This goal was a constant undertone during the development of the models described in section 2.4 and was seen as a valuable addition given the industrial context of the work presented here.

The strong bias towards keeping certain data structures easily interpretable and directly compatible on the outputs and data formats found in Composicad was a result of the heavy dependence of current CPV development on Composicad to define robot motions for filament winding. A result of centering further analysis processes around Composicad is a linear analysis process definition shown schematically in Figure 2.21

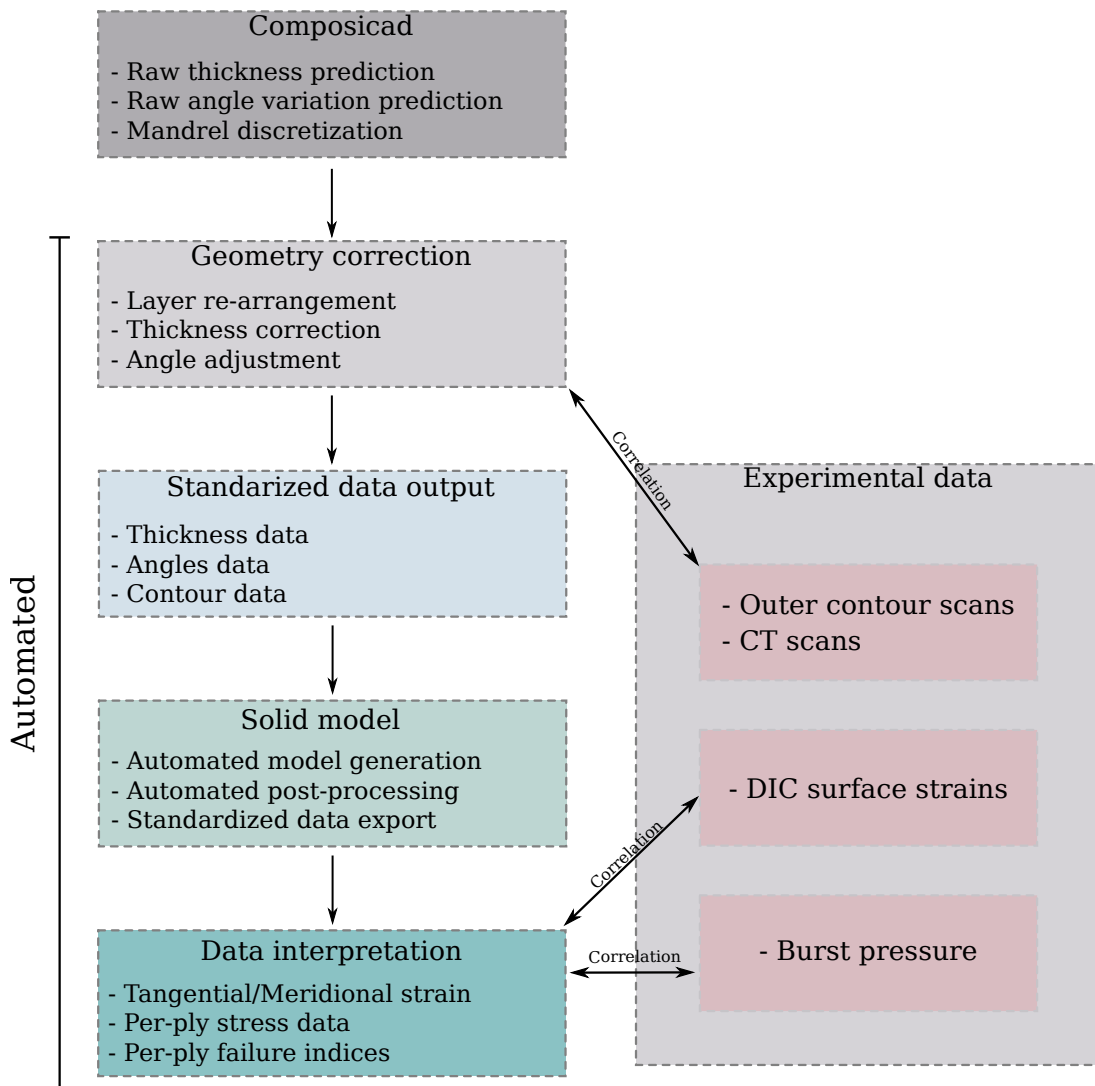


Figure 2.21: Overview of workflow from Composicad laminate definition to FE results

The chart in Figure 2.21 also highlights the main bottleneck for the full automation of CPV - Composicad. At the time of writing, this software had not been updated in years and with no indication of its inner workings moving into the open-source domain or at least for enabling some limited user-side automation. Nevertheless, Composicad has continued to define an industry standard in the field of filament winding and will likely continue to do so in the foreseeable future. Regardless, the analysis procedures of CPVs needs to become more streamlined if progress is to be made and compatibility with time efficient optimization methods is a

high priority in any engineering development process.

The work presented in this study regarding numerical modelling and geometry correction algorithm serves as an outline for how one of these processes may look like and highlights highly cost effective numerical solutions for the analysis of CPVs. In the future it is quite likely that the pre-processing steps shown in Figure 2.21 are to be replaced with more accurate, physical, models for thickness prediction that will be compatible with good CPV modelling practices. Furthermore, it should be made clear that the schematic shown is not a rigid one and that the implementation of an iterative process combining the fast modelling approaches presented previously with an optimization procedure can be made possible due to the time-efficiency between model generation and result generation.



# 3

## Experimental Plan & Results

The experimental characterization of CPV for the automotive industry is made complicated by the extreme operating conditions the structures are supposed to endure. An operating pressure of 70 MPa combined with the 2.25 safety factor results in very complex compositions of the orthotropic CFRP that they are currently made of. The facilities at Daimler AG are unique and offer the opportunity to do full-scale and sub-scale tests for custom manufactured CPVs while also allowing for a large amount of data collection for structural behavior characterization. In this chapter the experimental facilities used are first described. Afterwards, the rationalization and description of a comprehensive experimental plan aimed at investigating behavioral patterns in the cylinder-dome transition of CPVs is detailed. Finally, the results of the experimental plan are discussed and observations made.

### 3.1. Manufacturing and Testing

The facilities at Daimler AG offer an advanced towpreg filament winding facility and a unique test-bench capable of capturing an substantial amount of data on CPV behavior during pressurization. The manufacturing setup is centered around a KUKA KR-500, a 6 axis KUKA robot with a custom head attachment. The head attachment is a complex mandrel holder with built-in pressure outlets and an additional rotational axis to rotate the mandrel during winding. In front of the winding robot, a pillar with a hole running horizontal to the ground hold the eyelet in place. The eyelet on the pillar can rotate in order to allow for the deposition of fibers at certain angles. Behind the winding robot/pillar setup is the spool unwinding assembly where a set of controlled electric motors control the rate at which the spools are unwound and by doing so, regulate the tension of fiber application. An image of the manufacturing setup is visible in Figure 3.1. Throughout winding, the vessel mandrel is kept at a constant pressure to somewhat reduce liner deformation. After winding, the pressurized vessel is placed in an oven where it is cured at 170 degrees Celsius for 8 hours.



Figure 3.1: Robot-assisted filament winding system

Once a vessel is manufactured, it is tested in a one-of-a-kind burst chamber. A schematic overview of the burst chamber can be seen in Figure 3.3. The burst chamber is equipped with a total of 9 camera pairs distributed around the vessel at different heights. The camera pairs are used for the collection of DIC data and, when combined, provide full-field strain measurement of the CPV surface. The strain measurements produced are continuous along the surface and, at a frame-rate of one image per second, provide detailed description of outer surface strains at throughout the entire pressurization. Additionally, the chamber is equipped with 120 microphones distributed in a mathematically calculated array allowing for the collection and spatial localization of airborne acoustic emission data. The correlation of acoustic data is not the main focus of this study, but it should be noted that for all the tested vessels, acoustic data was collected - contributing to the constantly growing database of CPV acoustic behavior at Daimler AG.

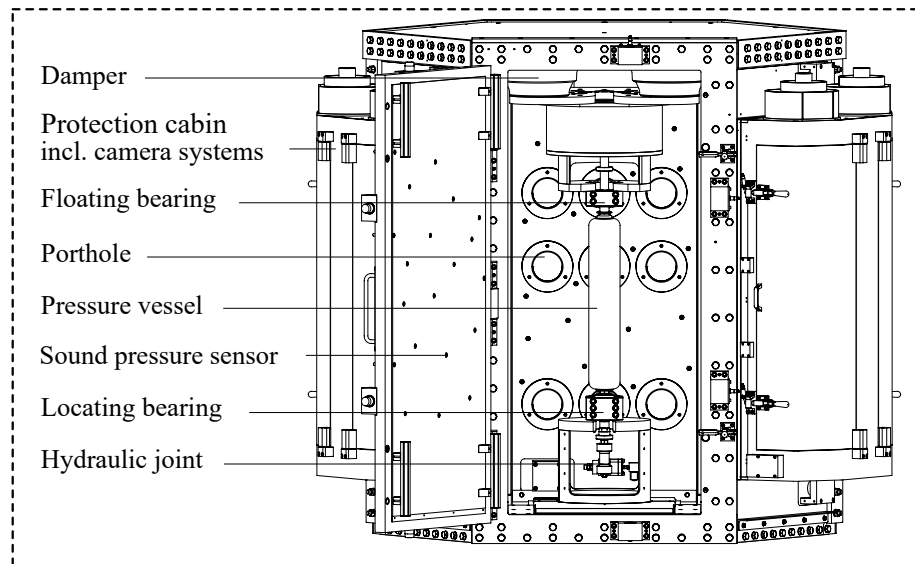


Figure 3.2: Burst chamber for the experimental characterization of CPVs

The DIC system present in the experimental testbench shown in Figure 3.3 operates by each camera pair measuring a segment of the CPV during pressurization at regular intervals. The sections are then assembled in 3D space using a industry standard software (GOM) in order to obtain a full 3D depiction of the deformations occurring in a CPV. For all the configurations present in this study, images of the vessels were taken once every second of pressurization. This corresponded to about a frame per 1 MPa of pressure increase. The data from the DIC measurements was extracted by evaluating tangential and meridional strains along a total of 15 lines spanning the length of the CPV - each side of the vessel containing a total of five lines. Due to the process with which GOM software generates data points along the lines, this resulted in each group of five effectively representing the average strain distribution along the length of each evaluated side of the vessel. The three sides were then averaged - resulting in a robust, representative measurement of the strains along the length of the tested **CPV**s. A schematic and graphical representation of the data provided by GOM is shown in Figure ??.

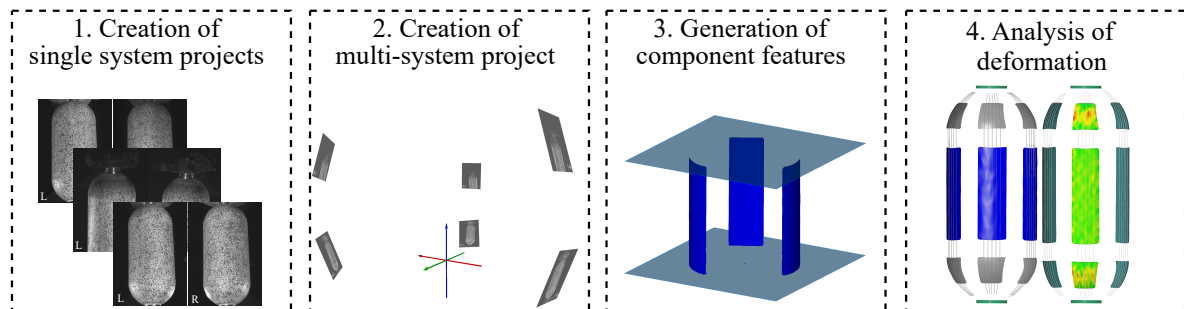


Figure 3.3: Data extraction methodology in GOM - Taken from [57]

## 3.2. Experimental Plan

The experimental plan and the numerical modelling represent the two main pillars upon which this study is founded. The setup was strongly inspired by the experimental work presented by Asijee [33] where the influence of stacking sequence on CPV performance was initially investigated using the same DIC test-bench as this study. That the cylinder-dome transition would represent a design critical region in pressure vessel development was an intuitively agreed upon fact, but its significance was quantified by Asijee [33]. The idea behind this study is to expand the data-set presented in [33] and apply a more focused approach to testing the cylinder-dome transition specifically in order to identify the interaction of two main variables:

### 1. Stacking Sequence

Due to the loading conditions of CPVs, the reinforcement distribution necessary to achieve structural integrity and safety usually results in asymmetric stacking sequences in the cylinder of the vessel. While the work presented by Asijee [33] describes observed effects of cylinder stacking sequence on CPV performance it also hints at non-negligible behavioral patterns in the cylinder-dome transition as a result of stacking sequence variation. This can easily be missed if the focus of a study is specifically the observation of average behavior in the cylinder region of the vessel since the symmetry of the cylinder would effectively cancel any bending-extensional coupling from occurring in the tangential direction. Where the bending extensional coupling is most expected is at the cylinder-dome transition as the symmetry of the vessel in the axial direction disappears and the asymmetry of the stacking sequence is free to manifest its mechanical response. It should be noted that a major purpose of this study is to provide additional data that will help in establishing whether the bending-extensional coupling is in-fact an observable phenomenon in CPVs of this type or if bending related phenomena observed previously are mainly caused by the geometric non-linearities inherent to these structures. Additionally, the variation of stacking sequence also has an effect on a variety of behavioral aspects of CPVs whose importance and impact on performance is not entirely understood. For instance, the placement of hoop layers through-thickness has a direct impact on the tangential deformation of the CPV. If the hoops are on the inside of the stacking sequence, the vessel will expand measurably less than if the hoop layers are on the outside of the sequence. This is due to the distribution of loads through-thickness in the cylinder during pressurization - the hoops on the inside are introduced to the load 'more efficiently' than when they are placed on the outside of the vessel stacking sequence. Another major parameter that may play a significant role in the cylinder-dome transition behavior is bending stiffness. Naturally, the stacking sequence directly determines the bending stiffness of the laminate. However, it is likely that the variation induced by stacking sequence manipulation also impacts the resulting deformation of the region under similar loading circumstances. It is complicated to make any real claims with certainty on what the exact importance and impact of each of these effects is which is why experimental studies are of crucial importance for the building of understanding on CPVs and their mechanical response.

### 2. Tangential Stiffness Variation Along the Meridian

That the tangential reinforcement varies in the cylinder-dome transition as a result of stacking sequence configuration was presented initially by Asijee [33] who noticed minor variations in CT scans of the vessels tested. Figure 3.4 shows a images cut-outs of a few representative configurations discussed in [33] where the difference in tangential reinforcement extent can be clearly examined by comparing the distance from the reference line to the tip of the hoop group/s extent into the dome region. Variation in meridional strain distribution of the 3 vessels can be seen next to the cut-outs. This points towards the necessity of examining the impact of varying tangential reinforcement extent in the cylinder-dome transition since the differences in response of each vessel make it difficult to claim that any one effect is taking precedent in causing the behavior observed.

That the meridional variation in tangential stiffness may contribute significantly to the overall behavioral patterns of CPVs was also pointed out by Soriano [27] who varied the hoop ply drop location and examined the tangential strain distribution of one of the configurations seen in Figure 3.4. The purpose of the experimental set executed as a part of this study is to provide a more refined description of the dominant effects that play a role in determining the behavioral response of CPVs. Figure 3.5 shows an overview of the configurations developed for this purpose.

Two baseline configurations are developed that applied relevant changes to the configurations used in [33] and aimed at improving the observability of effects in the cylinder-dome transition. The two baseline

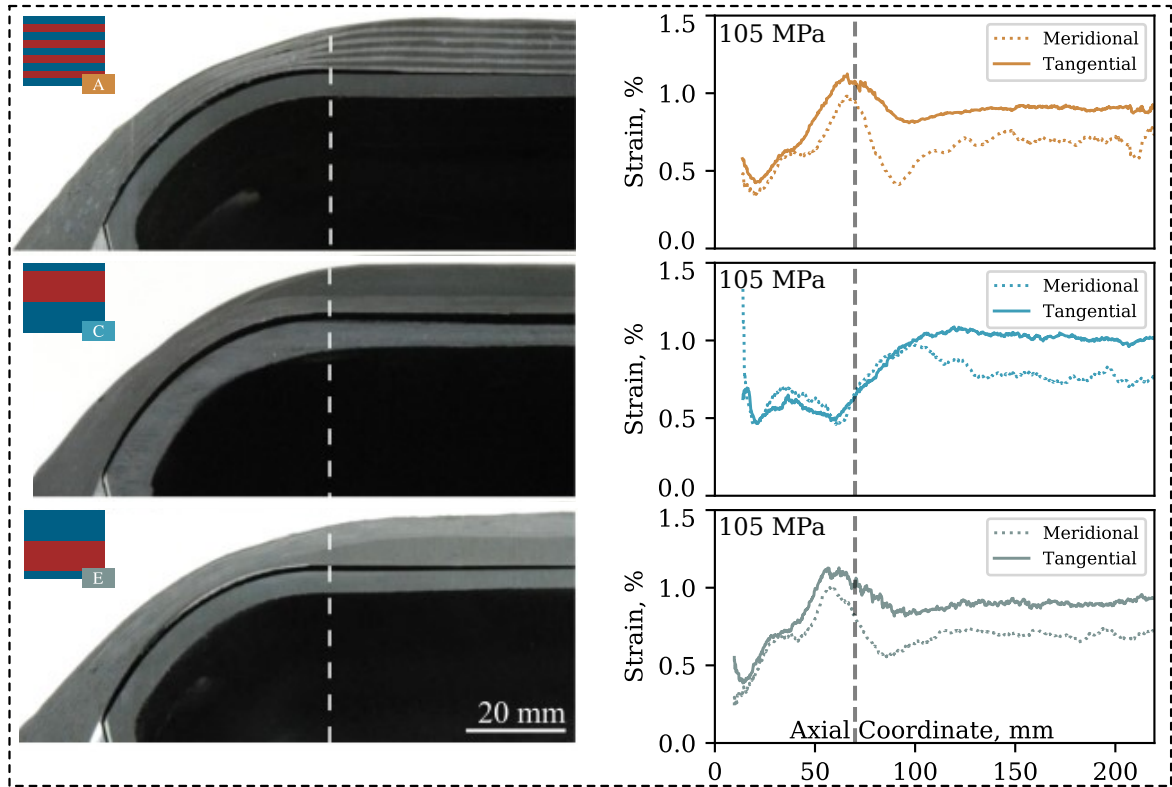


Figure 3.4: Variation in hoop group tapering between select configurations used by Asijee [33]

configurations are dubbed *BL* and *BC* where *L* symbolically stands for *legacy* as the overall distribution of layers and the hoop group extension/tapering was inherited from the best performing configuration in [33]. In *BL*, all but one low-angle helical layer is wound onto the mandrel followed by all the hoop layers. *C* in *BC* stands for *conjugate* as it represents a setup identical to *BL* in composition but produces an exactly opposite bending-extensional response to *BL* by inverting the stacking sequence - meaning that all the hoop layers are wound prior to all the helical layers. These two configurations present a baseline for the configurations aimed at investigating the changes in vessel response as a result of tangential stiffness variation. These configurations are dubbed *BL6*, *BL12*, *BC3* and *BC9* where the two letter code is the identifier of the stacking sequence and the number represents the distance *a* marked in Figure 3.5 which denotes the amount, in millimeters, by which the hoops were retracted towards the cylinder.

The main difference between the configurations presented here and the ones used in [33] is the introduction of high-angle helical layers. The decision to introduce additional layer groups to the stacking sequence was inspired by a couple factors. First, the observations made by Asijee [33] that can also be seen in Figure 3.4 where the variations in strain measurement between configurations is of such magnitude that making a conclusive remark on the influence of stacking sequence is difficult. The sensitivity in that study likely stemmed from the fact that only two layer orientations were used which increased the sensitivity of the vessel to variation in hoop drop-off location. The inclusion of high-angle helical layers allows for the gradual deposition of tangential material in the dome region of the vessel - helping 'normalize' the response in the cylinder-dome region between configurations and making comparison easier. This also goes hand-in-hand to allow for better comparison between configurations where the tangential reinforcement distribution in the cylinder-dome region is varied. Second, the introduction of high-angle helical layers provides an overall improvement of through-thickness stress distribution since it introduces intermediate layer orientations between low-angle and hoop layers. Previous studies that mostly focused on using two orientation groups in their configurations identified delaminations at the hoop-low-angle helical layer as the potential source of failure [47]. The introduction of high-angle helical layers can help reduce delamination-related damage progression. Additionally, the high-angle helical layers also play a significant role in expanding the design envelope. While the purpose of this study is not necessarily to examine the design envelope of any particular CPV configuration, the results presented here provide insight into the introduced interactions caused

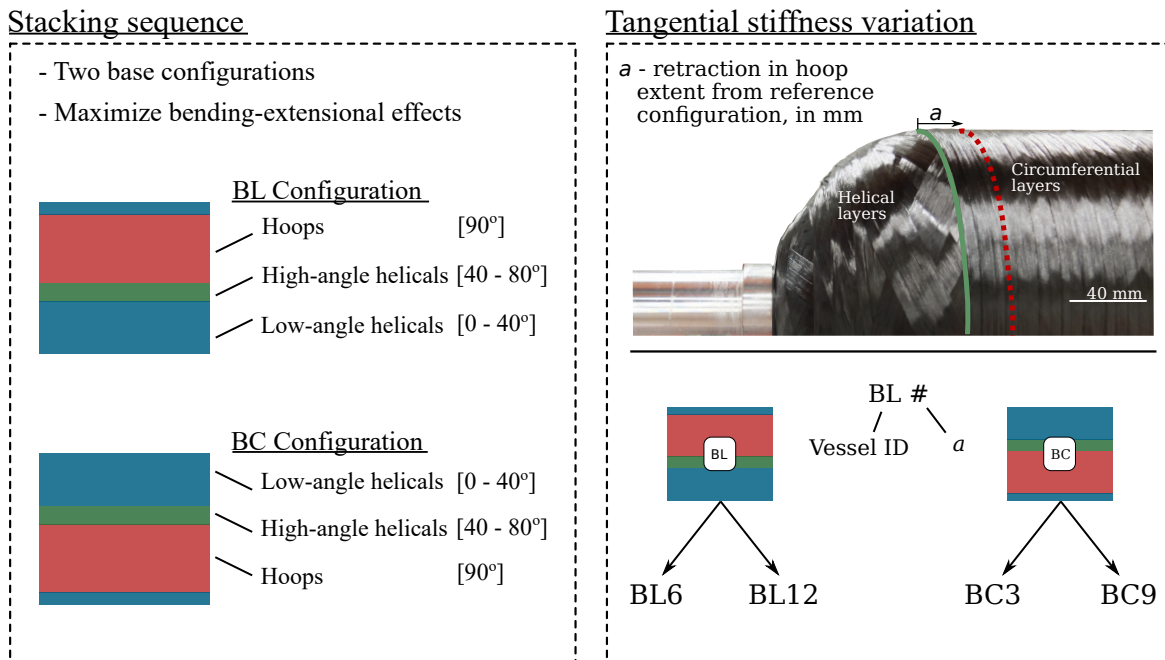


Figure 3.5: Overview of experimental configuration definition

by the presence of multiple layer orientations. Likewise, the geometry correction algorithm and its applicability to the manufacturing setup used at Daimler AG is also portrayed better since it can be tested against configurations with more than two orientations.

Of the total six configurations described, three samples of the configurations *BL*, *BL12* and *BC3* have been manufactured while one of each of the others was manufactured. The repeated vessels were chosen based on a pre-investigation in which all six configurations were manufactured and tested in order to make a preliminary observation of the magnitude of observed effects and results. These configurations were manufactured in multiple samples to allow for statistical analysis that would aid the results discussion later on. An additional overview of all configurations used together with a brief explanation of nomenclature is shown in Appendix B.

### 3.3. Overview of Result Consistency

Figure 3.6 demonstrate the reproducibility of results among repeated vessel samples. Ample care was taken to ensure that the manufacturing process of each vessel was as consistent as possible in order to minimize the possibility of external factors causing a significant change in vessel response. As a result, the consistency in measured response between any two repeated vessels is very high. The general response of each vessel in any repeated set is within the scatter of every other vessel in the same repeated set. This result gives legitimacy to the results of other vessels in this dataset which only had one copy manufactured.

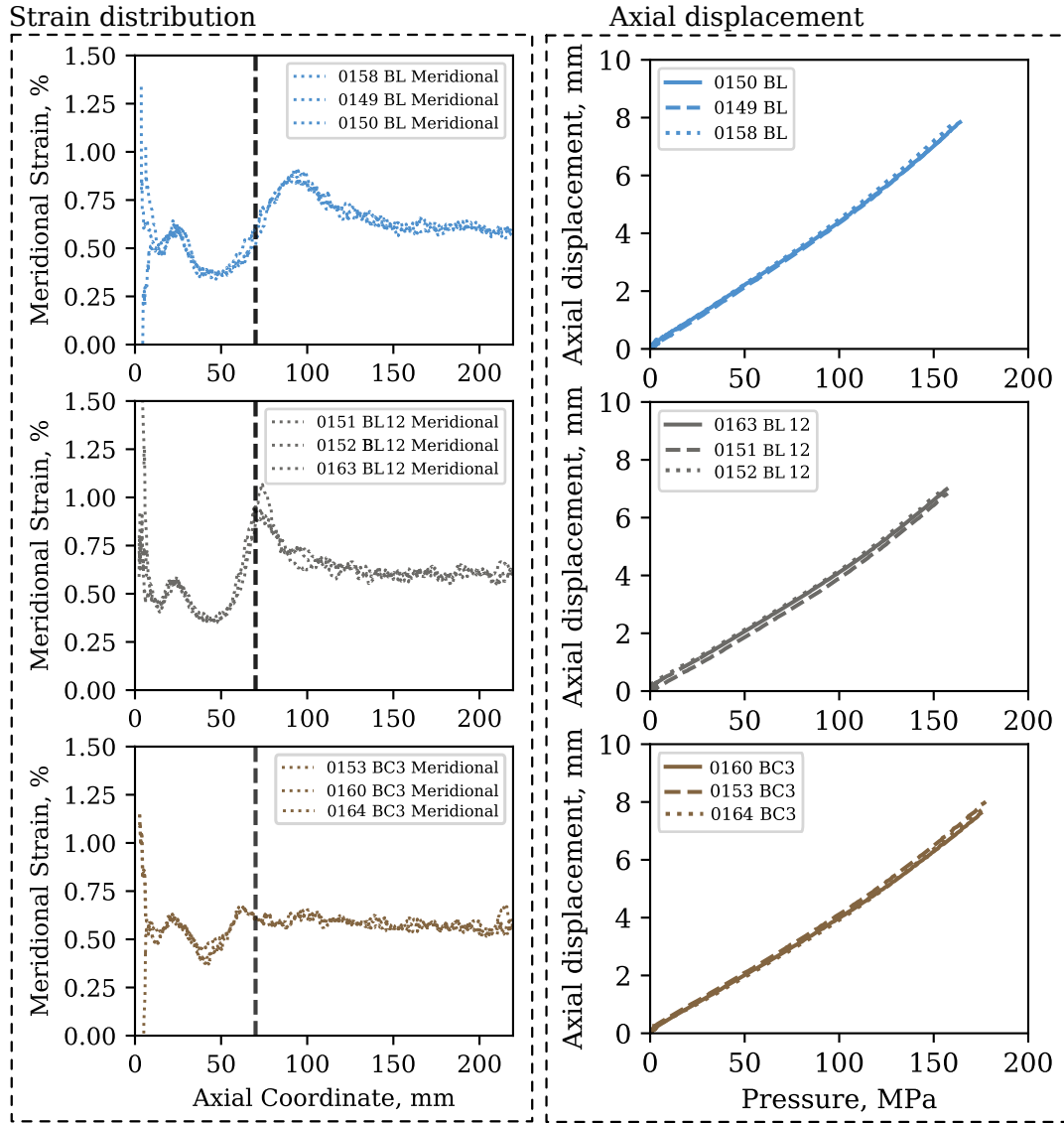


Figure 3.6: Overview of strain distribution and axial displacements for repeat configurations

### 3.4. Effect of Stacking Sequence Variation

The variation of stacking sequence has a variety of effects on the behavior of CPVs. These effects are manifested in overall mechanical response and highlight the criticality of specific design regions within a vessel. In particular, the variation of through-thickness positioning of hoop layers has an impact on the tangential expansion of the cylinder during loading. Additionally, varying the through-thickness position of the hoop layers within the laminate can directly influence the bending-extensional coupling response of the cylinder stacking sequence. This effect is most likely to manifest at the cylinder-dome transition since symmetry conditions diminish around it. The impact of stacking sequence variation is most readily observed between configurations *BL* and *BC* - shown in Figure 3.7.

Figure 3.7 shows the comparison of tangential and meridional strains in *BL* and *BC* vessels of the experimental set. Expectedly, the tangential strains in *BC* are noticeably lower than in *BL*. This is a result of load distribution through-thickness in the cylinder. In *BL*, the loads are first applied through the mass of low-angle and high-angle helicals and then transferred through to the hoop layers - which lowers the stress introduced to the hoop overall in comparison to *BC*. Contrarily, the *BC* configuration exposes the hoop layers to the load case first. Since the hoops are most effective at carrying tangential loads, they are loaded more than in *BL* and, logically, the helical layer mass is loaded comparatively less. This behavior was expected as it was also described by [33]. The introduction of high-angle helicals to the experimental set in this

study yielded the desired result - a relative normalization of the trends in the cylinder-dome transition. The cylinder-dome transition was a difficult area to compare in previous studies since configurations comparable to *BL* and *BC* had a severely different response - mainly *BC* equivalent configurations showed a large localized increase in tangential strains due to a lack of tangential reinforcement. This issue is virtually eliminated in the cases presented in this study. The general trends between *BL* and *BC* are fairly consistent and, disregarding the overall difference in magnitude in tangential strains, show a continuously decreasing strain around the cylinder-dome transition. Despite the intended impact of high-angle helical layer being fulfilled, the interpretation of the results presented in Figure 3.7 is not so trivial. While it is likely that the difference in bending-extensional coupling has a direct influence on the differences in the meridional strain between *BL* and *BC*, it is unknown what impact the difference in tangential strains has on determining the meridional strain trends. Here it is convenient to highlight the uniformity in cylinder meridional strains in both configurations since it highlights the possible role the tangential strain may have in "pulling" the meridional strains in the cylinder-dome transition. Additionally, it is nearly impossible to tell what the impact of the small differences in internal contour between the two configurations have on the mechanical response of the vessel. It should also be noted that the data presented in Figure 3.7 compares vessel deformation at 105. MPa. Given the differences in stacking sequence present in the two configurations, the damage progression is substantially different between the two. Namely, the fact hoops being placed on the outside of the stacking sequence in *BL* implies there is interfiber damage development in the helical layers under the hoop layers - causing a noticeable increase in loading presented to the hoops during pressurization. This effect was demonstrated through sophisticated numerical models by Soriano [27].

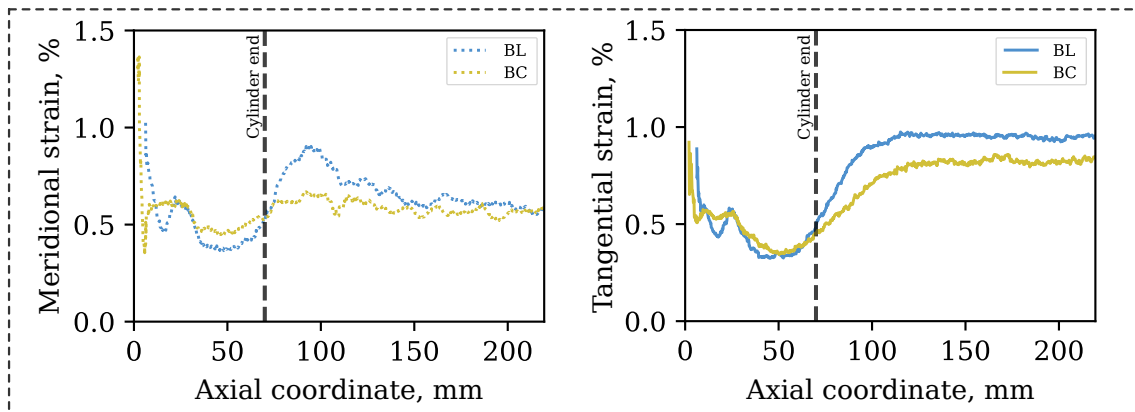


Figure 3.7: Strain measurement comparison of *BL* and *BL* configurations at 105 MPa

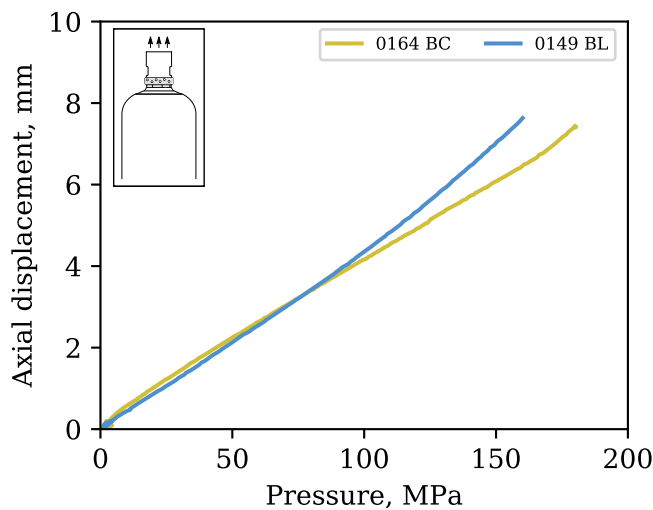


Figure 3.8: Axial displacement comparison of *BL* and *BC* configurations

Figure 3.8 shows the comparison of measured axial displacement between *BL* and *BC* cases. The immediately obvious is the inherently different axial extension trends between the two vessels. Where the slope of *BL* is consistently increasing with increasing pressure while the slope of *BC* varies with increasing pressure and only shows an increasing trend after 100 MPa. This difference is most likely related to the mechanical response described by external strain variation in Figure 3.7. The relatively larger meridional strain measured around the cylinder dome transition causes a larger axial extension to be measured in the *BL* case at earlier pressures. The exact impact of differences in axial displacement on burst performance is not entirely understood so it is not clear whether one of the other behavior is strictly beneficial. However, a general note in the context of product design can be made. The axial elongation of the vessel will play an important role in the viability of any given vessel design. A CPV must fit into a predetermined operating space within the vehicle and therefore cannot expand more than whatever the design margin allows for. With the two cases presented here, it is difficult to say which behavior is preferable since, at operating pressures of 70 MPa, both vessels expand similarly. One could argue that were operating pressures for CPVs to increase in the future, *BC* extensional behavior would be preferable as there is a significant difference in axial extension in the +100 MPa range.

### 3.5. Effect of Tangential Stiffness Variation

The potential impact of sensitivity to tangential stiffness variation was briefly discussed by Soriano [27] by a variation of hoop placement in CPVs with only two layer orientations (low-angle and hoop layers). The introduction of high-angle helicals in this experimental set allowed to investigate the impact of tangential stiffness variation around the cylinder-dome region while preserving comparability of results between configurations. The retraction of hoop layers from the cylinder-dome region is expected to cause a local increase in the tangential strains since the most tangentially stiff part of the structure is being removed from a region of the structure under sever tangential loading. Additionally, the retraction of hoop layers from the cylinder-dome region would presumably highlight the relative importance of specific loading elements that act in the cylinder-dome region. More specifically, the region is exposed to a highly complex loading case where tangential and axial loads of a pressurized shell are combined with bending loads stemming from the geometric non-linearities of the structure. These two are then compounded with the inherent bending-extensional response of the cylinder's stacking sequence. The combination of these three effects results in a design critical region the understanding of which can contribute greatly to the design strategies of CPVs. Figure 3.9 shows a comparison of the mechanical response of the *BL* sequence where hoops were retracted from towards the cylinder by 6 and 12 mm from the reference *BL* configuration.

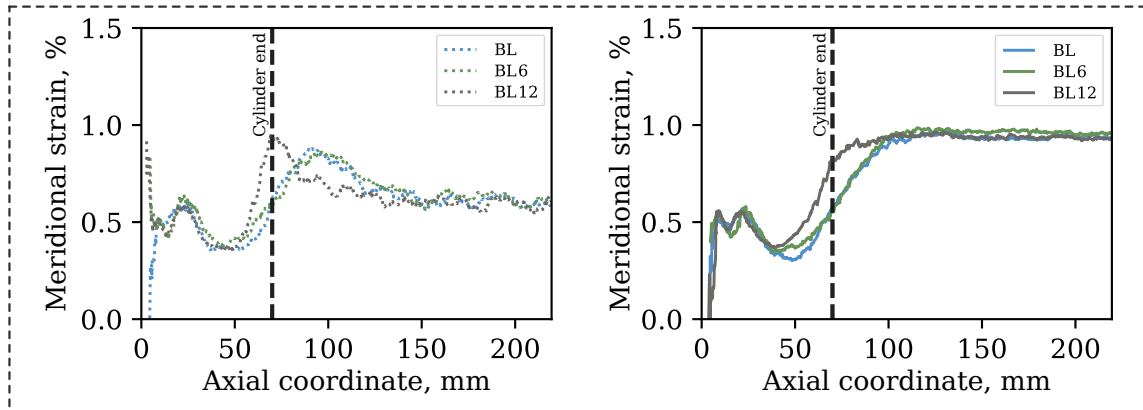


Figure 3.9: Strain measurement comparison of *BL* sequence configurations at 105 MPa

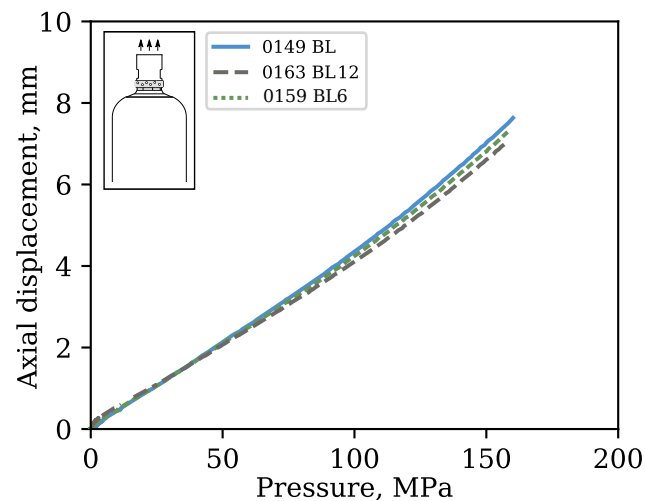


Figure 3.10: Axial displacement measurements of BL sequence configurations

The apparent increase in tangential strains in the cylinder-dome region is apparent in Figure 3.9. Interestingly, the differences between *BL* and *BL6* are rather small and highly localized to the region around axial coordinate 50. The expected increase in tangential strains is unambiguously clear between *BL* and *BL12* where the entire cylinder-dome region experiences a substantial increase in tangential strains. The meridional strains provide insight into an interesting occurrence. All three configurations have the same general trend in meridional strains. However, there is a distinct shift and increase in magnitude in global maximum measured in the cylinder-dome region between *BL* and *BL12*. The increase in magnitude is somewhat expected as a result of increased tangential strains. However, the maximum of meridional strains is seen to shift towards the cylinder-dome by retracting the hoop group away from the region. This result implies that, in relative terms, the geometrical bending loads present in the region are more severe than the bending-extensional coupling effects that are inherent to the stacking sequence of the cylinder. If the bending-extensional coupling effects were more significant, it would have been expected for the maximum meridional strain to shift towards the cylinder - closer to the edge of the complete cylinder stacking sequence. However, the exact opposite is observed and the maximum shifts towards the cylinder-dome joint which, generally, experiences the largest bending loads due to the geometry of the ellipsoidal end-caps. A relevant conclusion that can be extracted from this observed behavior is on the fine relationship between tangential stiffness, deformation, geometrical bending loads and resulting behavior. Removing tangential stiffness where it is needed results in a larger tangential deformations in the region - which increases the localized bending of the region. The increase in deformation and localized bending in the region causes an increase in damage which in turn causes an increase in deformation. This presents a positive feedback loop which effectively makes the need to account for loads stemming from geometry more relevant in design than the inherent laminate response resulting from stacking sequence.

The axial displacement comparison of the *BL*, shown in Figure 3.10, sequence is in line with expectations and follows closely the general trends described by Asijee [33]. All three vessel configurations show a monotonically increasing axial displacement with increasing pressure. The relative relationship between axial displacement at burst and the tangential stiffness variation is clearly exhibited with a gradual decrease within the sequence - *BL* being highest and *BL12* being lowest. This was expected since the removal of hoop layers from the cylinder-dome transition allows for relatively large localized expansion in the cylinder-dome region which promotes a bulge-like formation and acts to decrease the axial displacement of the boss ends.

The second sequence of configurations, as shown in Figure 3.11, describes the differences in behavior between *BC* cases at 105 MPa. Putting these results in context to the results in Figure 3.9 allows for the identification of comparable trends. The retraction of tangential reinforcement in the *BC* case, expectedly, shows the same type of increase in tangential strains around the cylinder-dome region. An interesting note is that for a comparatively smaller retraction of the hoops group, the increase in tangential strains measured in the region is significantly higher in the *BC* sequence than in the *BL* sequence. The impact on the meridional strain behavior is in line with what the observations made in the *BL* sequence - where the gradual retraction of tangential reinforcement causes a peak that tends towards the cylinder-dome joint. The formation of the global maximum in that region is caused by a combination of the bending loads and increase of tangential

strain to the region.

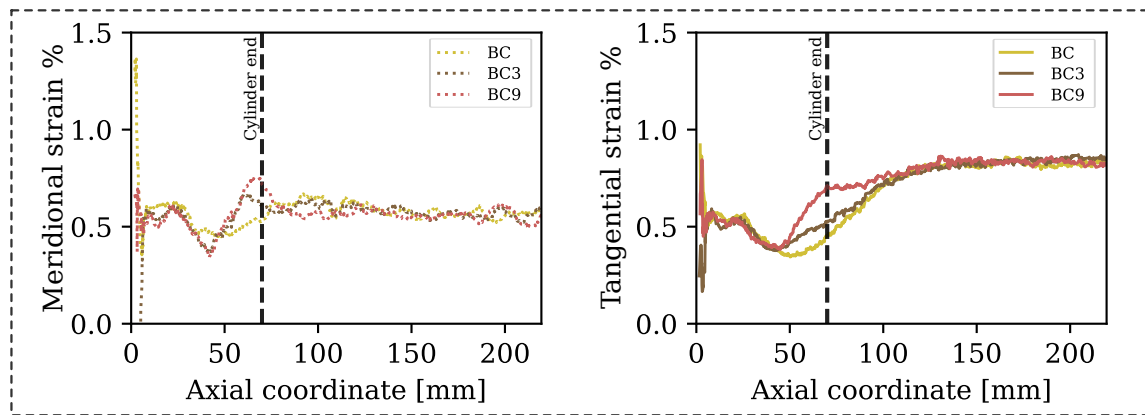


Figure 3.11: Strain measurement comparison of BC sequence configurations at 105 MPa

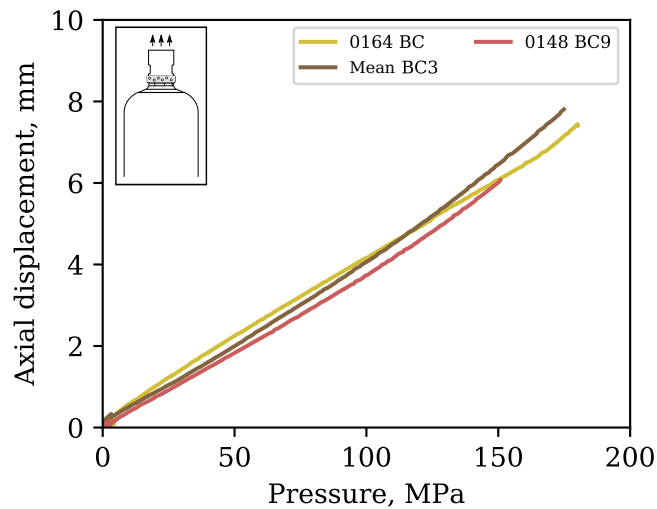


Figure 3.12: Axial displacement comparison of BC sequence configurations

The axial displacement comparison of the *BC* sequence shown in Figure 3.12 provides insights into correlating meridional and tangential strains to the axial displacement of the vessel. This is mainly exhibited by the differences between configurations *BC3* and *BC9*. *BC9* experiences a local increase in tangential expansion around the cylinder-dome transition which is manifested as generally lower axial displacement of the vessel ends. The same conclusion cannot be made for the *BC* case since its axial displacement behavior appears to be fundamentally different from the other two. Cases *BC3* and *BC9* show the same trend as *BL* with a constantly increasing rate of change in axial displacement. *BC* on the other hand shows a variation in the slope which is not readily explained from the observation of the strain distribution throughout pressurization. This can be interpreted by concluding that cylinder-dome transition deformation patterns have a significant impact on the resulting axial displacement response. The result is intuitive since it should be possible to relate meridional strains to axial displacement - where larger meridional strains would imply larger axial displacements. The variation in slope in the *BC* case is seen to take place around 100 MPa. After thorough analysis, there was no identifiable features in the strain fields that could be used to justify this variation in axial displacement rate.

### 3.6. Burst Performance Analysis

While the measurement of strain distribution and axial displacements can provide valuable insights into the mechanical response of CPVs, little can be said about relevant vessel performance without taking into consid-

eration burst pressure. Burst pressure allows the engineer to explicitly contextualize a vessel's performance relative to current standards. The burst pressure of all the vessels tested in this study was recorded in order to allow for relative analysis and the identification of trends within the tested configurations. Table 3.1 provides an overview of recorded burst pressures for all vessels within the *BC* and *BL* sequences. The mean column in Table 3.1 highlights the performance consistency of repeated samples since the standard deviation for repeated configurations was low.

The burst pressure measurements of this experimental set yielded highly unexpected results. Due to the large amount of data available before the vessels presented here were tested, it was reasonable conclude that the relative performance between the two baseline configurations would resemble the results presented by Nebe et al. [47]. In [47], configurations *C* and *E* (shown in Figure 2.12) are equivalent to the *BL* and *BC* configurations of the current experimental set due to their relative positioning of a single hoop group in the laminate. In [47], configurations *C* had a significantly higher burst pressure than *E*. When comparing the burst performance of the configurations in this study, configurations *BC* is found to have approximately 15.5 % higher than *BL*. This result is perhaps the most solid evidence that the high-angle helical layers were introduced to the tested configurations since the configurations in [47] were heavily influenced by the tangential stiffness variation in the cylinder-dome transition.

Matters are made more curious when the trends within *BL* and *BC* sequences are observed. Figure 3.13 shows a scatter plot relating measured vessel mass to recorded burst pressure. The plot shows a variation in vessel mass for repeated samples. The mass for a single vessel configuration was found to vary up to 4.5 % for *BC3* configuration. The exact source of this error is difficult to pinpoint since the winding programs for each vessel were identical between samples and all vessels in the set were manufactured using the same material batch. Regardless, there is no apparent correlation between mass increase and recorded burst pressure within repeated sample which is why this variation was not taken into account as impactful. A peculiarity to note is that only one sample in each repeated sample group has what seems to be an outlier recorded mass. It is possible that user error of the measuring device occurred causing the increase. This is not highly likely since the three outlying samples were not all manufactured and measured on the same day but is a source of error that should not be entirely eliminated. Analyzing the clustering of vessels in Figure 3.13 allowed for the observation of a substantial difference in behavior within the two sequences.

Table 3.1: Overview of recorded burst pressure results

Vessel	Burst pressure, MPa	Mean $\pm$ sd, MPa
BL	162.7	163.3 $\pm$ 1.3
	165.1	
	162.0	
BL6	163.9	163.9
BL12	158.5	160.2 $\pm$ 2.8
	158.0	
	164.2	
BC	188.7	188.7
BC3	177.2	177.8 $\pm$ 1.1
	176.9	
	179.3	
BC9	152.6	152.6

It was noted that the maximum and minimum recorded burst pressure varied by 25 % in the *BC* sequence and by only 1.9 % in the *BL* sequence. This difference was further visualized in Figure 3.14. This result holds great implications on vessel design since it implies that certain vessel configurations can yield a significant increase in performance at the expense of manufacturing robustness. The *BL* sequence burst pressure was found to be fairly stable within the entire experimental set, while the *BC* sequence burst pressure varied largely for smaller relative changes in tangential stiffness around the cylinder dome transition.

Representative photos of the remnants vessels *BL* and *BC* can be seen in Figure 3.15 - the effective disintegration of the cylinder with neatly expanded domes is highly indicative of cylinder-based failure. Both vessels *BL* and *BC* are considered to experience cylinder failures. With this in mind, an initial inspection would lead one to believe that the cylinder strength reduced between *BC* and *BL*. While this argument is not unreasonable, it is likely not the cause of the recorded difference in burst pressure. As discussed earlier

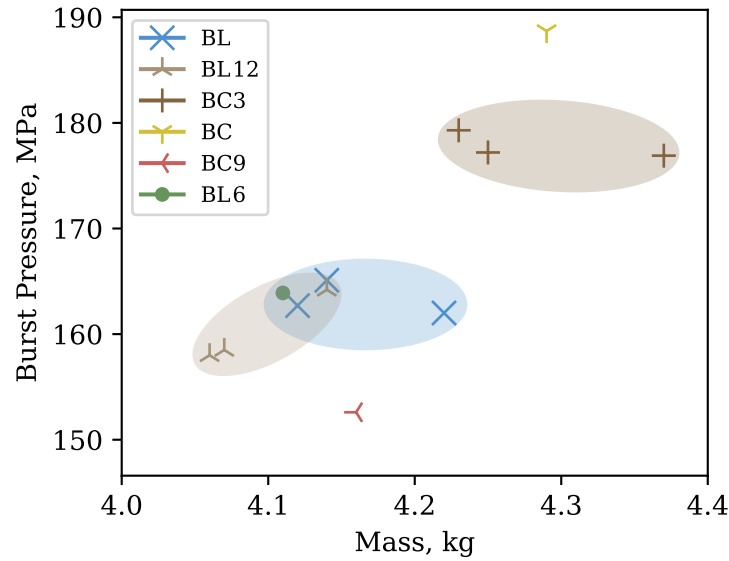


Figure 3.13: Overview of recorded burst pressure of tested vessels

in Chapter 2, changing the distribution of layers in a CPV directly impacts the compaction of said layers as well as damage development during pressurization. A higher compaction invariably implies a higher fiber volume fraction which could cause an increase in burst performance. However, it is difficult to measure and even more difficult to predict the fiber volume fraction changes through-thickness in a CPV. The variation of through-thickness properties is very small and highly contextual and dependent on manufacturing and environment parameters such as temperature during winding, tension, resin properties, etc. It is far more likely that the introduction of high-angle helical layers will have played a more significant role in determining the final burst pressure of the vessel. The potential criticality of high-angle helical layers will be further discussed in Chapter 4 with reference to predictions made by developed models. Of course, due diligence needs to be given to damage development patterns in both configurations where the *BC* configuration is perhaps more likely to fail at a later stage since its hoops are more directly exposed to tangential loads and 'shield' the other angles from excessive damage development. In the *BL* case the interfiber damage progression in the helical layers is likely to be a source of load increase on the hoop layers since *BL* is comparable in constitution to the *B+* case from [27].

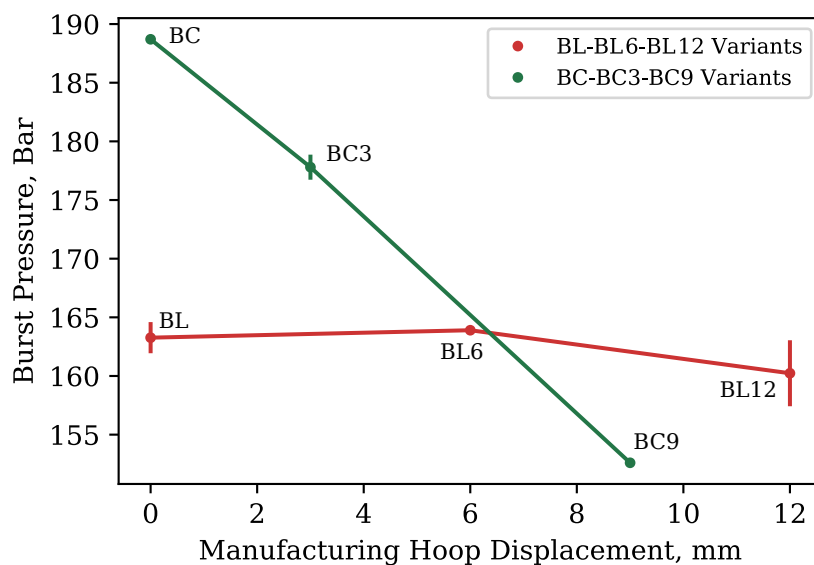


Figure 3.14: Recorded difference in impact of tangential stiffness variation on burst pressure performance

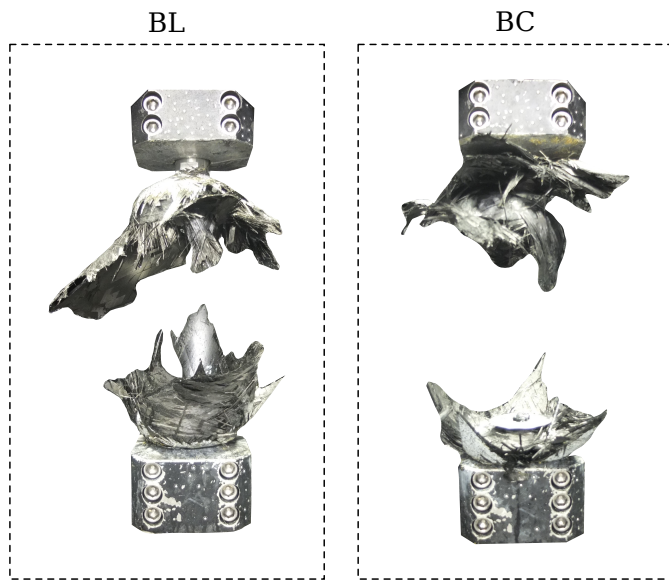


Figure 3.15: Photos of vessels after burst - *BC* and *BL* configurations



# 4

## Evaluation of Numerical Modelling Methods

The value of FE models only becomes visible through meticulous correlation with experimental results. The privilege of the study presented here is that it had access to a rather large dataset of previous experimental data and state-of-the-art test facilities which allowed for a comprehensive evaluation of the modelling efforts developed in tandem. The solid and the shell element models were compared to data gathered through the experimental part of this study.

The two models developed were compared to experiment through outer surface strains and burst pressure where a rudimentary estimate of burst pressure was made based on FPF. The limitations inherent to the thickness correction model were highlighted through the result comparison and a brief analysis was provided highlights the impact of a major assumption made in the geometry correction algorithm - constant inner contour. The following chapter provides an overview of experimental correlation and discussion on performance, sources of error and future outlook.

### 4.1. Shell Model Performance

CPVs manufactured for this experimental set fall well within the definition of thick laminates for CPVs as derived by Parnas and Katirci [31]. The laminate thickness for the specimens within this study goes to invalidate the use of elements constrained by the plane stress assumption. However, the development of a fully parametrized shell-element model such as the one described in Section 2.4 was motivated by previous studies that attempted developing a shell-element model without thickness correction [33]. Application of the developed thickness correction algorithm to a shell-element model yielded significant improvements in the prediction of general trends of CPVs. The a comprehensive overview of the model performance relative to DIC data is shown in Figure 4.1 which depicts the shell model predictions compared to measured vessel behavior at a pressure stage of 105 MPa for each vessel in the two main sequences of the experimental plan.

The shell model, is observed to have significantly improved by the addition of the thickness correction algorithm. Though regularly over-estimated, the general trends in tangential strains are consistently predicted by the shell model regardless of the configurations in question. The meridional strain, in contrast, are always underestimated. Additionally, the meridional strains are less accurately predicted than the tangential strains. The dome region and its non-linearities, when combined with the errors inherent to the thickness correction algorithm and the plane stress conditions result in an overestimation of response by a large margin - especially around the 150 mm axial coordinate. The shell model prediction seems to be generally more stable in the *BL* sequence than in the *BC* sequence where the dome region demonstrates significant deviation from measured strain trends. Two features demand attention - the apparent strain maximum at around 150 mm axial coordinate and the harmonic instability that follow it. The source of the harmonic instability was related to the ply drop-off of high-angle helical layers. Throughout testing, minor adjustments in the high-angle helical polar opening thickness build-up yield significant changes in the region. Since the shell model was relatively quickly supplanted by the solid model, the adjustment of high-angle helical layers to minimize these discrepancies was not seen as necessary.

The discrepancy in cylinder strain magnitudes can be linked to two major factors - thickness prediction

without material property correction and plane stress condition. The error in cylinder tangential strain prediction seems to increase between *BL* and the *BC* series. However, one should note that the predicted nominal cylinder strains in both series remains the same - a direct manifestation of the plane stress condition. In reality, the placement of the hoops will play a significant role in the cylinder expansion of a CPV as a result of load distribution. Since the shell model cannot account for the through-thickness variation of stresses in the cylinder, both cases have the same nominal cylinder strain, and logically the *BC* series is seen to have a larger error in cylinder strain. Additionally, the fact that strains are overestimated is not intuitive at first given that damage progression is not being taken into account. The reason for strains being consistently over-estimated lies in the thickness correction algorithm which, while accounting for layer compaction, does not account for fiber volume fraction variation and the resulting change in material properties per ply. Effectively, the thickness correction algorithm removes material in the interest of maintaining an accurate depiction of the vessel's outer contour underestimates the amount of reinforcement in the vessel. Overall, the marked improvement in performance of the shell model compared to previous studies is perhaps overshadowed by the aspects it still struggles to capture. It is evident that, while a reasonable representation of general trends in strain can be captured with shell-element based models, it is necessary to capture through-thickness effects in order to evaluate configurations of fundamentally different through-thickness configurations.

The discrepancy in the meridional strains is more difficult to pinpoint to a particular phenomenon. It was expected for the meridional strains to be consistently underestimated since damage is not considered. However, the inclusion of the imperfect thickness correction algorithm adds complexity to simply saying that the including damage progression would yield the 'correct' result. While accounting for damage would certainly improve the observed result, it is likely that the result is also influenced by some inaccuracy in the layer thickness prediction as well as inaccurate property depiction in the laminate. The low-angle helical layers are predicted to not compact as significantly as the hoop layers - this likely results in the geometry correction algorithm to not underestimate the amount of material in the low-angle helicals. Assuming material mass and properties were adequately accounted for, the inclusion of damage progression would certainly yield an improved result. Especially, in the configurations in this study since they contain high-angle helical layers where the matrix load bearing component becomes more important for parts of the laminate as discussed in Nebe et al. [12].

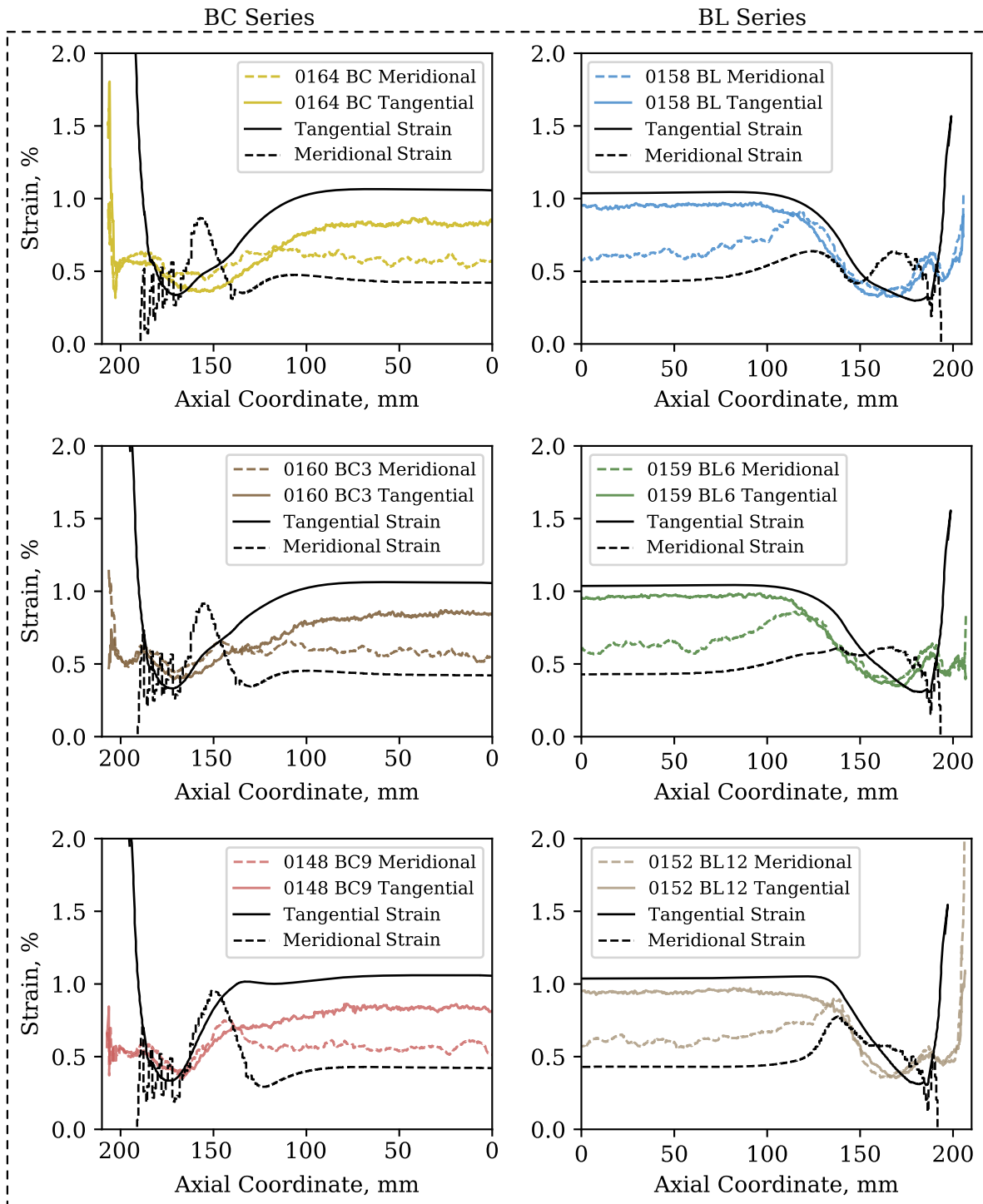


Figure 4.1: Overview of shell model predictions

## 4.2. Solid Model Performance

The use of solid elements provides the ability to account for through-thickness effects. As discussed in Subsection 2.4.2, solid elements have translational degrees of freedom but do not have any rotation degrees of freedom - making them overly stiff in bending. Figure 4.2 shows an overview of solid model predictions for the experimental set developed in this study. At first observation, the difference in performance between the shell model and the solid model is subtle, but the ramifications of the differences are substantial and imply a major improvement and potential for future development in the solid model.

The general depiction of tangential strains in the solid model closely resembles experiment and a major point that requires highlighting is the difference in predicted cylinder tangential strains between *BC* and *BL* sequences. The ability of the model to capture the through-thickness stress distribution causes the general trend of lower tangential expansion to be captured between the sequences. The error between measured and predicted is still seen to increase but by a smaller amount than in the shell model. The error increasing between the two sequences is still a result of thickness correction without material property adjustment which causes an effective underestimate of material present in the vessel as discussed previously. The meridional strain prediction is seen to have drastic improvement in the solid model over the shell model. The meridional strains in the *BL* sequence, while underestimated, show a strong trend correlation to measured strains with absolute errors being fairly consistent in all configurations in the sequence. The marked improvement in the meridional strain prediction is also likely directly related to the model's ability to account for through-thickness stress development.

The prediction of configurations in the *BC* sequence is critical in the dome region where vessel response can be seen to be largely overestimated. In the solid model the overestimation and the harmonic response is still visible but to a far lesser extent. The harmonic behavior which was linked to the high-angle helical drop-off locations is still a contentious point. Despite a significant amount of effort placed in fine tuning the ply drop-off locations and the thickness build-up around the layers' polar openings, it was not possible to completely eliminate the perceived harmonic response. Regardless, it would appear that accounting for through-thickness effects in the dome region bring the prediction closer to the observed behavior while highlighting aspects to improve in future iterations - mainly, the high-angle helical thickness build-up. The increase in error around the dome region of the vessels can also be tied to the impact of inner contour invariability. Since the models shown here do not take into account the change in inner contour, it is possible that the actual effect relatively small changes in liner geometry during winding is underestimated.

All results from the solid model in the experimental set shown in Figure 4.2 show a particular 'swelling' in the tangential strain response in the dome proper - for the *BC* sequence this can be seen aligning with the maximum in meridional strain, while in *BL* cases it can be seen in the dome proper right after the maximum in tangential strain. The exact source of this 'swell' is argued to be the overestimation of laminate response to meridional loading which increases closer to the polar opening. It is likely that this can be eliminated by a more refined through-thickness partitioning.

### 4.3. Burst Prediction Overview

The depiction of behavior trends, while valuable, can be further expanded and evaluated by the application of rudimentary failure prediction. Burst pressure can be estimated by applying any of a variety of composite damage criteria that allow for the prediction of first-ply failure. Hashin failure [44] was used to predict first-ply failure in both models while the solid model results were also used in tandem with Puck failure criterion in order to estimate burst pressure. Table 4.1 shows an overview of Hashin failure criterion used to predict burst pressure for the configurations within this study.

Table 4.1: Overview of predicted burst pressures via Hashin failure criterion

Vessel	Burst Pressure, MPa		
	Experiment	Solid Model   (% Error)	Shell Model   (% Error)
BL	163.3 ± 1.3	161.2   (-1.3)	181.9   (+11.4)
BL6	163.9	161.3   (-1.6)	181.4   (+10.7)
BL12	160.2 ± 2.8	161.3   (+0.6)	180.5   (+12.7)
BC	188.7	190.3   (+0.8)	163.9   (-15.1)
BC3	177.8 ± 1.1	193.2   (+8.7)	164.4   (-8.2)
BC9	152.6	122.8   (-24.3)	152.4   (-0.1)

Assuming first-ply failure is synonymous with catastrophic failure is, generally, a conservative assumption to make. Exactly how conservative depends on the failure criteria used. Therefore, one would intuitively expect the general trend for burst prediction using first-ply failure to be one of overestimation. However, in Table 4.1 we see a substantial amount variation in predicted results for both shell and solid models. The reasons for this require a more detailed look into the stress criteria and their results after application to configurations being inspected.

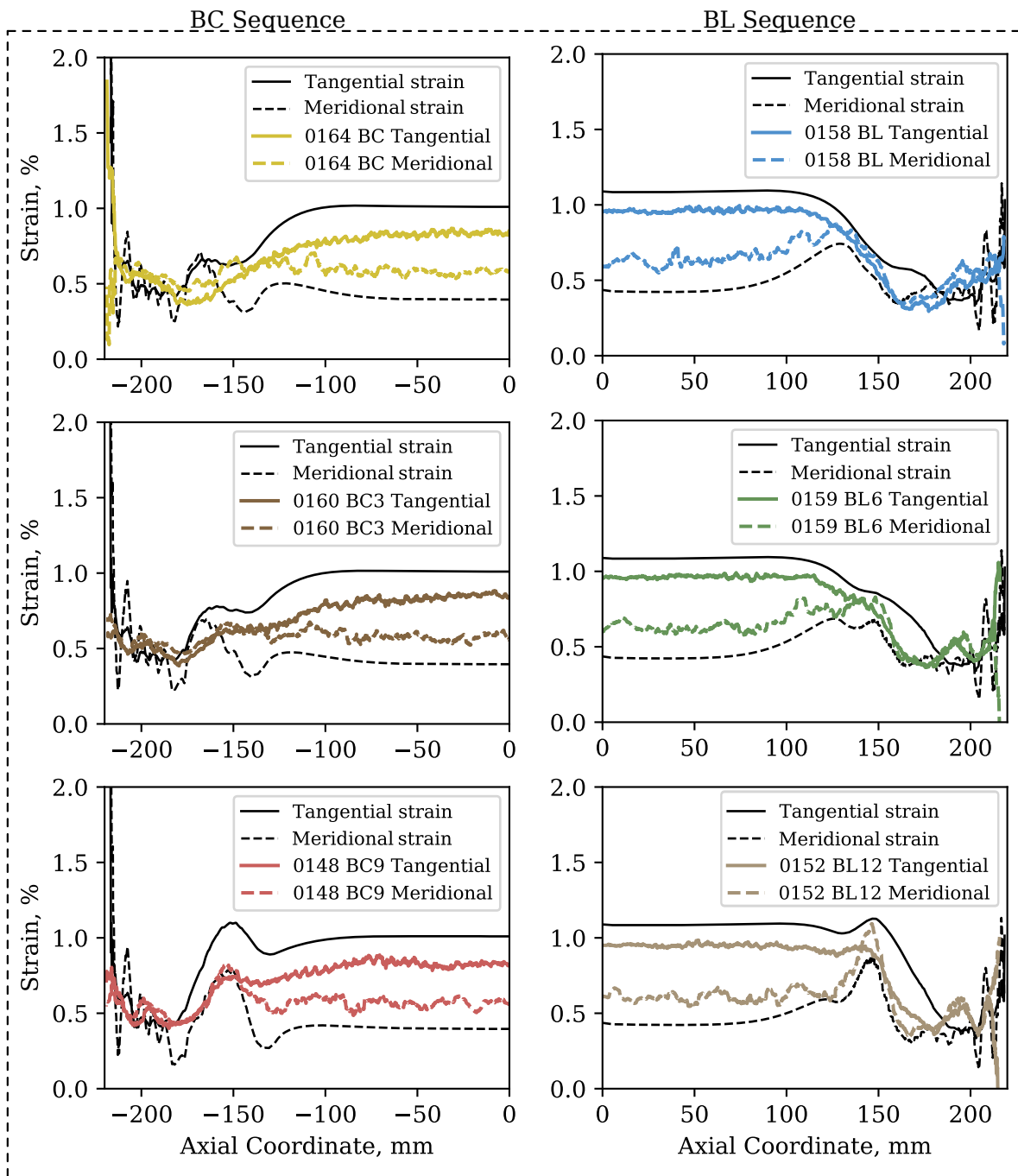


Figure 4.2: Overview of solid model predictions

### 4.3.1. Hashin Failure Criterion

Hashin failure criterion is a composite failure condition that was presented in 1981 by Hashin [44]. The criterion considers two main modes of damage occurrence in unidirectional fiber reinforced materials - fiber damage and matrix damage. The two modes can be summarized by the following equations:

Fiber Mode

$$\left(\frac{\sigma_{11}}{\sigma_A}\right)^2 + \left(\frac{\sigma_{12}}{\tau_A}\right)^2 + 1 \tag{4.1}$$

Matrix Mode

$$\left(\frac{\sigma_{22}}{\sigma_T}\right)^2 + \left(\frac{\sigma_{12}}{\tau_A}\right)^2 = 1 \quad (4.2)$$

Where  $\sigma_{11}$ ,  $\sigma_{22}$  and  $\sigma_{12}$  are fiber, transverse and shear stresses respectively,  $\sigma_A$  is material strength in the fiber direction,  $\sigma_T$  is the transverse strength and  $\tau_A$  is longitudinal shear strength of the material.

While the development of inter-fiber damage is a common and documented occurrence during the pressurization of CPVs, multiple studies show that it is not the primary cause of burst failure of pressure vessels [27, 50, 51]. Torres [50] and Cesari [51] show extensive experimental studies on airborne acoustic emission collection during the pressurization of CPVs while Soriano [27] numerically modelled damage progression within select examples of CPVs. As a result of their studies, it was concluded that considering inter-fiber damage as a source of burst failure for CPV structures was too conservative. Therefore, only fiber failure modes will be considered for the prediction of burst pressure within the models developed.

Hashin fiber failure is inherently limited as it only considers fiber and shear stresses to determine failure. This is a fairly rudimentary approximation since it neglects the stress development due to Poisson effects of the material. The implications of applying Hashin failure to the solid FE model will be discussed further in Section 4.3.3. The shell model FPF results will not be discussed in depth to limit the scope of the discussion to the solid model which shows more promise for future development.

### 4.3.2. Puck failure criterion

The main drawback of all currently known failure criteria is that their definition is inherently based on empirical data. Therefore it is often difficult to say with certainty which failure criteria gives accurate or most accurate results before a statistically significant amount of testing is performed. Regardless, there are no alternatives to currently defined failure criteria and their evaluation can provide perspective on the results. For this purpose, the Puck criterion was considered.

Puck failure criterion is particular since it offers a clear segregation of failure modes based on the stress state of the laminate [60]. A separation of fiber and transverse failure modes as well as three distinct matrix failure modes are specified. The fiber failure mode is presumed to be fiber dominated and is shown in the following equation:

$$\frac{1}{\pm X_{T,C}} \left[ \sigma_{11} - \left( \nu_{21} - \nu_{21,f} m_{\sigma f} \frac{E_{11}}{E_{11,f}} \right) (\sigma_{22} + \sigma_{33}) \right] = 1 \quad (4.3)$$

Where  $X_{T,C}$  is longitudinal tensile or compressive strength,  $\nu_{21}$  is Poisson ratio in the longitudinal direction due to transverse loading,  $E_{11}$  is Young's modulus in the longitudinal direction and  $E_{11,f}$  refers to fiber Young's modulus.  $m_{\sigma f}$  is an arbitrary factor that proposed to be 1.1 for CFRP.

Matrix failure is described by three modes shown below:

Mode A:

$$\sqrt{\left(\frac{\tau_{21}}{S}\right)^2 + (1 - p_{21}^t \frac{Y_T}{S})^2 \left(\frac{\sigma_{22}}{Y_T}\right)^2 + p_{21}^t \frac{\sigma_{22}}{S}} = 1 \quad \text{for } \sigma_{22} \geq 0 \quad (4.4)$$

Mode B:

$$\frac{1}{S} \left( \sqrt{\tau_{12}^2 + (p_{12}^c \sigma_{22})^2} + p_{12}^c \sigma_{22} \right) = 1 \quad \text{for } \sigma_{22} < 0 \quad \text{and} \quad 0 \leq \left| \frac{\sigma_{22}}{\tau_{12}} \right| \leq \frac{\tau_{23}^A}{\tau_{12}^c} \quad (4.5)$$

$$\sigma_{23}^A = \frac{S}{2p_{12}^c} \left( \sqrt{1 + 2p_{12}^c \frac{Y_C}{S}} - 1 \right); \quad \tau_{12}^c = S \sqrt{1 + 2p_{23}^c}; \quad p_{23}^c = p_{12}^c \frac{\tau_{23}^A}{S}$$

Mode C:

$$\left[ \left( \frac{\tau_{12}}{2(1 + p_{23}^c S)} \right)^2 + \frac{\sigma_{22}^2}{Y^c} \right] \frac{Y^c}{(-\sigma_{22})} = 1 \quad \text{for } \sigma_{22} < 0 \quad \text{and} \quad 0 \leq \left| \frac{\tau_{12}}{\sigma_{22}} \right| \leq \frac{\tau_{12}^c}{\tau_{23}^A} \quad (4.6)$$

Where  $p_{21}^t$  is equal to 0.3,  $p_{12}^c$  is equal to 0.2,  $p_{12}^{t,c}$  and  $p_{23}^{t,c}$  are defined as the slopes of the failure envelope for the in-plane and out-of-plane shear. Figure 4.3 shows an graphical description of puck failure modes.

As can be seen from Equations 4.3 - 4.6, the Puck failure criterion takes into consideration a much more complex set of stress interactions compared to Hashin. The main limitation of Puck stems in the fact that it does not account for shear stresses in the fiber failure mode, which is the mode being observed in this case. Similar to Hashin failure criterion, the Puck failure modes were developed/derived from a substantial experimental set. The empirical foundation of these failure criterion make them inherently difficult to classify in terms of how correct or applicable they are.

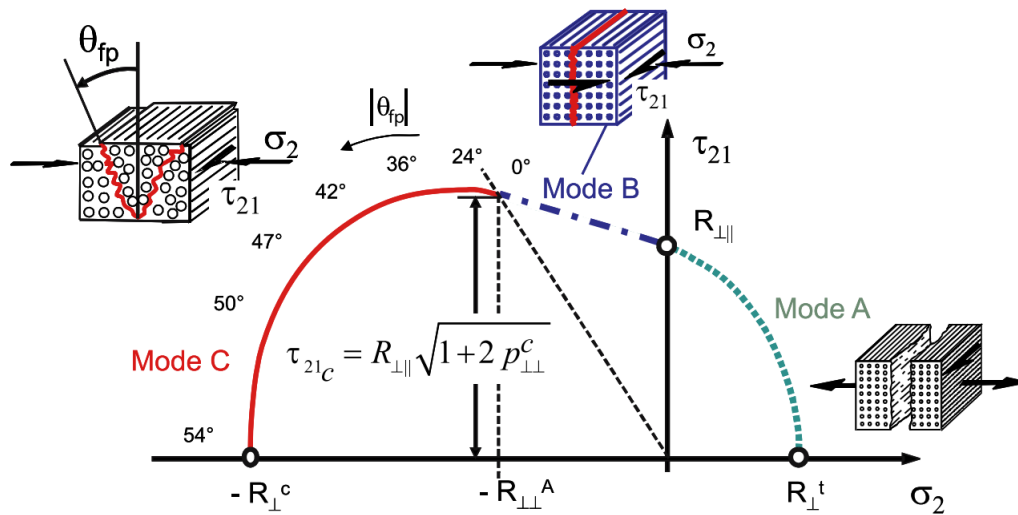


Figure 4.3: Failure envelope for inter-fiber failure according to Puck criteria - taken from [60]

### 4.3.3. Failure Predictions in Solid Model

The prediction of first-ply failure in the solid model is based on the extraction of per-ply stress data from the ABAQUS model and analyzing it by applying the failure criteria calculations. The solid model, unlike the shell model, provides additional data that allows for the application of Puck failure criteria - mainly the normal stresses related to normal ply directions.

Table 4.2 shows an overview of the predicted burst pressure as calculated Hashin and Puck criteria.

Table 4.2: Solid model predicted burst pressures according to Hashin and Puck failure criteria

Vessel	Burst Pressure, MPa		
	Real	Hashin	Puck
BL	163.3 ± 1.3	161.2	161.8
BL6	163.9	161.3	161.9
BL12	160.2 ± 2.8	161.3	161.9
BC	188.7	190.3	155.2
BC3	177.8 ± 1.1	193.2	155.5
BC9	152.6	122.8	147.1

The Hashin failure criteria is observed to have an overall lower error for nearly all cases in the experimental case. However, the interpretation of Hashin and Puck failure criteria is not straightforward. Interpretation problems stem from the issues in predictions of deformation behavior discussed previously. This is particularly true for the dome proper for the BC sequence, where the overestimation of laminate response is substantially larger than in BL sequence. Figure 4.4 shows the per-ply data on Hashin failure index in the BC sequence. The red x symbols in the plots represent the location of maximum failure index for every ply. To determine the burst pressure a simple linear extrapolation was made from the largest predicted failure index in the vessel at 105 MPa.

An observation that can be made about the Hashin failure criterion and its limitations. Since Hashin failure criterion only relates fiber and longitudinal shear stresses for the prediction of failure index, it tends to exaggerate failure prediction around the polar openings of layers. Note that failure indices past axial coor-

dinate  $> 150$  mm were not considered for failure prediction. The reason for this is due to the fact that shear stresses tend to increase rapidly around the polar opening of a helical layer due to the increase in orientation angle as the polar opening is approached. This increase in angle tends to happen in the dome region of the vessel where the longitudinal loads are high in the vessel and hence translate into shear stresses around helical layer polar openings. This presents a major limitation of the Hashin failure criterion in context of CPVs since it may be that Hashin can only provide some rudimentary information about cylinder failure, where nominal angle orientations are found for all layers in the stacking sequence. The issue is further amplified by the previously discussed overestimation of laminate response in the dome area for the *BC* series.

Further observation of Figure 4.4 a) makes it apparent the fact that all three cases of the *BC* sequence are predicted to fail in due to high-angle helical layers. This is surprising since, in all *BC* variants, the hoop layers are placed on the bottom of the vessel stacking sequence and are directly exposed to the loading case during pressurization. Interestingly, the burst pressure for the baseline *BC* case appears to be predicted fairly accurately. This apparent accuracy is likely to be circumstantial due to the lack of material property adjustment. With a more accurate material and through-thickness geometry description, it is likely that the burst pressure for the *BC* configurations would be more overestimated and would tend towards the measured value with appropriate damage modelling. Nonetheless, this result puts focus on the fact that introducing high-angle helicals to a stacking sequence may in fact be a critical vessel component.

Figure 4.4 b) also shows the Hashin failure index results of the *BL* sequence. Since the prediction for the *BL* sequence were generally more stable and there were no obvious unphysical trends predicted, the failure criteria plots are generally less ambiguous. This is not to say that they are more correct or more wrong since the general trend in burst prediction is affected with the same problems as the Hashin-based predictions for *BC* sequence. The main feature that is noticeably missing in the *BL* sequence is the relatively high failure indices at axial coordinate  $> 150$  mm. The lack of the overestimation of laminate response in that region reduces the perceived criticality of the region by effectively reducing the shear stresses present. Failure for all three configurations in the sequence is predicted to occur in the cylinder with noticeable changes in trends as result of tangential stiffness variation. The general trend was expected, however it is surprising that the vessel is still predicted to fail in the cylinder for the *BL12* configuration despite the cylinder-end being significantly under-reinforced compared to *BL*. Consistently with the *BC* series, all of the vessels are predicted to fail first in the high-angle helical layers. Expectedly, the failure index for the high-angle helicals has increased for the *BL* sequence due to the high-angle helicals being placed below the hoop layers in the stacking sequence - exposing them to larger tangential stresses than in *BC*. Unreasonably high failure-indices are encountered at the polar openings of low-angle helical layers for the same reason as discussed in previous paragraphs.

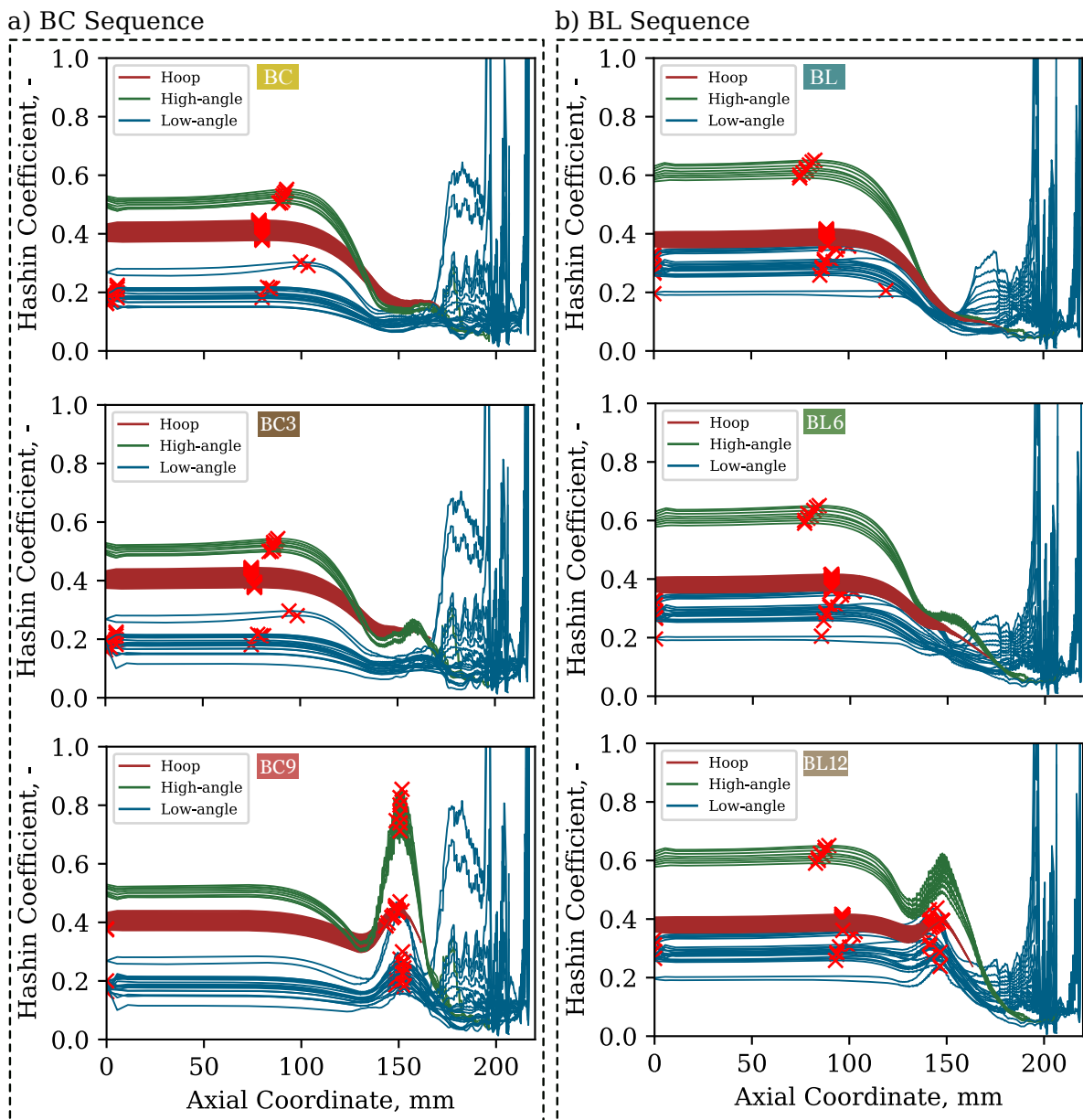


Figure 4.4: Per-ply Hashin failure coefficients along axial coordinate

Figure 4.5 shows an overview of failure indices as predicted by Puck fiber failure criteria. Since fiber failure criteria does not take into account longitudinal shear loading, the result shows a step-wise gradation of failure indices in the different types of layers. Therefore, Hoops being the most loaded in the fiber direction also have the highest Puck failure index followed by two different types of high-angle helical layers and low-angle helicals. The instability in the dome region of *BC* predictions is manifested here as well with a rather large increase in the low-angle helical layer failure index at axial coordinate  $> 150$  mm. Ignoring the shear stresses leads to a rather tame prediction of failure indices around the polar openings of layers which, given how *BC* sequence vessels failed is reasonable. The effect of retracting hoops is easier to recognize with the Puck criterion since the failure indices in the cylinder-dome transition region (between 140 and 170 mm axial coordinate) gradually increase and even become the predicted region of failure. Additionally, Puck also highlights the discussed drawbacks of the thickness correction algorithm by underestimating the burst pressure consistently. It is likely, that with further improvements in geometry depiction, Puck would be a better estimate for vessels that fail as a result of hoop layer failure in the cylinder. However, it is difficult to claim that Puck would be adequate for the determination of failure in the cylinder-dome transition or in the dome since it is unclear how failure is initiated in that region.

Applying Puck fiber failure criteria to the *BL* series provides similar results to applying the same to the *BC* sequence. The most notable behavior to observe in this series is the effect tangential stiffness variation around the cylinder-dome transition has on the failure indices distribution. Whereas Hashin did not really show the transition between *BL* – *BL6* and *BC* – *BC3*, Puck clearly shows there is an increase in fiber failure indices in the cylinder-dome transition between these intermediate cases. Additionally, Puck predicts the migration of failure location from the cylinder to the cylinder-dome transition within the *BL* sequence which is expected given the measured burst failures. With the current experimental setup it is impossible to pinpoint the actual burst initiation site so the validity of this result of evaluated based on intuition. Another point of note in the Puck figures is the noticeable increase in failure indices of the high-angle helicals between *BC* and *BL* sequence. This perceived increase and the fair proximity of the high-angle helical failure index magnitudes to the ones of hoop layers go towards supporting the prediction made by Hashin failure indices which make the high-angle helicals the source of failure in the cylinder.

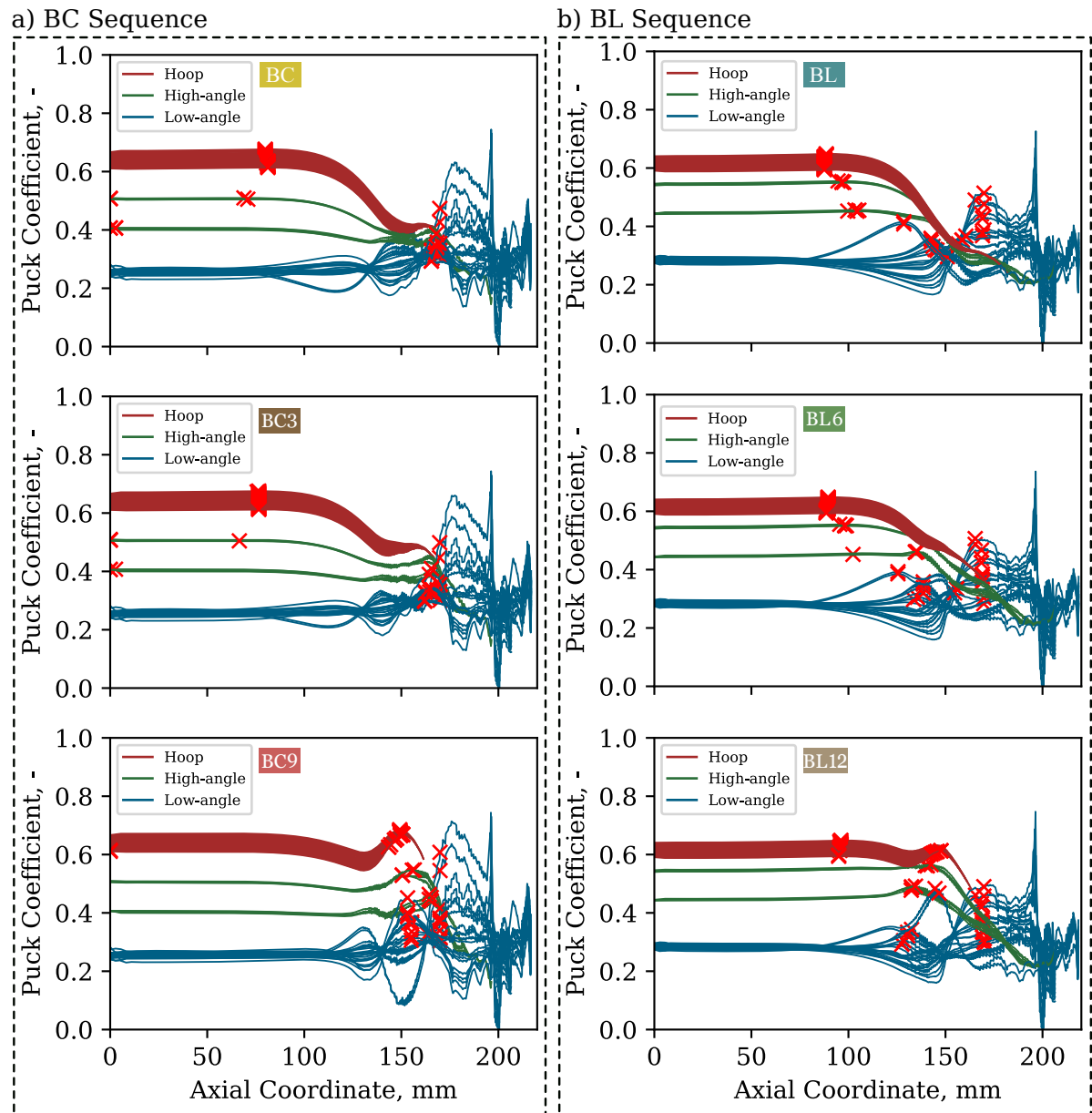


Figure 4.5: Per-ply Puck failure coefficient along the axial coordinate

An exemplary overview of failure remnants for all the vessels in the two sequences can be seen in Figure 4.6. It should be noted that significant variation in final failure remnants was observed and it was difficult to

correlate failure source to the predicted failure source via first-ply failure methods. The remnants of vessels presented in Figure 4.6 do imply that it is likely that most of the vessels failed either in the cylinder or the cylinder-dome transition. Of all the vessels, *BC9* is the most likely to have experienced a failure in the dome region of the vessel since nearly the entire cylinder remained intact.

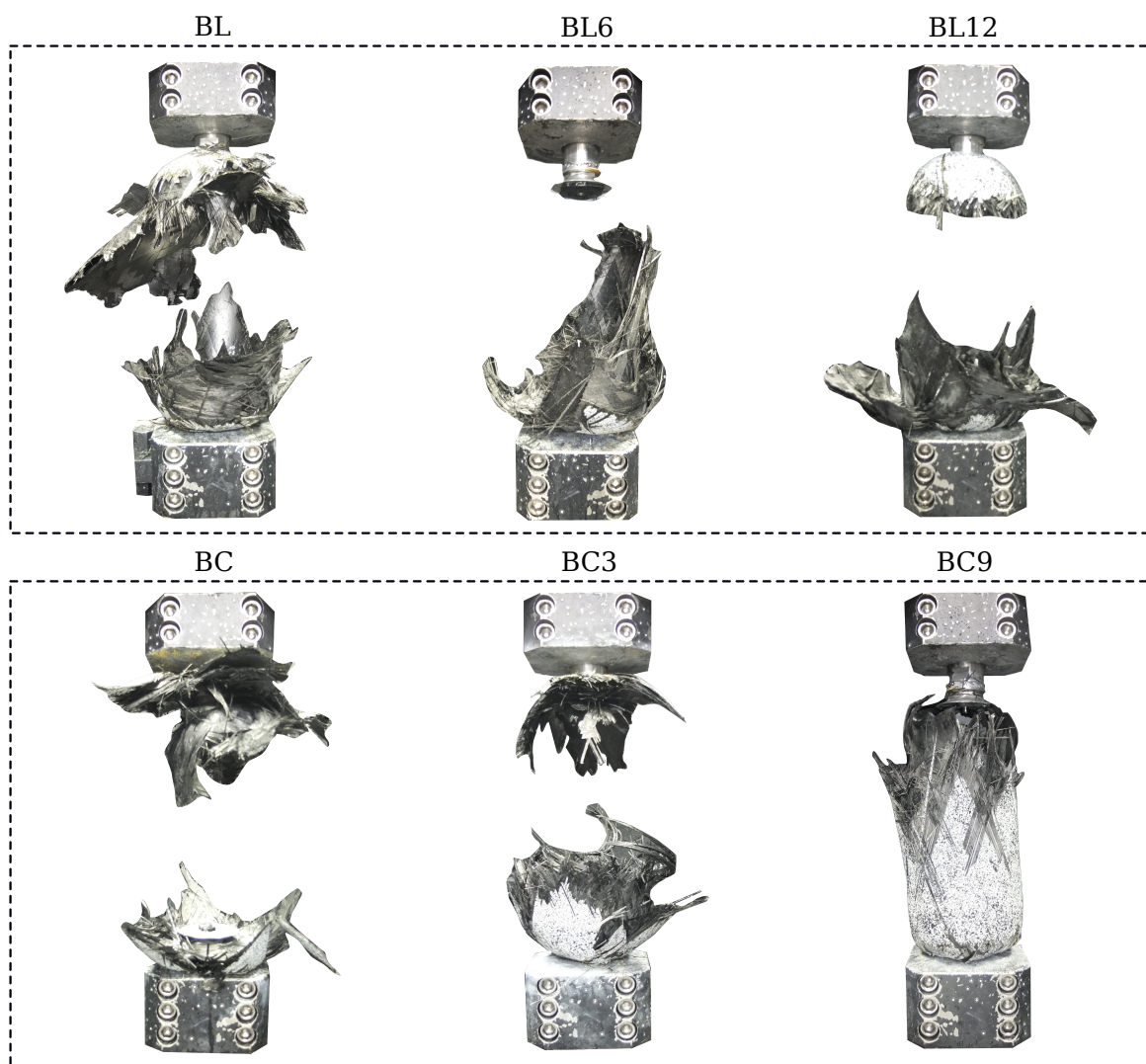


Figure 4.6: Overview of failure remnants of all configurations

#### 4.4. Impact of Inner Contour Variation on Prediction

A possible source of the errors in prediction observed in Figure 4.2 are inaccuracies in inner contour depiction. Since the distribution of tangential and axial loads in a pressure vessel is dependent on radius, it is clear that changes in the inner contour, or more specifically radius, would cause a change in the distribution of loads in a CPV. The exact impact this could have on results is unclear and uninvestigated within a comprehensive study. Initially, it was deemed unnecessary to account for changes in inner contour since the the Polyamide 6, PA6, liner provided a fairly rigid structure and was not expected to deform enough to affect results. A common theme that can be inferred from the results shown in Figures 4.2 and 4.1 is that developed FE models generally yield worse predictions in the dome region for *BC* than *BL* sequence. A rudimentary, manual, correction of the inner contour was attempted to highlight the potential impact small variations in the inner contour can have on the predictive ability of the developed models in order to highlight a potential course of future study.

#### 4.4.1. Contour Extraction

Inner contour adjustment is exemplified for the sequences *BC* and *BL*, given the readily availability of CT scans. The inner contour was manually extracted from CT scans of the *BC* and *BL* configurations. The extracted curves needed to be made compatible with Compositcad exported data, so an resampling procedure was needed to increase the point density of the extracted curves to match Compositcad's point density. Since the data extraction process was manual, the resampled curves were too discrete to work with. Therefore, a Savitzky-Golay filter [61] was applied to the data in order to achieve a smooth curve that was considered to be sufficiently close to the interpolated while still fitting against the constraints that were mainly imposed by the positioning of the boss in the FE model. An overview of the process can be seen in Figure 4.7. Furthermore, a detailed plot of the original liner contour and the corrected contours for the *BC* and *BL* configurations is shown in Figure 4.8.

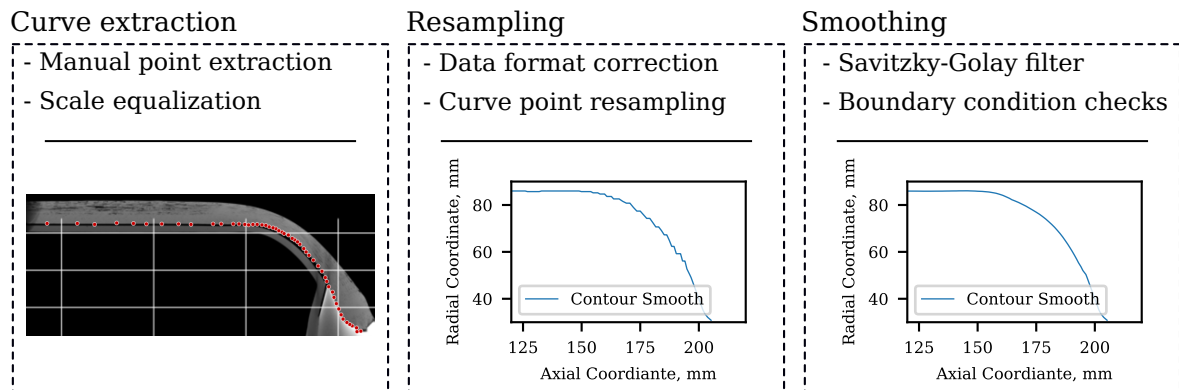


Figure 4.7: Overview of inner contour correction steps

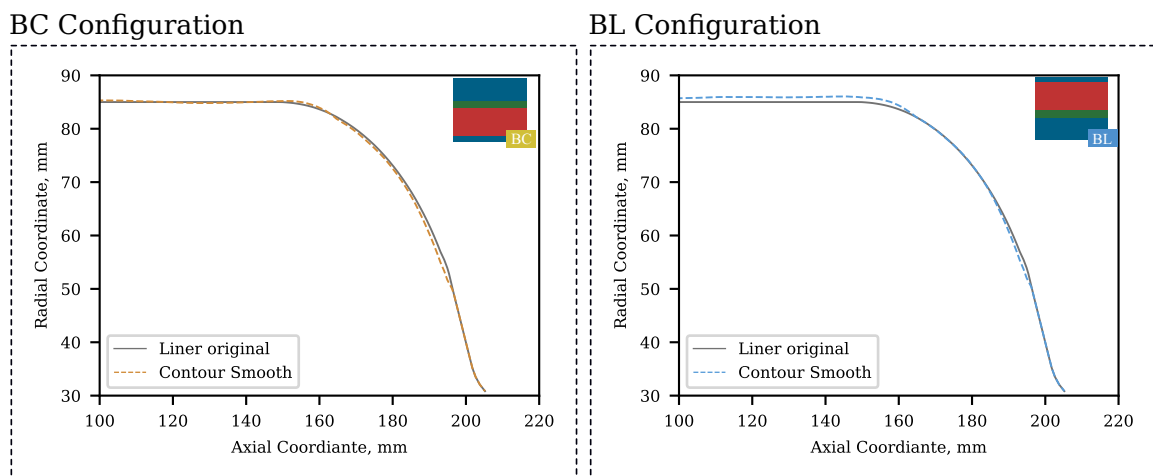


Figure 4.8: Comparison of adjusted and original inner contours

The differences in inner contour for both *BC* and *BL* cases are small. However, the observed differences are in line with intuitively expected deformation in the CPV liner given the layer distribution of the layers within their stacking sequences. The inner contour deformation can also be rationalized with reference to the vessel length variation during manufacturing - length data is shown in Figure 4.9. The liner is expected to deform most during the application of the first few layers since the more layers are applied to the vessel the more the radial forces introduced by further winding go toward compacting present layers. Therefore, the initial layers should be most significantly visible in vessel length measurements. So it is no surprise to see that applying hoop layers to the vessel in *BC* causes an increase in length while it doesn't appear to cause an increase in *BL* where a substantial amount of layers have already been deposited. The low-angle helical layers seem to have a comparable effect in both vessels however, the time of their placement is the cause of

the observed differences in extracted inner contour. In *BL* applying the majority of low-angle helical layers first would cause a contraction in length, but since there is virtually no support to the cylinder during the winding of these layers, the cylinder radius is expected to increase as a result of internal pressure. The radial increase is likely to be visible in the final inner contour because by the time high-angle helical and hoop layers are deposited a substantial enough amount of mass was deposited to not affect the inner contour as much. However, the deposition of high-angle helicals has a direct effect on the length which is seen to increase. This is likely to be manifested as bending around the cylinder-dome joint which is relatively unsupported by this point. The *BC* vessel first experiences slight elongation due to hoop placement which happens for the same reason a radial increase is seen for the *BL* case. It should be noted that the elongation due to hoop placement is less severe than the contraction experienced by *BL* due to low-angle helical deposition. This is due to the winding tensions used during manufacturing. helical layers are wound at  $2x$  higher tension than hoop layers. The deviation from nominal liner geometry in *BC* was expected to be seen in the dome proper since the placement of helical layers succeeds hoop placement therefore any length deformation is likely to be limited to the dome region assuming no liner-composite slipping.

Upon observation of Figure 4.8, the expected changes are indeed manifested in the extracted contours when placed against the original Compositacad contour. The changes are very small but they are present nonetheless. The derived inner contour was then applied to the solid FE model and solved to observe effects.

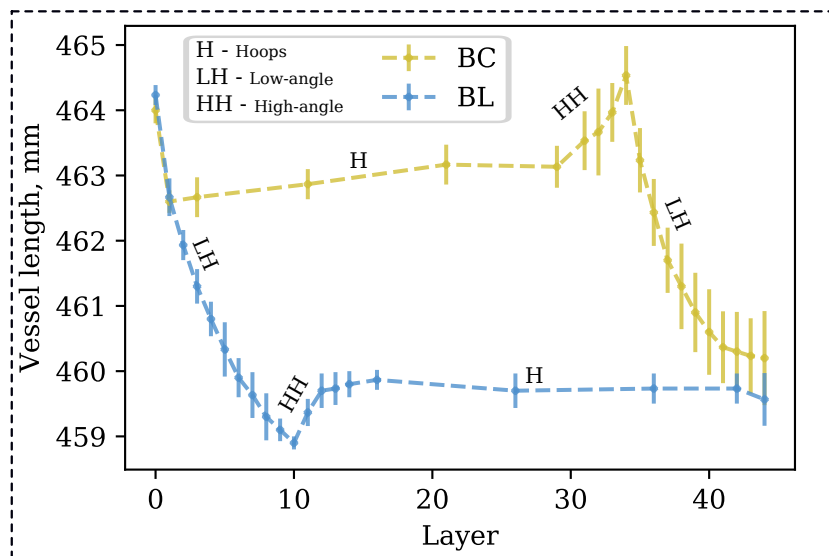


Figure 4.9: Length variation during manufacturing for *BL* and *BC*

#### 4.4.2. Inner Contour Results

Applying the extracted contours to the FE solid model was aimed at targeting the observed problems with the model's predictive ability for the dome region of the considered CPV configurations. The results obtained are summarized in Figure 4.10. While the results are not entirely conclusive, they do highlight the potential impact perceivably minor changes in the inner contour can have on the deformation prediction of the developed models.

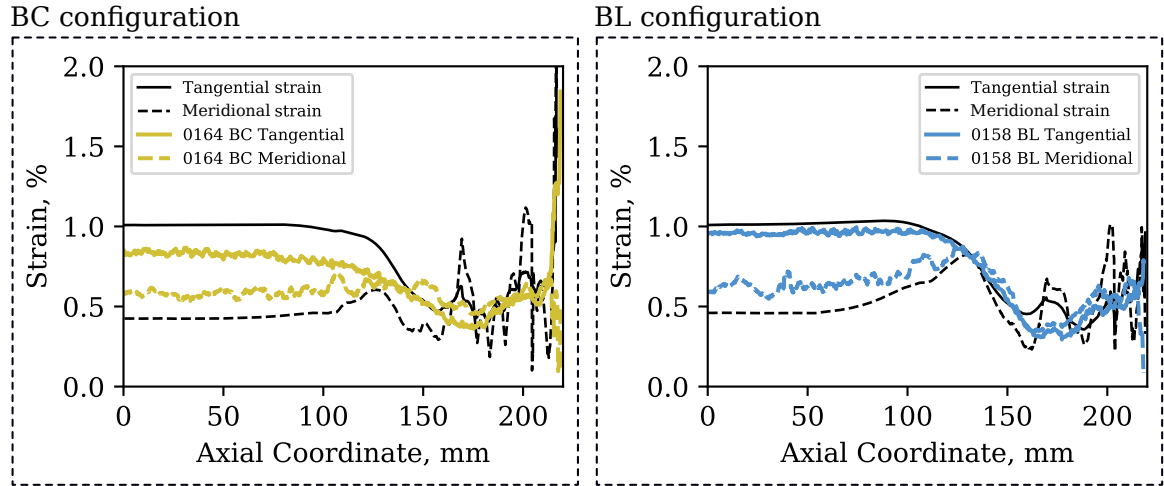


Figure 4.10: Strain predictions with inner contour adjustment

The results for the *BL* configuration benefit significantly from the inner contour adjustment. Interestingly, the predicted strains are seen to match better than before the inner contour adjustment. This is unexpected, since the cylinder radius for *BL* increases which increases the tangential loads in the cylinder. It is possible that the resulting change in the cylinder dome transition allows for compliance that causes an improvement in performance. It should be stressed once more that this perceived strong correlation should mainly be observed in terms of trends predicted instead of magnitudes since the limitations inherent to the geometry correction protocol cause an underestimation of reinforcement in the tangential direction. Therefore, a near match in predicted strain values in the cylinder does not imply high accuracy of predicted results. What does imply accuracy of results is the consistent prediction of deformation trends in the cylinder and cylinder-dome transition - which are fairly well presented.

Predictions for the *BC* configuration are slightly more ambiguous since the inner contour had very small adjustment applied to the dome region. The general trends in the tangential strain are largely unchanged compared to the results shown in Figure 4.2 but do show a less severe in tangential strain drop around axial coordinate 130. It is difficult to argue that the prediction of meridional strain has improved since the cylinder trends are basically unchanged and the dome region prediction is difficult to interpret. However, the focus should be on the fact that very small changes in dome curvature changed the predicted response to significantly and that it caused a difference for both cases. This result alone is sufficient to recognize the dome as a crucial aspect of the CPV's depiction within numerical models.

The predicted spike in meridional strains for both configurations goes to highlight the importance of developing better through-thickness definitions of layer distribution since it is highly likely that this inaccuracy is related to the treatment of high-angle helical layers and their predicted angles.

Finally, changes in the deformation behavior also has some impact on the predict burst pressure according to methods described in Section 4.3. Table 4.3 shows an overview of burst pressures deduced from FE models using adjusted inner contours.

Table 4.3: Overview of predicted burst pressures via Hashin failure criterion with new configurations

Vessel	Predicted Burst Pressure, MPa			
	Real	Hashin raw contour	Hashin	Puck
BL	163.3	161.2	189.8	169.7
BC	188.7	190.3	201.3	155.6

Expectedly, *BL* experienced an increase in predicted burst pressure since predicted strains in the cylinder were noticeably lower. *BC* response is more difficult to quantify since the dome response prediction did not markedly improve but changed substantially. This is indicative of the fact that both the inner contour adjustment process and the modelling of configurations with hoop layers on the bottom of the laminate is missing detail in some aspects.

## 4.5. Summary and Outlook of Modelling Techniques for Fast Behavior Prediction

The models presented in this study were evaluated by correlating predicted results to experimentally obtained values and measurements. Through comparing multiple aspects of the gathered results, some general conclusions about the validity of the models presented can be made. The initial goal of the models was to establish a foundation of functional FE models capable of providing reasonably accurate predictions of behavior in the cylinder-dome transition of an CPV while preserving low computational cost. The two models, suggestively named *solid* and *shell*, examined differ as a result of different finite element selection.

The shell model, based on 2D shell elements, when combined with the geometry correction algorithm from Chapter 2 was seen to provide significantly better results than presented in previous studies [33] where no geometry correction was attempted. The trends in the cylinder-dome transition were convincingly reproduced for the majority of cases. It can be said that tangential strains were generally predicted better than meridional strains. *BL* sequence was substantially more stable with no resonant-like behavior in the dome region while *BC* demonstrated an exaggerated prediction for laminate response in the dome region according to the shell model. The exact source of this discrepancy was connected to the limitations of the geometry correction model and the resulting inaccuracies in material estimation and high-angle helical layer tapering correction. Additionally, the use of shell elements was seen a severely limiting since no through-thickness effects could be captured in the cylinder. However, since shell element formulation accounts for rotational DOFs, differences in bending response between the two investigated sequences could be captured to some extent. The lack of through-thickness effects was also a likely contributor to the overestimation of response in the dome region of the CPV. Hashin failure criteria was applied to the shell model results in order to estimate burst pressure via FPF calculation. The burst pressure predictions suffered due to the recognized limitations in the thickness correction algorithm and the limitations of shell elements. Hence, no conclusive trends could be established from an attempted burst prediction. It is likely that the wall thickness of specimens investigated in this study makes shell elements wholly unsuitable for their analysis since the through-thickness effects are contributing to deformation patters in a non-neglectable amount. The shell element, however has been shown to have potential for the analysis of thin-walled CPVs (e.g. 35 MPa storage) since, when combined with a geometry correction algorithm, it is capable of reproducing trends in CPV deformation. It should be stressed that the performance of the model greatly depends on the accuracy of the geometry depiction. Therefore, if shell element modelling is desired, ample resources need to be placed on the accurate depiction of geometry correction and accompanying material properties.

The solid model, based on 3D solid elements, was observed to face a different set of challenges compared to the shell model but overall improved predictive ability for minor increase in computational costs. The general trends were represented reasonably well in all cases with meridional strains in the *BL* sequence seeing the most improvement compared to the shell model. The issue of response overestimation was still present in the *BC* sequence but was noticeably reduced both in terms of a local peak in the meridional strains and the perceived harmonic response in the dome region of the CPV. A major aspect of improvement with using solid elements is their ability to account for through-thickness effects. Through-thickness effects allow the solid model to describe the difference in tangential expansion of vessels relative to the positioning of tangential reinforcement within the stacking sequence of the vessel. The consideration of through thickness effects also results in a more realistic depiction of through-thickness stresses. The results from the solid model were also used to make a rudimentary FPF prediction of burst pressure. The results obtained from the solid model were promising but highlighted limitations of the geometry correction algorithm which made conclusive result interpretation problematic. However, the implementation of two Hashin and Puck fiber failure calculations allowed for the identification of a potential source of failure in CPVs with high-angle helical layers. The introduction of high-angle helicals, according the FPF failure results could also represent the introduction of a critical component for the CPV where the shear failure of high-angle helical layers may be sufficient for triggering global failure. However, further study is require in order to confirm the existence of this phenomenon. Nevertheless, it can be said that placing high-angle helical layers higher in the stacking sequence may cause an increase in performance since they would experience lower loads depending on the laminate thickness. It should be noted that the current implementation of the solid model only implements one through-thickness partition with a quadratic formulation of solid elements which effectively results in four partitions through-thickness. Tests were made that check result consistency with introducing more partitions which resulted in minor differences in predicted magnitudes, however these were seen as unnecessary given the increase in computational cost that follows. It is likely that the solid model would benefit greatly from alternative parti-

tioning methods which aim to maximize gains in accuracy while minimizing computational cost increase.

The development of both of these models was based on the desire to establish a solid foundation for the fast analysis of CPVs at Daimler AG. The developed models, and especially the solid model, showed great promise not just in the performance presented in this study, but also for future studies. With an average solving time of 30 minutes, it is relatively easy to imagine the paths this modelling baseline can take. An option is to further refine partitioning strategy with the aim of further improving prediction accuracy while also improving model robustness. The development of partitioning strategy should be combined with an effort to develop a accurate, physical, model of the thickness correction and layer distribution in CPVs. In fact, it is likely that the development of one such model would provide major improvements in the modelling efforts of CPVs in general. The solid model also provides a baseline for application of continuum damage mechanics CDM model which could be used for gains in prediction accuracy - especially for burst pressure predictions. The decision to model an 8th of a vessel in this study was mostly based on previously work at Daimler AG facilities. It would be highly beneficial to transition to modelling a smaller section of the vessel or axi-symmetric elements. This would reduce computational time significantly and would allow for more detailed modelling without increasing performance recorded in this study.

# 5

## Design Insights

CPVs are arguably one of the most complicated composite structure problems at present. It can be argued that a general lack of fundamental understanding is the bottleneck preventing these structures from being applied successfully in large scale serial products. Regardless, it is necessary to continue conducting academic studies which aim to build knowledge surrounding CPVs and their behavior in extreme loading cases such as the use case presented for the automotive industry. While a comprehensive set of best design practices is not yet available, general rules can be determined with already available knowledge. The experimental plan executed as part of this study alongside data from previous experimental studies made at Daimler AG allow for a retrospective approach to currently understood and speculated design decisions that could result in beneficial changes for CPV performance. The privilege of this study's context is in the large amount of data from which general design rules can be inferred and hypothesized. Therefore, an overview of observed phenomena and their implications on potentially beneficial design rules will be discussed in the following chapter and a hypothetical improved stacking sequence will be proposed through the use of tools developed as part of this study.

### 5.1. Design Practices and Implications

The two variables examined in this study represent a continuation of studies on the influence of stacking sequence on CPV performance done in the past. The most notable of those was presented in the works by Nebe et al. [47] and Asijee [33] where the CPVs with two layer orientations were considered and a variety of layer groupings were tested. The results obtained by these studies pointed to a variety of configuration-vs-performance trends that seemed to be consistent with some studies made on composite pipes. More specifically, an outcome of these studies was to claim that placing hoops on the outside of the CPV stacking sequence yielded an increase in burst pressure due to a relative reduction in stresses experienced by the hoop layers. While this conclusion was consistent with a results presented by Mertiny et al. [35], it did neglected the implications of using two layer orientation groups and their potential impact on the structural response in the cylinder-dome transition.

The results of the experimental plan in this study allowed to highlight the limitations of using only two layer orientations in a stacking sequence and additionally outlined some rather impactful results that can be used to develop some general ideas about design rules for CPVs. Using two layer orientations for the development of a stacking sequence forces one to meticulously investigate the placement of the hoop layers and tangential reinforcement in the cylinder dome transition in order to avoid premature failure due to excessive deformation in the region. The introduction of high-angle helicals provides a window to the development of varied stacking sequences that open the design space of CPVs by allowing the design to provide tangential reinforcement to virtually any part of the dome. The configurations used within the current experimental study provide results that directly oppose the conclusions from previous study - namely that placing hoop layers on the inside of the stacking sequence can actually increase burst performance significantly. Additionally, the introduction of high-angle helical layers introduced behavior that shed light on the interaction between manufacturing and performance.

When a CPV designer makes the choice to include high-angle helical layers to provide tangential reinforcement in the dome region of the vessel, they also inevitably initiated a discussion on their manufacturing

practices. This is now known because of the relative changes in burst pressures between *BC* and *BL* sequences. The designer is then faced with a choice - place hoops on the inside of the stacking sequence to presumably gain in vessel strength at the cost of having to ensure that their manufacturing process is precise enough to ensure highly consistent tangential reinforcement placement *or* place the hoops on the top of the vessel in order to allow for rather significant variation in the manufacturing process without significantly changing the expected burst pressure. Naturally, these points are only valid for configurations in which all hoop layers within a CPV are placed into a single group. Additionally, either direction of the two mentioned have heavy implications on other CPV properties, such as laminate porosity variation, which can also have an impact on the burst performance of the structure.

Effects of hoop layer grouping was an important focal point of previous studies [33, 47]. Grouping all hoops into a single large group is a design decision that causes a significant amount of issues from a damage progression perspective. That large inter-fiber cracks can form in hoop groups was shown by [50]. The exact impact of these is not yet quantified but some clarification on their effect was shown by [57] where a full-scale vessel was seen to lose 15% in burst pressure performance after some 22,000 pressurization cycles. After single pressurization tests the burst pressure of configurations with large hoop groups was not observed to decrease [33, 50, 57]. While these factoids only provide two limited data points, when combined with general rules of composite design, it can be said that grouping all hoop layers into one large group is likely not optimal for cyclical performance. Additionally, increasing hoop group size also increases the through-thickness stress gradients between the main layer groups. If long-term performance is of more note than mass savings, than it is likely that fragmenting the stacking sequence into repeating patterns would perform more consistently over longer periods of time. This change would likely come at the expense of mass increase compared to configurations where maximum burst pressure is sought due to more material being required in order to achieve similar strength performance and the introduction of connector layer mass which is necessary when transitioning from hoop groups to helical layer groups.

Questions regarding tangential reinforcement around the cylinder-dome transition are plentiful and every single one is difficult to provide a certain answer for. The question of how much reinforcement is sufficient is still not possible to answer and perhaps is not the "correct" question to ask. Perhaps it is more appropriate to ask whether one can introduce tangential reinforcement into the cylinder-dome region to cause failure. This answer is not possible to answer conclusively from the results of this study. However, it is possible to provide a sort of preamble to the answer. With certainty one can say that variation of tangential reinforcement around the cylinder-dome transition has significant impact on the vessel response in the region. The *BL* sequence provides insight into a very particular interaction of bending loads in the region which implies that the perhaps the bending loads caused by geometry/deformation interactions are much more important to mitigate than ones caused by bending-extensional coupling. The *BC* case possibly provides a coincidental example of vessel response when the tangential reinforcement in the region is sufficient to cause a uniform meridional strain distribution due to even expansion around the cylinder-dome region. While it is impossible to make claims with certainty whether extending tangential reinforcement into the dome would cause detrimental effects, it can be said with certainty, within the context of this study, that having tangential reinforcement in the cylinder dome transition is generally better than not having it. This is especially shown to be true if hoop layers are placed on the inside of the CPV stacking sequence.

The choice of liner material likely plays a much more crucial role than can be described using just the results of this study. The inner contour's impact on the vessel deformation potentially has a significant impact on the vessel's deformation. It could be said that, generally, a stiffer vessel liner could prove to be more robust for vessel design purposes since the designer could get away with assuming constant inner contour. If a liner would be made out of a very soft rubber like PA6, the deformation caused by winding would likely be too severe to ignore. Of course, the inner contour deformation also has implications on storage volume which, within an industrial context, is probably close in important to structural integrity. Having a malleable liner also limits the designers ability to use higher winding tensions since it would inevitably deform the inner contour and cause a lower storage volume. The inner contour deformation is also interesting given the length variations observed in this study. A reduction in same-layer group sizes would inevitably reduce the relative impact of each group on the liner deformation and the vessel length. So some benefit for inner contour preservation can be found in varying layer groups every so often in the stacking sequence.

Additional notes should be made on the observed impact high-angle helical layers can have on CPV design. While the burst analysis conducted in this study is rather rudimentary, it does point towards a previously un-investigated phenomenon - potential burst caused by fiber failure in high-angle helical layers that are primarily loaded in shear. The question of high-angle helical criticality requires further investigation. However,

that placing high-angle helical layers on the outside of the stacking sequence would be beneficial to the internal stress state is not difficult to imagine. High-angle helicals are effectively intermediate layers that are not effective at carrying tangential or axial loads since most of them are manifested in shear loading in the layer. Therefore, minimizing their stress exposure by placing them on the outside of the stacking sequence would reduce the stresses they experience while still providing the tangential reinforcement in the dome for which they were introduced. Arguably placing them on the outside would change the distribution of loads in the dome, however, since the thicknesses in the dome-proper region are somewhat lower than in the cylinder, this would likely not play a significant role.

## 5.2. An Improved Stacking Sequence

The discussion in the previous provides description of a few strongly interconnected generally observed behaviors of CPVs and what implications the decisions relating to them may have. To pinpoint general rules of CPV design, one would need to define a set of limitations to constitute a design case. Regardless, the observations listed above allow to make a suggestion for a potentially improved stacking sequence that should result in a marked improvement in burst pressure. A short investigation on the effects of varying layer placement was done using the CPV analysis tools developed as part of this study in order to determine the potential gains in performance and mass savings that could potentially be achieved for the CPV geometry relevant to this study. It should be stressed that this is by no means a proposition for an optimized design of CPVs, but it aims to present a hypothetical prototype configuration that, if built, would likely provide further insight into CPV mechanics and good design practices.

The evaluation of FPF derived burst pressure led to the identification of high-angle helical layers as a potential source of failure. Since the burst pressure of the *BC* configuration was unquestionably the highest of all tested vessels, the tangential reinforcement distribution was kept the equivalent in all three configurations additionally evaluated with the high-angle helical layers being distributed in different patterns within the stacking sequence. Figure 5.1 shows an overview of the evaluated cylinder stacking sequences.

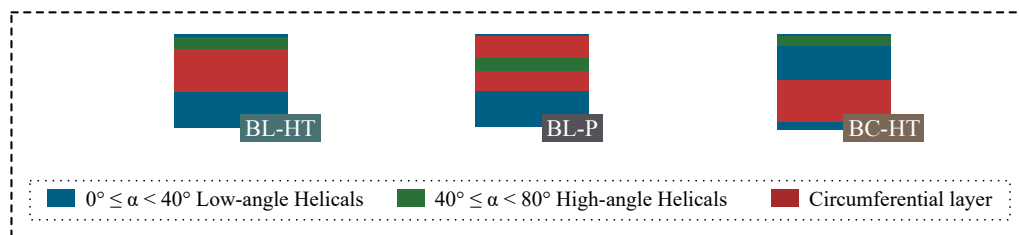


Figure 5.1: Design study stacking sequence configurations

The three configurations represent an investigation into the effects of helical placement on the deformational behavior and, within the limitations of current methods, the predicted burst pressure of CPVs. The three configurations are named with reference to their initial stacking sequence, *BL* or *BC*, with one of two suffixes, *HT* (High-angle Top) or *P* (Parted). The general idea behind the configurations presented here is founded in the possibility of high-angle helicals being the source of failure in *BC* and *BL* configurations. By placing the high-angle helical layers on top of the stacking sequence the stresses they are exposed to are minimized - effectively reducing their criticality in equal conditions. The *BL-P* configuration is a test that examines the behavior of the vessel in the case of hoop group partitioning. Splitting the hoop group in half with high-angle helicals and ordering high-angle helicals in such a way to minimize angle differences between the hoop and the high-angle helical layers. Figure 5.2 shows the distribution of layers through-thickness and the predicted outer contours of the investigated configurations.

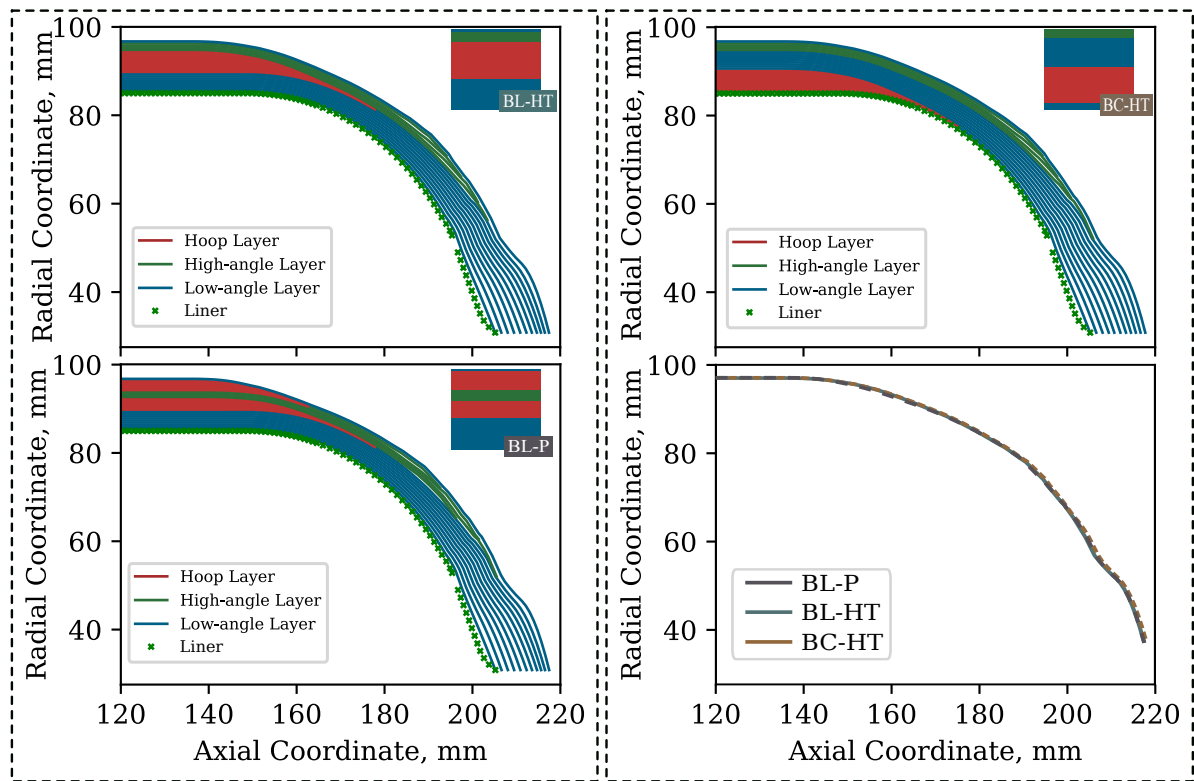


Figure 5.2: Predicted geometry description of new configurations

Figure 5.3 shows the per-ply failure indices according to Puck and Hashin along the axial coordinate. Perhaps attention should be set towards trends observed in the Hashin failure criteria since the trends recognized in through it in the original configurations are what caused this investigation. The relocation of the high-angle helicals causes exactly the desired effect in all three configurations - a general reduction in the failure indices of the high-angle helical layers. In fact, according to Hashin failure criterion, the resulting reduction in loading of high-angle helicals is so severe in the  $BC-HT$  configuration that the criticality is again found in the hoop layers - arguably the preferred state of loading since regulation mandates failure to occur in the cylinder. The same change in the high-angle helical failure indices is observed in the other two configurations but not to the same severity. This trend was expected since the high-angle helical layers are displaced by a smaller amount in the  $BL-HT$  and  $BL-P$  cases compared to the  $BC-HT$  case. That fiber loads are reduced in the high-angle helical layers is also visible according to Puck failure criteria since, when compared to their baseline configurations, the stresses in the high-angle helical layers has significantly reduced. This is not entirely correct for the  $BL-P$  configuration since the high-angle helical layers have not been placed much higher than their original position and are now more under the influence of their surrounding hoop layers and their loading case. Another important note is that all failures are unambiguously predicted to occur in the cylinder region of the vessel. The configurations that actually failed in the cylinder in experiment were the ones that had the closest prediction by Hashin failure criterion. While this is not conclusive proof of the fact that the burst pressures predicted from these results, it is a circumstance that increases the likelihood of representative trends being predicted. Table 5.1 shows an overview of the predicted burst pressures for new layouts and their baseline configurations.

Table 5.1: Overview of predicted burst pressures via Hashin failure criterion with new configurations

Vessel	Predicted Burst Pressure, MPa	
	Hashin	Puck
BL	189.8	169.7
BC	190.3	155.2
BC-HT	241.2	157.0
BL-HT	208.7	157.0
BL-P	197.5	158.6

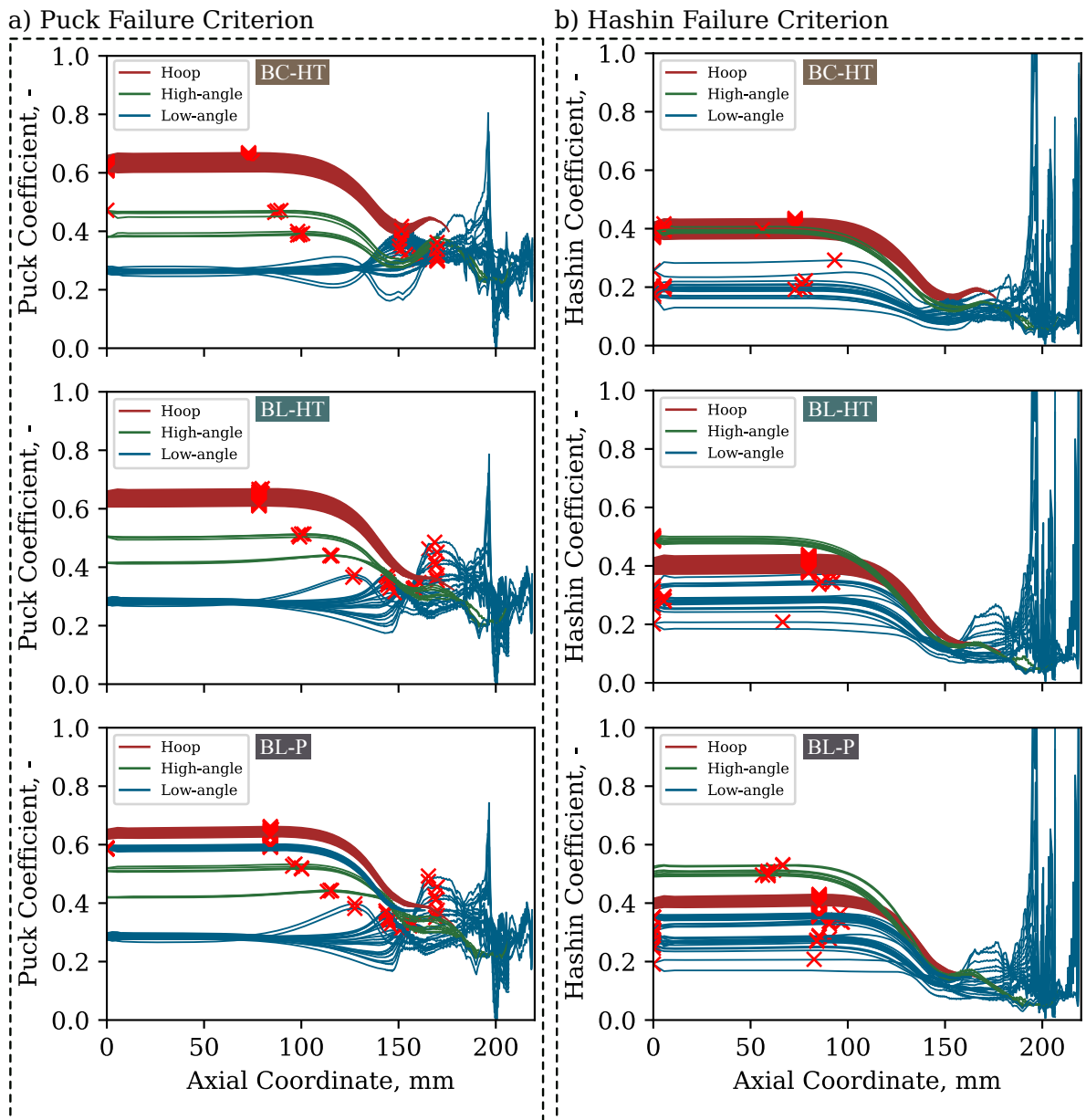


Figure 5.3: Per-ply failure indices according to Puck and Hashin criteria

An interesting occurrence that becomes apparent in Table 5.1 - the burst pressure for configurations *BC – HT* and *BL – HT* decreased according to Puck while the same configurations see a drastic increase in predicted burst pressure compared to their baseline stacking sequence according to Hashin failure condition. Of course, this is a result of the limitations of each failure criterion - mainly, Puck does not account

for shear stresses at all in its calculation of fiber failure indices. Therefore, with the alternate placement of high-angle helical layers resulting load increase in the hoop layers, the failure indices for hoops increase significantly. Contrarily, the Hashin failure criterion does not account for normal and transverse stresses in the prediction of fiber failure indices, and so does not predict the increase in tangential loads to the hoops as a significant contributor to their failure index. It is difficult to interpret these results conclusively since they also need to be considered within the context of the limitations of the thickness correction algorithm which, to some extent, underestimates the amount of material present and does not account for material property variation as a result of compaction effects. Regardless, these results can be used at face value with the fact that Hashin was shown to be better at predicting cylinder failure than Puck within this experimental set.

Assuming that previously observed trends in burst prediction hold. The  $BC - HT$  configuration can be comfortably adapted by the removal of layers providing tangential reinforcement to increase structural efficiency while preserving the minimum required burst pressure of 157.5 MPa. No formal optimization procedure was adapted for this process due to time restrictions so a 5 hoop layers were removed from the configuration in order to gage differences in results. Figure 5.4 shows a comparison of the failure index variation in the less reinforced,  $BC - HT2$  configuration and  $BC - HT$ . Following is a table that summarizes the final burst pressure for each of the two configurations - Table 5.2.

Table 5.2: Comparison of predicted burst pressures between  $BC - HT$  and  $BC - HT2$

Vessel	Predicted Burst Pressure, MPa	
	Hashin	Puck
BC-HT	241.2	157.0
BC-HT2	195.4	143.8

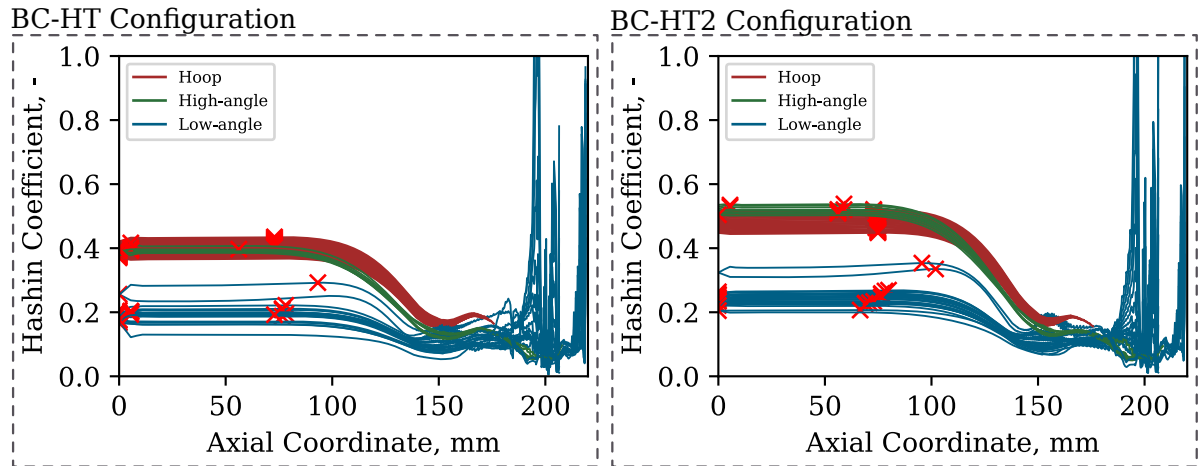


Figure 5.4: Per-ply failure indices according to Hashin criteria for  $BC-HT$  and  $BC-HT2$  configurations

The inherent limitations of the current modelling approach makes it difficult to make any certain conclusions about CPV design. However, that this kind of study can be made at all is an encouraging fact as there are numerous areas of improvement for the modelling approach that can improve its validity and make the framework discussed in this thesis useful for CPV optimization in the future. Additionally, the results from the three additional laminates tested provide a solid base for future investigations. While it is unlikely that placing the high-angle helical groups on the outside of the laminate will increase the burst pressure to 240 MPa, it is quite possible that it will increase the burst pressure somewhat. Confirming that trend would actually go toward establishing, as a design rule, that high-angle helical layers should be placed closer to the outside of the stacking sequence. Gaining this knowledge would make a significant difference in current ideas about the general approach to CPV design.

# 6

## Conclusions and Outlook

### 6.1. Summary

Composite Pressure Vessels (CPVs) are crucial structures for the functioning of a Fuel-cell Electric Vehicle (FCEV). The reduction of used material and further structural optimization is necessary if future products using Fuel Cell (FC) technology are to be made economically viable. This report presents the development of an automated, computationally efficient, numerical analysis framework for CPVs. The goal of the framework is to obtain reasonably accurate predictions on the mechanical response of CPVs and make future research on the topic more accessible and efficient by lowering configuration-to-result time. Additionally, the study aims to expand the understanding of the structural response of CPVs through an experimental study examining the cylinder-dome transition of the vessel by varying two design-relevant variables - stacking sequence and tangential stiffness distribution in the cylinder-dome transition.

#### 6.1.1. Numerical Analysis Framework

The numerical framework described in this study is founded on the use of an industry standard filament winding software, Compositcad, which allows the user to generate filament winding paths for the manufacturing of pressure vessels. The software also provides a rough estimate of CPV geometry which is heavily adjusted in order to better resemble reality. Initially, the analysis framework corrects the Compositcad output through the adjustment of layer distribution and layer thickness via the application of engineering and analytical solutions respectively. The geometry correction algorithm was found to provide highly usable results for a wide variety of used configurations and was demonstrated to provide a good outer contour match between virtually all configurations measured in the cylinder and cylinder-dome region.

The results from the geometry correction algorithm were formatted into standardized output compatible with ABAQUS FE software where two models, a shell element and a solid element, were developed to simulate the CPV response. While the shell element's main drawback was its inability to account for through-thickness effects, it was clear that the general trends in the cylinder-dome transition were consistently predicted and so it could be concluded that a shell element modelling approach is arguably useful for use on thin CPV applications (e.g. 35 MPa storage) where thick-wall effects would play a less substantial role. The solid model was found to consistently generate good predictions for vessel response in the cylinder and cylinder-dome transition for virtually all configurations. The through-thickness effects that were captured by the solid model also allowed for the capture of cylinder deformation trends as a result of stacking sequence variation. The solid model was also found to provide somewhat ambiguous results for the burst pressure prediction of CPVs where specific failure criteria provided very low error burst pressure prediction in cases where failure occurs in the cylinder of the vessel. Granted the source of the ambiguity stemmed from only considering First Ply Failure (FPF) and not accounting for damage modelling.

The solid model also allowed for the identification of a potential source of criticality - high-angle helical damage development during pressurization. It is unclear how a high-angle helical layer behaves during the pressurization up to 157.5 MPa but it is certain that, in the cylinder, the majority of its loading will be manifested as shear stresses. As an attempt to further investigate the potential impact of this supposed criticality and to demonstrate the modelling frameworks ability to rapidly generate results for a wide variety of CPVs configurations, three hypothetical configurations were tested and analyzed using the framework in order to

establish potential trends. While the certainty of results obtained from this study are somewhat ambiguous, the potential of the framework was clearly shown and future development is certain to result in significant improvement in both analysis time and result quality/accuracy.

### 6.1.2. Experimental Plan

The extensive experimental plan consisted of testing two variables of high-relevance to CPV design - stacking sequence and tangential stiffness variation in the cylinder-dome transition. A total of six configurations were developed for the experimental plan with a total of 12 CPVs were manufactured for the experimental set. The experimental results yielded two major observations that may have a significant impact on both future studies and CPV design. The apparent increase in burst pressure performance due to placement of hoop layers on the inside of the stacking sequence being one and the observed, highly-sensitive, relationship between tangential stiffness variation, burst pressure and hoop group placement being the other.

Configurations with hoop groups placed on the inside of the stacking sequence (*BC*) showed up to 15.5% higher burst pressures than their counterparts. This result is of high importance as it directly opposes the results of some previous studies and has strong implications on CPV design and potential mass savings if further investigated and quantified. The apparent increase in strength however comes at a cost of apparently lower margin for manufacturing error. The variation of tangential stiffness around the cylinder-dome transition can be described as testing the configurations robustness against manufacturing error. It was observed that the *BC* configurations also showed a significant decrease in burst performance for comparable reductions in tangential stiffness in the cylinder-dome region - with 12% difference from highest to lowest performing. Contrarily, the configurations with hoop groups towards the outside of the stacking sequence (*BL*) showed a relatively low reduction in burst pressure due to reduction in tangential stiffness to the same region - with only 6% between the highest and lowest performing configuration.

## 6.2. Conclusions

To provide an arranged overview of the conclusions for this thesis, a brief discussion on each of the initially posed question is presented below.

1. *How can the influence of manufacturing related phenomena as well as distinct laminate responses be captured by computationally efficient numerical models?*

Previous studies brought into question whether or not relatively simple and computationally efficient models can be utilized in the analysis of CPVs while preserving a high level of predictive ability. The development of the modelling framework presented here showed that, with the adequate description of vessel geometry, a significant improvement in vessel behavior can be acquired and expected for a large variety of different configurations. The essence of capturing laminate response of a CPV within a numerical model seems to be heavily focused around the geometry description. This is also why an entire chapter of this thesis is devoted to the explanation of the various processes applied and developed to generate a reasonably good description of the CPVs used.

While the geometry correction process utilized here yielded good results, it should be stressed once more that the process developed here is highly limited to the manufacturing processes at Daimler AG facilities. This is especially true for the definition of *context* which would require major adaptation for either a significant change in geometry or in manufacturing method. Additionally, the process developed for this particular study did not take into account the variation of material properties as a result of compaction which, if accounted for adequately, would likely result in substantial impact on model predictive ability. Additionally, the angle variation of helical layers was not correlated to measurement as measuring angle variation. Accounting for angle variation to a high degree of accuracy should be strong priority in the future in order to ensure result accuracy.

It was shown that low-cost models can provide highly consistent and reasonably accurate results across a variety of configurations and with minimal user input. The results of this study provide a solid baseline for future development since models of this type can be easily used in conventional optimization applications due to their high rate of results output. Naturally, these kinds of studies are relatively far in the future as a lot more knowledge is required before quality cost functions for the optimization of CPVs can be made.

2. *How does changing laminate properties of the cylinder affect the behavior of the cylinder-dome transi-*

*tion region?*

The variation of stacking sequence was investigated by the variation of the main hoop layer group placement within the stacking sequence with two major configurations being considered - (*BC*) and (*BL*). Both *BC* and *BL* tackled the cylinder-dome variation through the introduction of high-angle helical layers which aimed to normalize the deformation for both cases and make comparison easier than it was in previous studies.

The results of this change yielded an expected result - the cylinder expansion being markedly higher in the *BL* case than in the *BC* case. In the *BL* case, the low-angle helicals, that need to transfer high tangential loads to the hoop layers above, are more compliant and expand more. During this expansion, they also experience damage which also causes a relative increase in the load distributed to the hoops.

Additionally, the choice of the two configurations was made due their maximizing effect on bending-extensional coupling of the cylinder laminate. Specifically, *BL* and *BC* have exactly opposite bending-extensional responses and were expected to behave substantially differently in the region as a result. However, the difference in cylinder expansion made it difficult to conclude whether the variation in behavior in the cylinder-dome transition originated from the laminate response or differences in tangential expansion in the region. The exact impact of bending-extensional coupling on CPV response and its relevance for their design remains a question for future studies.

*3. How sensitive is the cylinder-dome transition to varying tangential stiffness by the introduction of hoop layer tapering into the transition region?*

The variation of tangential stiffness in the cylinder-dome transition was made by shifting the ply-drop off region of the main hoop layer group towards the cylinder - effectively reducing the tangential reinforcement in the CPV. The movement of the hoop group toward the cylinder allowed for the evaluation of significance of the two main sources of bending loads in the CPV - bending caused by geometry and bending caused by the coupling response of the cylinder laminate.

The general trends in deformation were consistent for both *BC* and *BL* configurations, with a clear local maximum in meridional strains appearing with the reduction of tangential stiffness in the cylinder-dome region. However, an important note for this trend is that the location of this local maximum is roughly constant among all configurations that exhibit it regardless of stacking sequence. This implies that bending loads stemming from vessel geometry may play a more significant role in the deformational behavior of CPVs than the coupling response of the laminate. The main difference in response around the cylinder-dome transition between *BL* and *BC* configurations stems from the apparently higher meridional strains recorded in the *BL* case. However, this likely does not stem from higher bending loads but rather due to the higher compliance of the *BL* case whose hoop layers are on the outside of the stacking sequence - causing a larger tangential expansion and subsequently, higher meridional strains. This is mitigated in *BC* by the hoops being on the inside of the laminate.

It should be stated that due to both groups of configurations (those based *BC* and *BL*) have been similarly affected by the variation of tangential stiffness in the region. But while the measured deformations in the cylinder-dome region are comparable, the value of this observation becomes clearer with the consideration of impact on burst pressure of the vessels.

*4. How do laminate properties and changing hoop layer tapering affect burst performance?*

Major differences in burst pressure were recorded between *BC*-based configurations and *BL* based configurations. The best performing *BC* configuration outperformed the best performing *BL* configuration by 15% burst pressure. This significant difference has major implications on the mass savings potential for the two design approaches and it is likely that, with further study, a "better" practice for a stacking sequence configuration may be identified between the two.

This finding is also put into context when accounting for configurations that vary tangential stiffness around the cylinder-dome transitions. The configurations based on *BC* were found to be substantially more sensitive to tangential stiffness variation than their counterparts based on *BL* stacking sequence. This implies a very intricate relationship between internal stress distribution, burst performance and manufacturability.

At this point it can be postulated that *BC*-like configurations have, on average higher mass savings potential than *BL*-like configurations but come at a cost of low tolerances during manufacturing. Where an

error in hoop layer placement of 6mm can cause a drop in performance of 12%. Contrarily, *BL*-like configurations present a solution with apparently lower mass savings potential but at the benefit of highly robust manufacturing - where hoop layer placement errors of 12mm result in a burst pressure reduction of 6%.

While both these statements require further studies in order to corroborate on their implications, the results presented in this study provide a solid foundation for future studies examining the phenomena identified through the current experimental set. Additionally, it should be stressed that these findings are also dependent on layers used within the stacking sequence. SO it is likely that varying results would be found if sufficiently different layer orientations were used.

#### 5. *What design rules can be determined from the experimental set provided in this study?*

It is difficult to present any certain design rules from the results of this study since most of the results prompt further investigation rather than a quantitative impact on performance. Furthermore, it is necessary to state that a good design of a pressure vessel will depend greatly on the use case in question and its inherent design constraints.

This study allows for some statements on hoop group placement. If dealing with a configuration where only one hoop group is present, its position in the stacking sequence has implications past its burst pressure. Namely, cylinder expansion. In the automotive industry, packaging is an important aspect of design and displacements usually have to fit within a tight operating range. Hence it is likely that, despite the apparent sensitivity to manufacturing error, configurations with hoop groups closer to the inside of the stacking sequence are a preferred choice due to the marked decrease in both tangential and axial expansion of the CPV. The contrary is true for configurations with hoop group placement towards the outside of the CPV, since those are bound to expand more both tangentially and axially. Of course, space considerations are not the sole outcome for either of the two configurations. Placing hoop closer to the outside of the stacking sequence results in better layer consolidation, arguably better laminate properties and generally lower wall thickness. All factors whose exact impact is not entirely understood at the moment, but are highly important for good understanding.

The range within which tangential reinforcement is introduced to the cylinder-dome transition is beneficial remains unknown. From the results of this study, it can only be said that the introduction of tangential stiffness to the cylinder-dome transition yielded an improvement in burst pressure. Naturally, the extension of hoop layers in the cylinder dome transition or the introduction tangential reinforcement via high-angle helicals directly implies an increase in mass. Hence, while there is benefit to be had by limiting the tangential expansion in the cylinder-dome transition, it is not yet possible to make claims on general design rules for CPVs on this note.

Hoop layer grouping is also a question that comes to attention. Previous studies [33, 51] highlighted the presence of inter-fiber fracture (IFF) propagation in layer groups. This is especially true for hoop group where the majority of the fibers are close to uni-directional. The consolidation of all the hoop layers into a single group has good implications on resulting laminate quality, but also has poor implications on crack propagation as it allows for large IFF surfaces to be created. This is merely an observation and it is not possible to make concrete conclusions on best design practice at this time.

This study also allowed for the identification of a hypothetical criticality point - high-angle helical damage progression/occurrence. This perceived criticality stems solely from the analysis of First-Ply-Failure (FPF) results of the analysis framework and is one that definitely requires further study. It is possible that placing high-angle helical layers on the outside of the stacking sequence would yield improved performance as it could alter the tangential stresses carried by them by some margin. If true it is likely that this effect would be rather significant in future development and design of CPVs.

### 6.3. Future Work

It is important to once again highlight some of the outstanding issues present in the current methodology. Assuming that some of the future studies to be carried out at Daimler will base some of their analysis on the developed modelling approach, quite a few areas of improvement can be identified.

Starting with the geometry correction algorithm. While the thickness correction algorithm was shown to work very well for all sub-scale vessel configurations tested in the past and in this study, it is likely that a significant change in the liner geometry would affect its performance significantly. This statement is valid for both the thickness correction and the layer re-arrangement algorithms. The layer re-arrangement algo-

rithm is by definition an 'engineering' solution - meaning that it is tailor made for observations made during manufacturing at Daimler AG. As it was stressed before, the future invention of similar geometry correction protocols is not a valid method of providing a good answer to the solution since the methodology is not based on a robust physical model. Real progress is likely to be seen once efforts are invested into developing a physical model to depict not just the layer re-arrangement phenomena, but also the inner contour changes during winding. Granted this effort alone could likely satisfy the amount of work required to obtain a PhD. A slightly smaller task could, for starters be to develop a computationally efficient method of determining inner contour changes as a result of winding - this would already eliminate aspects of the geometry correction algorithm while also accounting for inner contour changes which were shown to have significant impact on model prediction in Section 4.4.1. Similar work was already presented by Zhang et al. where highly accurate modelling techniques were used to determine mandrel buckling as a result of winding tension. [62]

The thickness correction procedure is one that likely requires assumption adjustments if its performance is to be improved for future studies. The most troublesome assumptions being made in its current installation is the scaling of fiber tension into force tangential to the circumference. The current implementation scales the fiber tension strongly which causes the helical layers to be very poorly compacted - while this is not a problem in the cylinder, in the dome region it is. The dome region is discretized and treated as a series of sequentially decreasing cylinders. The general trend for layer compaction makes intuitive sense but it was impossible to validate results against measurements. A potential direction for future study could also be a study attempting to experimentally determine layer thicknesses with aim to compare it to and improve the thickness correction algorithm. Alternatively, one could attempt to expand the current thickness correction model to include the changes in thickness resulting from curing processes - this is already a possibility given the work presented by Kang et al. [58] but would require currently unavailable information on material properties. Additionally, the compaction of layers has heavy implications on material properties of the laminate - namely porosity and fiber volume fraction. To accurately account for these in future modelling efforts would strongly add to the reliability of results and make similar analysis frameworks more robust for a larger variety of configurations.

The further development of the presented models is likely the most substantial and versatile platform for future studies. Given the thickness of the structures required for automotive applications, it is unlikely that the shell model will see any substantial improvement. The solid model, on the other hand, serves as a solid platform for future development. Redefining through-thickness partitioning strategies is a direction that has a lot of potential to result in accuracy improvement. The model ability is also strongly related to its through thickness geometry prediction - so any improvement made to the geometry correction algorithm is also likely to result in a performance improvement of the solid model. As for potential modelling improvements - a large aspect that was not investigated within this study is damage progression. While it is likely too early to implement a damage progression model into the current model definition, it is a direction that future research should consider since the model is already fairly good at predicting general observed trends in the CPV and would likely result in good insights on damage progression in CPVs.

The future of CPVs is difficult to predict. The time of writing this thesis is likely the best time to be involved in the development of pressurized storage systems due to essentially every major truck manufacturer having announced a portfolio of new FCEV products. On top of the automotive industry, the aviation industry seems to be leaning heavily towards a sustainable future with hydrogen taking center stage. However, while the stage appears to have been set, a lot of work remains. Despite the topic of CPVs being known and discussed for around 60 years by this point, we still don't fully understand the fundamentals of these structures and before any sort of meaningful optimization can be made, there must be a significant amount of work applied to the accurate description of the small infinity of effects that play a role in determining the performance of a CPV. It should be stressed that without these studies taking place, and without the necessary knowledge being developed it is not difficult to imagine CPVs and FC propelled transportation solutions being dwarfed by battery powered alternatives in the next 20 years or less.



# A

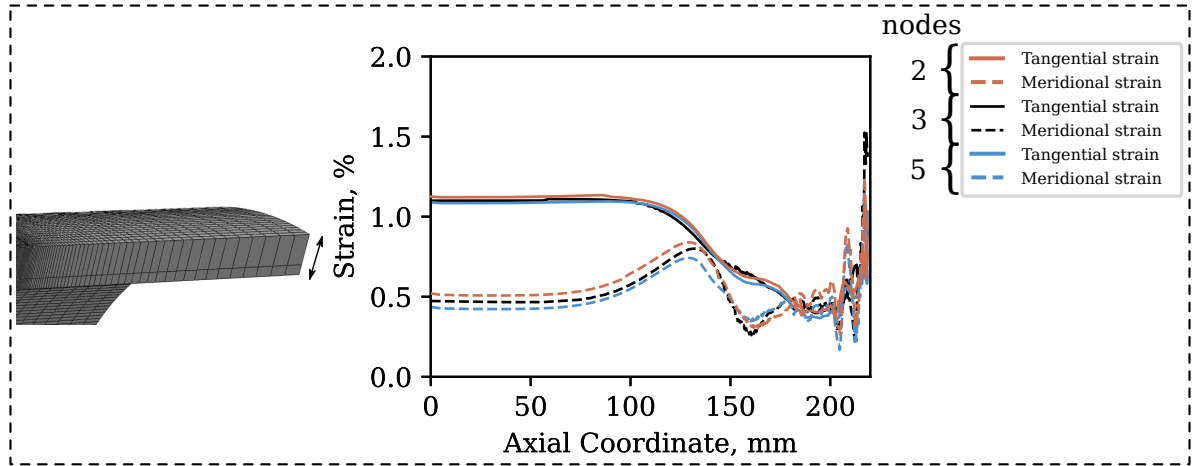
## Mesh Study

Nothing is perfect and neither is the codebase developed for the modelling framework. Certain limitations inherent to the coding approach combined with the time restrictions implied with this project made it difficult to code every aspect of the framework in a robust manner. This eventually limited some of the automated meshing controls. The reader should keep in mind that this following mesh study is more of a guideline to emphasize areas where mesh refinement is necessary and not a claim that an ideal meshing strategy has been used in the study.

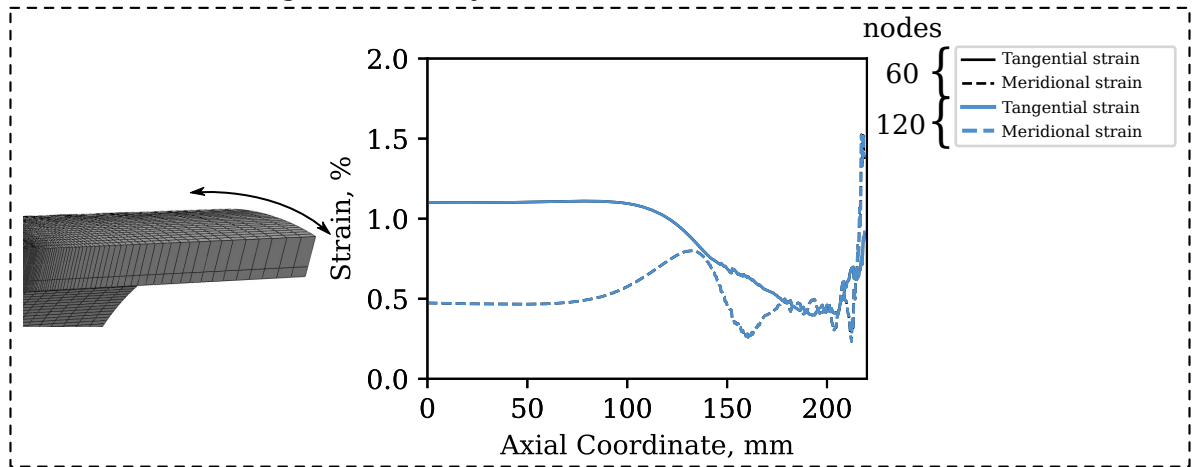
Figure A.1 shows a summary of the mesh study where the mesh density was varied in the radial, circumferential and meridional directions in order to further evaluate the performance of the model used in this study. Of the three result groups shown in Figure A.1, the radial mesh density is most crucial to make note of. It is clear the results, while relatively close together, still do not show clear signs of convergence with the tested mesh densities. Only a maximum of 5 nodes were tested because of the methodology used to generate the through-thickness partitions in the vessel geometry. The partitioning strategy was not investigated further due to time restrictions. While it is clear that an improvement in partitioning strategy and an increase in mesh density would likely yield further change in results, it can be said that the overall trends are unchanged between the extreme case of 2 nodes through-thickness and 5 nodes through-thickness. An encouraging observation is found in the tangential strains which decrease with increasing mesh density - implying that the overestimation of the results is also partly caused by insufficient mesh refinement in through-thickness.

The meridional and circumferential strain predictions are essentially unaffected by the used cases. The meridional mesh density is limited to a minimum number by the distribution of points along the meridian as defined by Compositcad. This limitation leaves much to be desired since it also indirectly determines the point density for angle variation along the meridian - increasing the point density in Compositcad may yield better predictions for the dome region behavior prediction as a result of a more accurate depiction of the angles found in the dome. The accuracy of the angle predictions coming out of Compositcad was not correlated to measurement and represent a challenging task for future research.

Radial Density



Circumferential/Tangential Density



Meridional Density

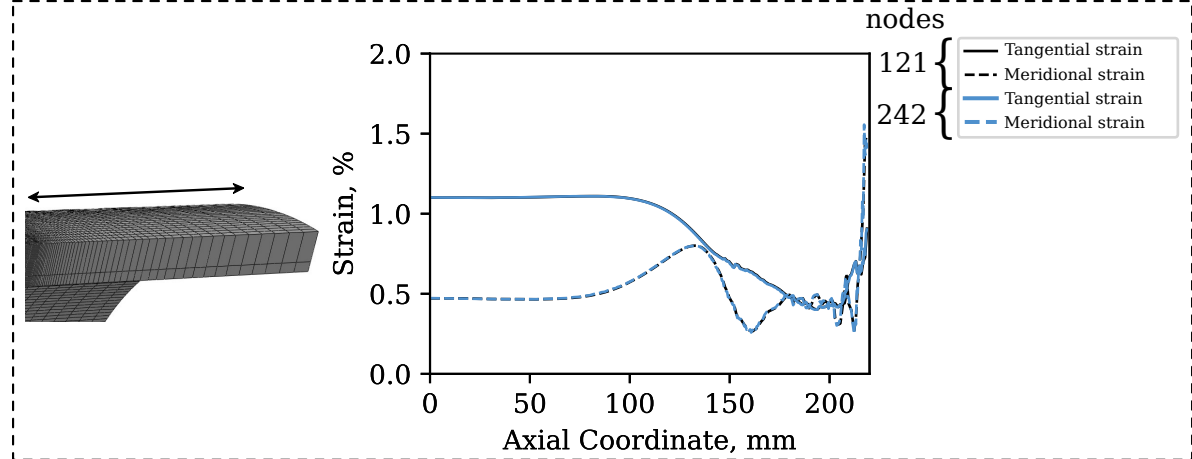


Figure A.1: Summary of result sensitivity on mesh density in major directions

# B

## Layup Configurations Overview

Figure B.1 shows a similar overview as seen in Chapter 3 with an expanded section to allow for a listed overview of all configurations used in the experimental plan of the study.

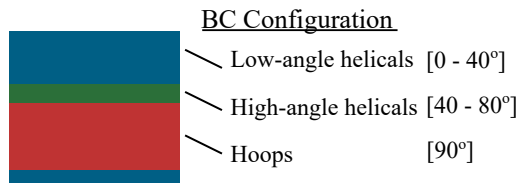
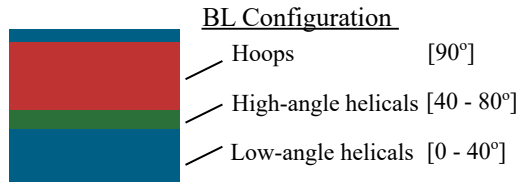
The two variables varied were stacking sequence and tangential stiffness variation. Two main configurations were developed as part of the stacking sequence variation - *BL* and *BC*. The *L* in *BL* stands for 'legacy', as the distribution of hoop and low-angle helical layers was configured according to an inherited configuration from Asijee [33]. The novelty of these configurations in comparison to [33] is found in the addition of high-angle helical layers - two groups, in particular at different angles. Both *BC* and *BL* have the same number of layers and both have a total of four different layer orientations. The *BL* configuration also inherits the circumferential tapering distribution from a configuration found in [33]. Hence, *BC* is a direct conjugate of *BL* with a slight variation in the circumferential tapering that was identified to vary by a 2mm from the *BL* configuration based on CT measurements. These two configurations test the stacking sequence impact on the CPV performance.

The tangential stiffness variation causes an expansion to the nomenclature used. Namely *BL* and *BC* configurations with an appended number. In the case of *BL*, the resulting configurations are *BL6* and *BL12* while in the case of *BC*, *BC3* and *BC9* are defined. These vary from their baseline configuration by the extent their hoop group is pushed into the cylinder. Their suffixed number symbolizes the exact amount, in mm, that the hoop group tapering was pushed towards the cylinder relative to their baseline configuration as shown in Figure B.1. This results in a total of six configurations displayed in the middle section of Figure B.1. Notice that the schematics for each triplet shows the same stacking sequence because the cylinder stacking sequence remains unchanged, only the tapering region in the cylinder-dome transition changes between each sequence. Colors are used to distinguish between each configuration and ensure easy distinction between each variant of the baseline *BC* and *BL* configurations.

Additionally, at the bottom of Figure B.1, the configurations used by Asijee [33] are listed using the same color schematics to designate layer types. While no configuration from this study was repeated, the numerical analysis models and the geometry correction algorithm were benchmarked against all configurations listed during development.

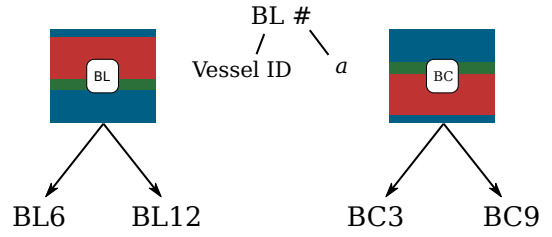
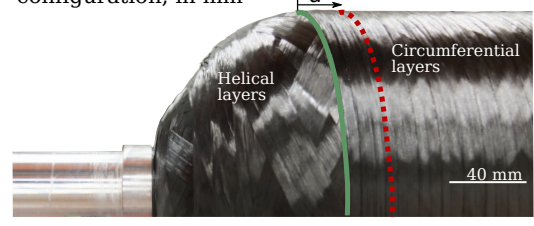
Stacking sequence

- Two base configurations
- Maximize bending-extensional effects

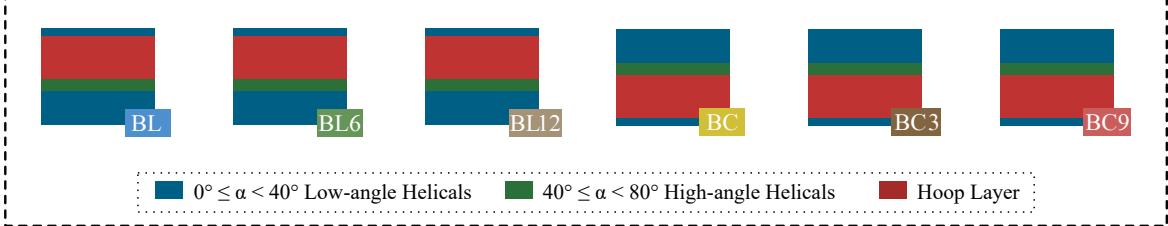


Tangential stiffness variation

$a$  - retraction in hoop extent from reference configuration, in mm



Current Experimental Configurations



Asijee [33] Experimental Configurations

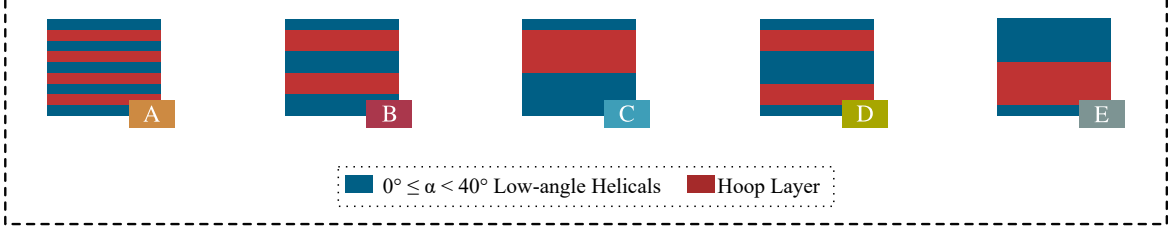


Figure B.1: Summary of nomenclature and all stacking sequence configurations and color schemes

# Bibliography

- [1] M. Ehsani, Y. Gao, S. E. Gay, and A. Emadi. *Modern electric, hybrid electric, and fuel cell vehicles: Fundamentals, theory, and design*, pages 1–396. Modern Electric, Hybrid Electric, and Fuel Cell Vehicles: Fundamentals, Theory, and Design. 2004. URL [www.scopus.com](http://www.scopus.com). Cited By :921.
- [2] Economic Commission for Europe of the United Nations (UN/ECE). Regulation no (EU) 134 - uniform provision concerning the approval of motor vehicles and their components with regard to safety-related performance of hydrogen fuelled vehicles (hfcv), 2015.
- [3] The official blog of toyota uk. <https://blog.toyota.co.uk/toyota-mirai-safety-facts/toyotablog-h2-safety-pict-n2>. Accessed: 2020-11-03.
- [4] International Standards Organization, Geneva, Switzerland. Gaseous hydrogen - lang vehicle fuel containers, 2018.
- [5] International Standards Organization, Geneva, Switzerland. Gas cylinders - high pressure cylinders for the on-board storage of natural gas as a fuel for automotive vehicles, 2013.
- [6] D. Leh, P. Saffré, P. Francescato, and R. Arrieux. Multi-sequence dome lay-up simulations for hydrogen hyper-bar composite pressure vessels. *Composites Part A: Applied Science and Manufacturing*, 52:106–117, 2013. URL [www.scopus.com](http://www.scopus.com). Cited By :14.
- [7] L. Zu, S. Koussios, and A. Beukers. Design of filament-wound domes based on continuum theory and non-geodesic roving trajectories. *Composites Part A: Applied Science and Manufacturing*, 41(9):1312–1320, 2010. URL [www.scopus.com](http://www.scopus.com). Cited By :48.
- [8] J. S. Park, C. S. Hong, C. G. Kim, and C. U. Kim. Analysis of filament wound composite structures considering the change of winding angles through the thickness direction. *Composite Structures*, 55(1):63–71, 2002. doi: 10.1016/S0263-8223(01)00137-4.
- [9] F. C. Shen. A filament-wound structure technology overview. *Materials Chemistry and Physics*, 42(2):96–100, 1995. Cited By :48.
- [10] S. T. Peters. Composite filament winding. *ASM International*, 1995.
- [11] J. Rojek, S. Joannès, M. Mavrogordato, L. Laiarinandrasana, A. Bunsell, and A. Thionnet. Modelling the effect of porosity on the mechanical properties of unidirectional composites. the case of thick-walled pressure vessels. In *ECCM 2018 - 18th European Conference on Composite Materials*, 2020. URL [www.scopus.com](http://www.scopus.com).
- [12] Nebe, M., Soriano, A., Braun, C., Middendorf, P., and Walther, F. Analysis on the internal pressure loading of composite pressure vessels: Fe modeling and experimental correlation. *Composites Part B*, 2020.
- [13] De Carvalho, J., Lossie, M., Vandepitte, D., and Van Brussel, H. Optimization of filament-wound parts based on non-geodesic winding. *Composites Manufacturing*, 6(2):79–84, 1995. doi: 10.1016/0956-7143(95)99647-B.
- [14] William F. Trench. *Elementary Differential Equations with Boudnary Value Problems*. Brooks/Cole Thomson Learning, 2001.
- [15] Wang, R., Jiao, W., Liu, W., and Yang, F. Dome thickness prediction of composite pressure vessels by a cubic spline function and finite element analysis. *Polymers and Polymer Composites*, 19(2-3):227–234, 2018. ISSN 0967-3911. doi: 10.1177/0967391111019002-327.
- [16] Wang, R., Jiao, W., Liu, W., and Yang, F. A new method for predicting dome thickness of composite pressure vessels. *Journal of Reinforced Plastics and Composites*, 29(22):3345–3352, 2010. ISSN 0731-6844. doi: 10.1177/0731684410376330.

- [17] James R. Faddoul. Structural considerations in design of lightweight glass-fiber composite pressure vessels. 1973. URL [www.scopus.com](http://www.scopus.com). Cited By :5.
- [18] Vasiliev, V. V., Krikanov, A. A., and Razin, A. F. New generation of filament-wound composite pressure vessels for commercial applications. *Composite Structures*, 62:449–459, 2003. URL [www.scopus.com](http://www.scopus.com).
- [19] Fukunaga, H. and Uemura, M. Optimum design of helically wound composite pressure vessels. *Composite Structures*, 1(1):31–49, 1983. doi: 10.1016/0263-8223(83)90015-6.
- [20] M. Hojjati, V. Safavi Ardebili, and S.V. Hoa. Design of domes for polymeric composite pressure vessels. *Composites Engineering*, 5(1):51 – 59, 1995. doi: 10.1016/0961-9526(95)93979-6.
- [21] Liang, C.C., Chen, H.W., and Wang, C.H. Optimum design of dome contour for filament-wound composite pressure vessels based on a shape factor. *Composite Structures*, 58(4):469–482, 2002. doi: 10.1016/S0263-8223(02)00136-8.
- [22] Koussios, S., Bergsma, O.K., and Beukers, A. Filament winding. part 1: Determination of the wound body related parameters. *Composites Part A: Applied Science and Manufacturing*, 35(2):181–195, 2004. doi: 10.1016/j.compositesa.2003.10.003.
- [23] Zu, L., Xu, H., Wang, H., Zhang, B., and Zi, B. Design and analysis of filament-wound composite pressure vessels based on non-geodesic winding. *Composite Structures*, 207:41–52, 2019. ISSN 02638223. doi: 10.1016/j.compstruct.2018.09.007.
- [24] D. K. Roylance. Netting Analysis for Filament-Wound Pressure Vessels. Technical Report AMMRC TN 76-3, Composites Division Army Materials and Mechanics Research Center, 1976.
- [25] Zhou, J., Chen, J., Zheng, Y., Wang, Z., and An, Q. Dome shape optimization of filament-wound composite pressure vessels based on hyperelliptic functions considering both geodesic and non-geodesic winding patterns. *Journal of Composite Materials*, 51(14):1961–1969, 2017. doi: 10.1177/0021998316662512.
- [26] Leh, D., Magneville, B., Saffré, P., Francescato, P., Arrieux, R., and Villalonga, S. Optimisation of 700 bar type iv hydrogen pressure vessel considering composite damage and dome multi-sequencing. *International Journal of Hydrogen Energy*, 40(38):13215–13230, 2015. ISSN 03603199. doi: 10.1016/j.ijhydene.2015.06.156.
- [27] Soriano Sutil, A. *Analysis strategies for as-manufactured composite pressure vessels*. MSc Thesis: Delft University of Technology, 2020.
- [28] Wang, H., Zheng, C., Wei, S, and Wei, Z. Micromechanics-based progressive failure analysis of carbon fiber/epoxy composite vessel under combined internal pressure and thermomechanical loading. *Composites Part B: Engineering*, 89:77–84, 2019.
- [29] Tew, B. W. Preliminary design of tubular composite structures using netting theory and composite degradation factors. *Journal of Pressure Vessel Technology*, 117:390–394, 1995. doi: 10.1115/1.2842141.
- [30] Jones, R. M. *Mechanics of Composite Materials*. CRC Press, Virginia, 1999.
- [31] Parnas, L. and Katirci, N. Design of fiber-reinforced composite pressure vessels under various loading conditions. *Composite Structures*, 58(1):83–95, 2000. doi: 10.1016/S0263-8223(02)00037-5.
- [32] M. Xia, H. Takayanagi, and K. Kemmochi. Analysis of multi-layered filament-wound composite pipes under internal pressure. *Composite Structures*, 53(4):483–491, 2001. ISSN 02638223. doi: 10.1016/S0263-8223(01)00061-7.
- [33] Asijee, T. *Experimental and numerical investigation into the influence of layup sequence on the mechanical performance of composite pressure vessels*. MSc Thesis: Delft University of Technology, 2020.
- [34] Ramos, I., Ho Park, Y., and Ulibarri-Sanchez, J. Analytical and Numerical Studies of a Thick Anisotropic Multilayered Fiber-Reinforced Composite Pressure Vessel. *Journal of Pressure Vessel Technology, Transactions of the ASME*, 141(1):011203, 2019. doi: 10.1115/1.4041887.

- [35] P. Mertiny, F. Ellyin, and A. Hothan. Stacking sequence effect of multi-angle filament wound tubular composite structures. *Journal of Composite Materials*, 38(13):1095–1113, 2004. URL [www.scopus.com](http://www.scopus.com). Cited By :20.
- [36] Jack R. Vinson. *The Behavior of Shells Composed of Isotropic and Composite Materials*. 1993.
- [37] Baličević, P., Kozak, D., and Mrčela, T. Strength of pressure vessels with ellipsoidal heads. *Strojnikski Vestnik/Journal of Mechanical Engineering*, 54(10):685–692, 2008.
- [38] K. Magnucki, W. Szyc, and J. Lewiński. Minimization of stress concentration factor in cylindrical pressure vessels with ellipsoidal heads. *International Journal of Pressure Vessels and Piping*, 79(12):841–846, 2002. URL [www.scopus.com](http://www.scopus.com). Cited By :29.
- [39] Isotensoid related composite structures. In *Technical Conference of the American Society for Composites*, 2006.
- [40] Zu, L., Koussios, S., and Beukers, A. Design of filament-wound isotensoid pressure vessels with unequal polar openings. *Composite Structures*, 92(9):2307–2313, 2010. doi: 10.1016/j.compstruct.2009.07.013.
- [41] Alcántar, V., Aceves, S. M., Ledesma, E., Ledesma, S., and Aguilera, E. Optimization of Type 4 composite pressure vessels using genetic algorithms and simulated annealing. *International Journal of Hydrogen Energy*, 42(24):15770–15781, 2017. doi: 10.1016/j.ijhydene.2017.03.032.
- [42] D. Leh, B. Magneville, P. Saffré, P. Francescato, R. Arrieux, and S. Villalonga. Optimisation of 700 bar type iv hydrogen pressure vessel considering composite damage and dome multi-sequencing. *International Journal of Hydrogen Energy*, 40(38):13215–13230, 2015. URL [www.scopus.com](http://www.scopus.com). Cited By :6.
- [43] Leh, D., Saffré, P., Francescato, P., Arrieux, R., and Villalonga, S. A progressive failure analysis of a 700-bar type iv hydrogen composite pressure vessel. *International Journal of Hydrogen Energy*, 40(38):13206–13214, 2015. ISSN 03603199. doi: 10.1016/j.ijhydene.2015.05.061.
- [44] Z. Hashin. Fatigue failure criteria for unidirectional fiber composites. *Journal of Applied Mechanics, Transactions ASME*, 48(4):846–852, 1981. URL [www.scopus.com](http://www.scopus.com). Cited By :47.
- [45] Berro Ramirez, J. P., Halm, D., Grandidier, J. C., Villalonga, S., and Nony, F. 700 bar type iv high pressure hydrogen storage vessel burst – simulation and experimental validation. *International Journal of Hydrogen Energy*, 40(38):13183–13192, 2015. ISSN 03603199. doi: 10.1016/j.ijhydene.2015.05.126.
- [46] FA. Leone, A.C. Bergan, and C.G. Dávila. CompDam - Deformation Gradient Decomposition (DGD), v2.5.0, 2019. [https://github.com/nasa/CompDam\\_DGD](https://github.com/nasa/CompDam_DGD).
- [47] Nebe, M., Asijee, T., Braun, C., van Campen, J.M.J.F., and Walther, F. Experimental and analytical analysis on the stacking sequence of composite pressure vessels. *Composite Structures*, 247:112429, 2020. ISSN 0263-8223. doi: 10.1016/j.compstruct.2020.112429.
- [48] Meng, L. B., Jin, G. C., Yao, X. F., and Yeh, H. Y. 3D full-field deformation monitoring of fiber composite pressure vessel using 3D digital speckle correlation method. *Polymer Testing*, 2006. doi: 10.1016/j.polymertesting.2005.09.011.
- [49] Gasior, P., Malesa, M., Kaleta, J., Kujawińska, M., Malowany, K., and Rybczyński, R. Application of complementary optical methods for strain investigation in composite high pressure vessel. *Composite Structures*, 203:718–724, 2018. doi: 10.1016/j.compstruct.2018.07.060.
- [50] Torres, A. I. *Experimental and analytical determination of interfiber fracture mechanisms and patterns in type IV composite pressure vessels*. MSc Thesis: Delft University of Technology, 2019.
- [51] Cesari, E. *Combined acoustic and optic characterization of damage mechanisms in internally pressurized composite pressure vessels*. MSc Thesis: Delft University of Technology, 2020.
- [52] Michigan scientific corporation website. <https://www.michsci.com/what-is-a-strain-gauge/?cn-reloaded=1>. Accessed: 2020-11-10.

- [53] Pavel Dokoupil. Determination of measurement uncertainty of strain and stress using strain gages. *Transactions of the VŠB – Technical University of Ostrava - Mechanical Series*, 63(1), 2017.
- [54] Hao, J.-C., Leng, J.-S., and Wei, Z. Non-destructive evaluation of composite pressure vessel by using fbg sensors. *Chinese Journal of Aeronautics*, 20(2):120–123, 2007. ISSN 10009361. doi: 10.1016/S1000-9361(07)60017-X.
- [55] Kang, D. H., Kim, C. U., and Kim, C. G. The embedment of fiber Bragg grating sensors into filament wound pressure tanks considering multiplexing. *NDT and E International*, 39(2):109–116, 2006. doi: 10.1016/j.ndteint.2005.07.013.
- [56] Nebe, M., Braun, C., Gebhardt, T., Hülsbusch, D., and Walther, F. *Optische und akustische Analyse der Schadens- und Versagensmechanismen in CFK-Druckbehältern*. Werkstoffprüfung 2018 – Werkstoffe und Bauteile auf dem Prüfstand, Hrsg.: G. Moninger, Stahleisen, 2018. ISBN 978-3-941269-99-6.
- [57] Nebe, M. *In situ characterization methodology for the design and analysis of composite pressure vessels*. Springer Vieweg, 2020.
- [58] C. Kang, Y. Shi, B. Deng, T. Yu, and P. Sun. Determination of residual stress and design of process parameters for composite cylinder in filament winding. *Advances in Materials Science and Engineering*, 2018, 2018. URL [www.scopus.com](http://www.scopus.com). Cited By :4.
- [59] S. Koussios, O. K. Bergsma, and A. Beukers. Filament winding. part 1: Determination of the wound body related parameters. *Composites Part A: Applied Science and Manufacturing*, 35(2):181–195, 2004. URL [www.scopus.com](http://www.scopus.com). Cited By :29.
- [60] M. Knops. *Analysis of failure in fiber polymer laminates: The theory of alfred puck*, pages 1–205. Analysis of Failure in Fiber Polymer Laminates: The Theory of Alfred Puck. 2008. URL [www.scopus.com](http://www.scopus.com). Cited By :140.
- [61] A. Savitzky and M. J. E. Golay. Smoothing and differentiation of data by simplified least squares procedures. *Analytical Chemistry*, 36(8):1627–1639, 1964. URL [www.scopus.com](http://www.scopus.com). Cited By :12167.
- [62] Zhang, Q., Xu, H., Jia, X., Zu, L., Cheng, S., and Wang, H. Design of a 70 mpa type iv hydrogen storage vessel using accurate modeling techniques for dome thickness prediction. *Composite Structures*, 236: 111915, 2020. ISSN 02638223. doi: 10.1016/j.compstruct.2020.111915.